Tissue-engineered models of the glioblastoma tumor microenvironment

A Dissertation

Presented to
the faculty of the School of Engineering and Applied Sciences
University of Virginia

in partial fulfillment
of the requirements for the degree of

Doctor of Philosophy

by

Jessica X. Yuan

August 2018

Approval sheet

The dissertation is submitted in partial fulfillment of the requirements for the degree of

Doctor of Philosophy in Biomedical Engineering

Jessica X. Yuan
Author

This dissertation has been read and approved by the examining committee:

Jennifer M. Munson, Ph.D.
Dissertation Advisor
Department of Biomedical Engineering

Shayn M. Peirce-Cottler, Ph.D.
Committee Chair
Department of Biomedical Engineering

Bethany J. Horton, Ph.D.
Committee Member
Department of Public Health Sciences

Jason A. Papin, Ph.D.
Committee Member
Department of Biomedical Engineering

Benjamin W. Purow, M.D.
Committee Member
Department of Neurology

Accepted for the School of Engineering and Applied Science:

Craig H. Benson, Ph.D.
Dean
School of Engineering and Applied Science

Summary

A tumor is made of more than only cancer cells. The tissue surrounding the tumor, referred to as the tumor microenvironment, is highly complex and comprised of many various factors, such as stromal cells, extracellular matrix, chemokines, and biophysical forces. These factors have been shown to contribute to therapeutic resistance in many cancers. However, in one of the deadliest and most invasive types of cancers, glioblastoma, the tumor microenvironment is understudied, and links to patient survival are unknown. Glioblastoma is a cancer that simultaneously invades and grows, therefore tumor cells aggressively and diffusely infiltrate the brain. This defining feature, as well as the need to minimize damage to the healthy brain tissue in order to preserve neural function, makes complete surgical resection of glioblastoma tumors exceptionally difficult. An infiltrative edge remains post-resection, and it is these invading tumor cells that interact with and transform the previously healthy brain for inevitable recurrence of glioblastoma tumors.

The brain microenvironment is particularly unique compared to other tissues within the body, thus making the tumors that arise here challenging to understand and treat. Glia, the supporting cells exclusive to the brain have unique biological functions to promote and protect the brain. The brain extracellular matrix is primarily composed of hyaluronan, with no collagen, a normally prevalent component of other tissues. The blood-brain barrier protects the brain from foreign substances, and therefore limits therapeutic access to tumors. Brain tumor growth and recurrence is mediated by multiple factors from this complex

microenvironment, and it is this complexity that makes studying the microenvironment difficult. Previously limited to costly *in vivo* experiments or non-representative 2D *in vitro* studies, the advent of tissue engineering brought a technology for incorporating defined populations of multiple cell types in extracellular matrix, to represent the microenvironment more realistically and more similarly to *in vivo* tissues without sacrificing the ease of implementation associated with *in vitro* experiments. When applied to the study of cancer, tissue engineering can be used to replicate complex tumors *in vitro* to more easily tune and study contributions of specific microenvironment components and better understand the tumor microenvironment as a whole.

The overall objective of this dissertation work was to use tissue engineering to build a patient-driven and physiologically relevant 3D *in vitro* model of the glioblastoma tumor microenvironment to study microenvironmental contributions and therapeutic response. Through development of quantitative techniques for histological analysis of the glioblastoma cellular microenvironment, we built statistical models for predicting patient survival based on the cellular microenvironment makeup of their tumors (Chapter 2). Based on the histological analyses of patient tumor samples, a 3D *in vitro* model, specifically mimicking the post-resection infiltrative edge of the glioblastoma tumor microenvironment, was designed and optimized (Chapter 3). Taking advantage of the tunable nature of the tissue-engineered model, we demonstrate assessment of multiparametric effects of the microenvironment *in vitro* (Chapter 4), ability to identify microenvironment intercellular signaling targets (Chapter 5), as well as therapeutic responses to standard of care, and to

clinically relevant chemotherapeutics *in vitro* and *in vivo* (Chapter 6). In all, this dissertation encompasses work to understand contributions of the cellular microenvironment to glioblastoma malignancy across the spectrum – from analysis of patient tumor samples to *in vitro* tissue-engineered modeling and *in vivo* xenograft studies.

Acknowledgments

First, I must thank my advisor, Jenny Munson, for convincing me to dive headfirst into cancer tissue engineering. Your energy and enthusiasm for research is contagious, and I am grateful you chose me as your first graduate student. Thank you for all the guidance and encouragement, and providing a plethora of opportunities to learn, explore, and grow over the last four years.

Throughout my time here at the University of Virginia, I received tremendous support and encouragement from my colleagues and peers. To my committee members, Shayn Peirce-Cottler, Jason Papin, BJ Purow, Beth Horton, and Jeff Saucerman, thank you for all your knowledge, recommendations, and insight. I really appreciate all the time you have each committed to helping me. Special thanks to Shayn for providing space at UVa for me to finish out my research. To all the Munson Burners, Kathryn Kingsmore Allison, Ali Harris, Matt Perez, Chase Cornelison, Daniel Logsdon, and Caleb Stine, thank you for all the troubleshooting, advice, and support, amongst the fantasy football trash talk. It has been a pleasure to work alongside and learn from each of you. In particular, Kathryn and Ali – thank you for being my cheerleaders, helping me push through the toughest of times. Chase – thank you for teaching me, providing feedback, and being an invaluable second pair of hands. This work would not have been possible without the help of the extremely talented undergraduates I had the honor of mentoring and working with: thank you Alexandra Berr, Samantha Schwager, Garrett Beeghly, Nikhith Kalkunte, and Lynette Sequeira. To Kellen

Chen and TK Phung, thank you for always being willing to listen to me vent, and to eat Al Carbon, Brazo's, Marie Bette, Mellow, and Pie Chest (just to name a few).

Absolutely most of all, thank you to my family. My father came to the US over thirty years ago to become the first Dr. Yuan and inspired my path to become a scientist. My mother did everything, big or small, in her power to help and support me. Every single day, I am grateful for your dedication and perseverance, and for the enormous sacrifices you both made to leave your homeland and start a new life in the US. Thank you for teaching me to work hard and do my best. My older sister, the second Dr. (Dr.) Yuan, inspired me to not only become a biomedical engineer, but more specifically, a tissue engineer. Thank you, Jenny, for helping pave my way through this minefield, and never missing an opportunity to grill me on my research. My brother-in-law taught me 3D cell culture back when I was an undergrad, a skill without which I would not have this thesis. Thank you, Quentin, for all your encouragement and advice. Even though my career choices so far may not be the most unique in our family, I am so lucky to be a part of a household full of role models. I absolutely have to thank my sweet baby James P. Sullivan for being my loyal companion, and bringing me endless amounts of joy through all the Ph.D. hardships. Last, but certainly not least, Joshua provided more love, patience, motivation, and support than I could have ever thought possible. Thank you for never hesitating to try and help me in any way you can, despite almost 3,000 miles of distance, and always making sure I have something to look forward to, with Disney trips and ramen spots across the world. I cannot wait for all our next adventures together.

Table of Contents

List of tables

List of figures

List of symbols and abbreviations

ρ	Spearman's coefficient
μL	Microliter
μm	Micrometer
μM	Micromolar
ACUC	Animal Care and Use Committee
ANOVA	Analysis of Variance
AM	Astrocytes and Microglia
BCNU	Bis-chloronitrosourea (Carmustine)
CCL2	Chemokine (C-C motif) ligand 2 (also known as MCP-1)
CCR2	Chemokine (C-C motif) receptor 2
CI	Confidence Interval
cm	Centimeter
CXCL1	Chemokine (C-X-C motif) ligand 1 (also known as Gro-1)
CXCL8	Chemokine (C-X-C motif) ligand 8 (also known as IL-8)
CXCL12	Chemokine (C-X-C motif) ligand 12 (also known as Stromal-cell derived factor 1)
CXCR2	Chemokine (C-X-C motif) receptor 2
CXCR4	Chemokine (C-X-C motif) receptor 4
DAPI	4',6-Diamidino-2-phenylindole
DMEM	Dulbecco's Modified Eagle's Medium
DNA	Deoxyribonucleic Acid
ECM	Extracellular matrix
EGF	Epidermal Growth Factor
EGFR	Epidermal Growth Factor Receptor
ELISA	Enzyme-linked immunosorbent assay
FBS	Fetal bovine serum
FDA	United States Food and Drug Administration
FGF	Fibroblast Growth Factor
GBM	Glioblastoma
GFP	Green fluorescent protein
GSC	Glioblastoma stem cell
Gy	Gray
H&E	Hematoxylin and eosin

HIF-1α	Hypoxia inducible factor 1 alpha
HR	Hazard ratio
IC50	Inhibitory Concentration 50%
IDH1	Isocitrate Dehydrogenase Enzyme Isoform 1
kg	Kilogram
mg	Milligram
MGMT	Methyl-O6-Guanine-Methyltransferase
mm	Millimeter
MMP	Matrix metalloproteinase
MRI	Magnetic resonance imaging
nm	Nanometer
nM	Nanomolar
OCT	Optimal cutting temperature compound
OSP-1	Oligodendrocyte specific protein 1
PBS	Phosphate buffered saline
PDGF	Platelet-derived growth factor
PEG	Polyethylene glycol
RT	Radiation therapy
TBS	Tris-buffered saline
TME	Tumor microenvironment
TMZ	Temozolomide
TPER	Tissue Protein Extraction Reagent
VEGF	Vascular Endothelial Growth Factor

Chapter 1: Introduction

Although cancer is still the second leading cause of death in United States [1], in the last few decades, better surveillance, understanding of tumor biology and novel treatment discoveries have led to patient survival in many cancers improving greatly [2]. However, brain cancers are notoriously difficult to treat, and for the most common and malignant form, glioblastoma, the survival rate is dismally low. Recent advances in clinical treatments for glioblastoma have only increased the median survival time to 16 months after first diagnosis [3, 4]. Brain tumors are unique in treatment regimens and progression patterns from other cancers due to the distinct environment these tumors grow within, the types of cells they develop from, as well as how they interact with their native tissue environment.

1.1 Glioblastoma overview

Although brain cancers only affect a small population of adults, the most common and malignant form, glioblastoma (GBM), has such poor prognosis that they are a significant clinical problem [3]. Glioblastoma claims 12-14,000 lives annually in the United States, with a median survival of 16 months after diagnosis [3]. Glioblastoma is characterized by diffuse invasion from the primary tumor bulk into the healthy brain tissue [5]. These invading cells remain after surgical resection, and are considered the cause for inevitable recurrence [6–8].

When a patient displays symptoms of a brain tumor, such as chronic headaches, loss of consciousness, seizure, and/or loss of sensory or motor functions, the patient will undergo

magnetic resonance imaging (MRI) to detect the tumor. The patient will then undergo surgery to remove as much of the tumor bulk as is safely possible. After surgical resection of the tumor bulk, a portion of the resected tumor sample is biopsied and after hematoxylin and eosin (H&E) staining for nuclei and protein content, is graded by a neuro-pathologist to identify the type of cancer.

Brain tumors typically arise from glial cells, the unique support cells of the brain, giving the term "gliomas" when referring to brain tumors. There is further delineation for gliomas, based on the specific glial cell of origin. The most common type of glioma is the astrocytoma, arising from astrocytes, the star-shaped, supporting brain cells. Brain cancers have four grades, increasing in malignancy. Lower grade gliomas (grade I and II) are typically easier to treat, and patient survival is higher than higher grade gliomas (grade III and IV). Unlike other cancers, gliomas are not given stages, as these tumors rarely metastasize. Grade is determined by pathologists upon examination of biopsy samples. Glioblastoma is classified as a grade IV astrocytoma, indicating the most malignant grade in the most common type of glioma. According to the World Health Organization (WHO) classification, histological criteria for glioblastoma diagnosis is nuclear atypia, cellular pleomorphism, mitotic activity, vascular thrombosis, microvascular proliferation, and necrosis [9]. Glioblastoma is considered highly malignant due to the large number of tumor cells that are capable of reproducing rapidly, as well as the large network of blood vessels nourishing the tumor. Astrocytes are the most abundant cells in the brain, and as a grade IV astrocytoma,

glioblastoma tumor cells are readily capable of invading through the brain tissue, but very rarely metastasize outside the brain.

Glioblastoma was previously named glioblastoma multiforme, a name that reflects the highly heterogeneous morphology and pathology of these tumors. Although multiforme has since been dropped from its clinical name, the key pathological features of glioblastoma, originally identified by Hans Scherer in 1938 – perivascular invasion, perineuronal satelliotosis, subpial spread, and white matter tract invasion – continue to persist for diagnosis of this cancer [10]. These features reflect the characteristic invasive nature of glioblastoma. Pseudopalisading necrosis, a distinct pathological feature of glioblastoma, results from an abundance of growth in cells in a small area, resulting in hypoxia and cell death at the center of area, followed by cell migration away from the dead regions. This induces growth factors and angiogenesis, production of blood vessels, to support and select for the most aggressive cancer cells. These factors together contribute to the highly malignant nature of glioblastoma.

1.2 Treatment of glioblastoma

The standard of care therapeutic strategy for glioblastoma is surgical resection of the tumor bulk, followed by multiple rounds of pulsed oral temozolomide (TMZ) chemotherapy and radiation therapy to the brain. Despite this highly aggressive standard of care, glioblastoma always recurs and patient survival is dismally low, at less than 2 years after diagnosis [3].

The first line of treatment is surgical resection, when a neurosurgeon removes the tumor from the primary site within the brain. This surgery involves a craniotomy to open the skull, followed by cutting of the tumor out of the brain. This process is not an exact science; neurosurgeons operating rely primarily on "feel" of the tumor and brain, developed from experience over time. MRI guides surgeons by creating a map to view the general tumor shape and placement. However, the image acquired via MRI typically does not have enough resolution to visualize all the invasive paths glioblastoma cells take outside the primary tumor bulk border. In order to preserve neural function, neurosurgeons focus on resecting as much of the tumor bulk as possible without affecting the healthy brain tissue. Sometimes, they will resect millimeters of extra border around the tumor bulk to attempt to remove the diffusely invaded cells that are not macroscopically visible or tactile. The experience and skill of the neurosurgeon operating is integral to successful resection of the tumor [11].

Radiation therapy utilizes gamma-irradiation to directly damage DNA in cells. This type of therapy is common in the majority of cancer patients. For brain tumors, gamma rays are directly sent through the tumor site to not only directly damage DNA at the treatment time, but also to generate free radicals that can cause more damage over time [12, 13]. The radiation is limited to a 1-2cm region surrounding the tumor bulk in an effort to minimize damage to the healthy tissue while still treating as many of the invasive cancer cells as possible. However, there are typically adverse effects regardless. Patients can experience loss of neurological function after undergoing radiation therapy to the brain.

Furthermore, glioblastoma recurrence occurs just outside the radiation field, within a 2-cm margin from the original tumor primary site in a majority of patients [14].

Systemic chemotherapy after post-surgical resection is given to all patients via orally delivered temozolomide (TMZ) and enters the brain tumor via blood vessels. TMZ is a DNA alkylating agent that induces apoptosis of cancer cells by randomly silencing genes epigenetically [4]. This chemotherapy has been effective in yielding a significant increase in survival time compared to surgical resections with only radiation therapy [4]. However, 30% of malignant glioma patients express methyl-guanine-methyl-transferase (MGMT) hypermethylation, which undoes the TMZ methylation mechanism and thus makes these patients resistant to treatment [15, 16]. Despite this, the MGMT methylation is a strong predictive factor for favorable survival as the median survival for patients with MGMT methylation is 21.7 months compared to those without at 12.7 months [17].

Secondary therapies are beneficial in 25% of patients with recurrence [18]. In the past, BCNU chemotherapy has been administered to glioblastoma patients via poly lactic-co-glycolic acid wafers applied into the resection site [19]. This treatment resulted in a slight increase in survival, but patients still recurred and the usage of such wafers never became common. After the standard-of-care regimen fails, and a patient recurs, the neuro-oncologist may prescribe anti-angiogenic therapies to halt or slow down glioma growth by controlling blood vessel growth. Anti-angiogenic therapies, such as monoclonal antibodies targets to vascular endothelial growth factor (VEGF), aimed to prevent a tumor from undergoing angiogenesis necessary to supply the tumor with nutrients. For glioblastoma patients,

bevacizumab (Avastin ®) was shown to slow tumor growth but did not significantly affect overall survival [20].

A number of therapies that have been approved and successful in treating other cancers, have also been tested for glioblastoma post-standard of care. However, there has been very limited success on this front, with no therapy significantly improving overall survival compared to the standard of care. Glioblastoma is particularly difficult to treat due to the brain-blood barrier which limits therapeutic access, as well as the unique cell types that are not found in other tissues of the body [21]. On a practical level, the short survival times of glioblastoma patients, sadly, also makes multiple therapeutic regimens infeasible. There is also no strategic selection process in place for recurrent glioblastoma therapy, as selection of a therapeutic strategy depends solely on physician experience and a trial-and-error approach with readily available chemotherapeutic drugs.

The high therapeutic failure rate for treatment of glioblastoma occurs not just because cells continue to survive post-treatment, but because those remaining cells are able to repopulate, invade, and proliferate to form new tumors [22, 23]. In many cancers, high-throughput therapeutic screening strategies use single cell types in 2D, or the recent emergence of 3D spheroid culture, for assessment of cell survival post-therapy in order to quickly and easily eliminate non-beneficial therapeutics [24, 25]. These assays are overlooking important malignancy outcomes that are contributing to recurrence. And furthermore, these types of assays are not representative of the native brain environment, as tumors are composed of more than just cancer cells, as described in the following section.

1.3 The tumor microenvironment

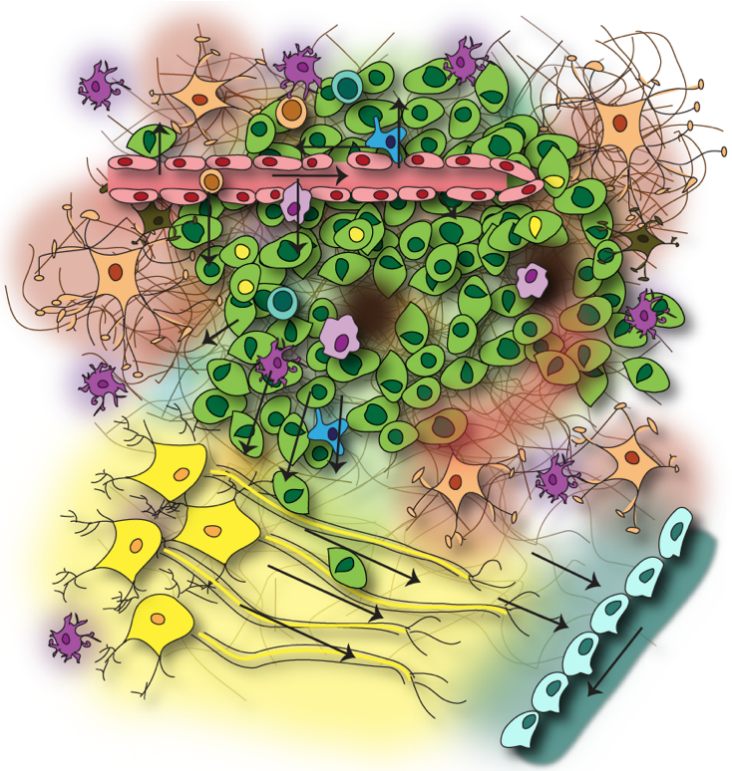

Figure 1.1: The brain tumor microenvironment is unique and comprised of many factors other than tumor cells. In addition to cancer cells and cancer stem cells (green), the brain tumor microenvironment includes stromal cells, such as astrocytes (orange), microglia (purple), epithelial cells (pink), and neurons (yellow), as well as extracellular matrix, soluble factors, biophysical forces, and more.

The tissue surrounding the cancer cells is referred to as the tumor microenvironment (TME) (**Figure 1.1**). It is an emerging theme that the tumor microenvironment is important in promoting treatment resistance via multiple mechanisms – enriching cancer stem cells, increasing apoptosis resistance, proliferation, and invasion, and reducing drug transport to tumor cells [26]. Although the tumor microenvironment for each cancer can vary depending on the tissue of origin, the general components include stromal cells, extracellular matrix,

soluble factors, and biophysical forces, in addition to the cancer cells and cancer stem cells [27].

Glioblastoma usually relapses within 2-3cm of the original surgical resection cavity [14, 28], suggesting the anatomy of glioblastoma and its surrounding brain microenvironment contain many features that support and contribute to the malignancy of the disease. From autopsy findings in 1938, Hans Scherer suggested gliomas migrate along existing brain structures triggered by interactions of the glioma cells with the brain microenvironment [10]. Glioblastoma tumors most commonly occur in the subcortical white matter of the cerebral hemispheres, and follow white matter tracts for growth and infiltration [29]. Scherer's structures – perivascular invasion, perineuronal satellitosis, subpial spread, and white matter tract invasion – are optimized for diffuse spread of glioblastoma tumors throughout the brain microenvironment [10, 30, 31].

1.3.1 Stromal cells

Stromal cells are normal cells, native to the tissue of origin, which can be transformed from interactions with the cancer cells. In many tissues, fibroblasts, macrophages, and other immune cells are shared and common stromal cells across multiple cancers. However, the brain has a unique microenvironment. The brain has two main types of cells – neurons and glial cells. Neurons are the messenger cells of the brain and process and transmit information through electrical and chemical signaling. Glial cells provide support for neurons and help regulate signal transmission. There are roughly ten times as many glial cells as neurons in the central nervous system. Brain tumor growth and recurrence is likely mediated by

multiple factors from the complex microenvironment, but in particular, glial cells have been implicated [32–34].

Microglia are the resident macrophages, or immune cells, of the brain, and therefore the main form of immune defense for the central nervous system. Similar to macrophages, the primary functions of microglia include scavenging for foreign or damaged cells and materials, phagocytosis – engulfing of these various debris, maintaining brain homeostasis, and promoting inflammation in damaged tissue. As such, microglia play a large and vital role in the body's own effort to combat glioblastoma. We and others have seen microglia and tumor-associated macrophages accumulate within and around glioma [35, 36]. Due to the extreme difficulty of distinguishing brain-specific microglia from macrophages residing in the brain, for this dissertation, they will be discussed as one cell population. In normal brain, microglia account for 10% of brain cells, but in glioblastoma, this percentage increases significantly [35, 36]. In normal brain, microglia are typically in a resting, or "ramified" state with a small cellular body and long branching processes as cell turnover is relatively low. In glioma and other infectious or inflamed states of the brain, microglia change morphology to respond to the attacks, becoming activated and reactive, with large cellular bodies from phagocytosis of cells.

Researchers have long been interested in the role and contribution of microglia to glioma growth. Microglia have been shown to promote migration of murine glioma cells, and this migration promotion is preferential for microglia over other brain cells, such as oligodendrocytes and endothelial cells [37]. Glioma cell invasion was significantly reduced in

mouse brain slices depleted of microglia via clodronate filled liposomes, compare to control brain slices with original microglia populations [38]. Crosstalk between glioma cells and microglia include a host of factors, including CXCL12, EGF, periostin, TGFβ, interleukin-10, and many more, promoting glioma cell proliferation and invasion [39–42].

Astrocytes are the most abundant cell in the brain and the original normal cells from which glioblastoma arises. The primary function of these star-shaped glial cells includes structural support, nutrient supply, neural repair, and support and maintenance of the blood-brain barrier. Astrocytes highly populate the brain, and there is no region of the central nervous system where astrocytes cannot be found. Activated, or reactive, astrocytes are both beneficial and harmful to brain tissue [43]. After injury, reactive astrocytes form a glial scar tissue surrounding the impaired area to contain and suppress inflammation but can persist and form a barrier against regeneration [43].

Studies have shown astrocytes are involved in glioma remodeling and disruption of the blood brain barrier to increase glioma cell invasion [44]. Astrocytes have been shown to increase glioma cell invasion via production of the metalloproteinase, proMMP2 [45] and to increase glioma cell proliferation via CXCL12/CXCR4 signaling [46]. Direct contact between glioma cells and astrocytes protects glioma cells against chemotherapeutics, and might reveal underlying mechanisms for poor chemotherapeutic efficacy in glioblastoma [47]. Astrocytes produce the enzyme, heparanase, to degrade proteoglycans within the extracellular matrix and promote invasion of cancer cells [48]. Astrocytes secrete many factors and play a role in signaling pathways that have been implicated in glioma growth. Astrocytes mediate

activation of sonic hedgehog signaling, a pathway that is activated in glioma, and has been shown to have an active role in glioma stem cell self-renewal and growth [49]. Astrocytes downregulate TNFα, a proinflammatory chemokine utilized by microglia to carry out immune system function, thus suppressing immune reactions and promoting glioma growth [50].

1.3.2 Vasculature

Angiogenesis, or the recruitment of blood vessels and vasculature to provide and sustain nutrients, is a hallmark of all cancers [51]. As a tumor grows from an individual cell into a complex mass, the cells are proliferating at a high rate with a lack of nutrient supply. Cells will either die via necrosis, or secrete growth factors, such as Vascular Endothelial Growth Factor (VEGF) and angiopoetin, to recruit blood supply to sustain them [52]. Although there are many therapeutics aimed to inhibit angiogenesis in order to starve tumors from nutrients, these treatments have been more harmful than beneficial in glioblastoma. Studies have shown inhibiting angiogenesis has increased invasion and malignancy [53, 54]. Systemic delivery of therapeutics requires blood vessels to enter the tumor, and without these vessels, therapeutics are unable to enter the tumor. As such, researchers have focused on normalizing the tumor vasculature, as opposed to inhibiting blood vessel growth, in order to continue delivery of chemotherapeutics to the tumor and hopefully reduce the invasive potential of the cancer cells [55].

Gliomas, in particular, are highly vascularized tumors. Initial brain tumor growth occurs via co-opting pre-existing blood vessels – glioma cells migrate along the blood vessels

causing them to compress and destabilize, and eventually leading to vessel regression, hypoxia, and tumor cell death [56, 57]. Accumulation of hypoxia inducible factor 1α (HIF1 α) induces VEGF and drives angiogenesis to support the tumor. Once glioblastoma tumors are symptomatic and diagnosed, the tumor has already generated a complex and aggressive vasculature that is difficult to surgically resect. A common histopathological feature unique to glioblastoma, "pseudopalisading" necrosis, connects multiple characteristics of glioblastoma (invasion, hypoxia, and angiogenesis), as tumor cells rapidly proliferate, necrose, invade, and recruit blood vessels [58].

Normal brain tumor vasculature is specialized and composed of astrocytes, endothelial cells, and pericytes, to form the blood-brain barrier [59]. The blood-brain barrier protects the brain by selectively restricting molecules from entering the intracranial circulatory system, thus compromising the ability for many chemotherapeutics to cross. However, the blood-brain barrier itself can become compromised with the growth of tumors in the parenchyma, and while it is easier for chemotherapeutics to now enter the brain, the inherent protection of the blood-brain barrier is no longer intact.

1.3.3 Extracellular matrix

The extracellular matrix (ECM) is composed of macromolecules that provide tissues with structural integrity. These macromolecules (proteoglycans, glycosaminoglycans, and glycoproteins) create a randomly oriented scaffold for cells to adhere, grow, and develop. The major components of the ECM are tissue-specific – the breast ECM is primarily collagen type I, while lung ECM is primarily collagen type IV [60]. In the brain, hyaluronan, an

unbranched and negatively charged glycosaminoglycan, is the most common ECM, and there is no collagen present [61, 62].

Stromal cells, such as fibroblasts, are not only embedded within the ECM, but are also primarily responsible for ECM remodeling by aiding deposition and degradation of ECM components via secretion and regulation of factors and enzymes [63]. Tumor ECM is significantly altered from normal tissue ECM. In general, cancer cells and cancer associated stromal cells can actively increase ECM deposition [64]. Furthermore, in parallel, matrix degradation enzymes, such as matrix metalloproteinases, are downregulated, leading to further increases in ECM deposition [65, 66].

In glioblastoma, hyaluronan is upregulated and contributes to cancer progression by cancer cell invasion and proliferation, as well as therapeutic resistance and recurrence [61, 62, 67–69]. Many studies have shown interactions between CD44, a transmembrane glycoprotein that acts as a receptor for hyaluronan, and hyaluronan promotes glioblastoma growth, invasion, and therapeutic resistance [70]. Furthermore, hyaluronanidases and hyaluronan synthases are overexpressed [71], and these factors together likely contribute to the highly aggressive and therapeutically resistant nature of glioblastoma. Other glycoproteins and proteoglycans, such as tenascin C, brevican and versican are also upregulated in glioblastoma [61, 72], thus demonstrating the glioblastoma ECM is architecturally distinct from normal brain ECM.

1.3.4 Biophysical forces

As described previously, cancer cells, as well as stromal cells, significantly alter the ECM by depositing and degrading ECM components [73, 74]. These changes, along with the activation of stromal cells, cause the tissue stroma to stiffen [73]. Tissue stiffening has been correlated with disease progression and metastasis, as well as poor prognosis in many cancers. Since the mechanical stiffness of tumors can increase up to 100 times the original healthy tissue stiffness, this phenomenon has been used as diagnostic tool and surgical aid in cancers of the breast, skin, liver, lung, and brain [75, 76]. Changes in the biomechanical environment of the tissue creates physical barriers that hinder therapeutic efficacy [75].

The increase in ECM, as well as other hallmarks of cancer – unchecked cellular growth and increased abnormal angiogenesis – results in elevated pressure in the tumor bulk [51, 52]. This elevated pressure is high throughout the tumor bulk, while the pressure at the tumor border leading into the surrounding stromal tissue is normal, generating a pressure gradient that causes the fluid found in the tissue stroma to flow from the tumor bulk into the surrounding stroma [52, 77–79]. This fluid flow is termed interstitial fluid flow, or simply interstitial flow. The lymphatic system primarily regulates flow of interstitial fluid to bring nutrients and oxygen throughout the tissues and stromal space [80]. In cancers, the increased interstitial pressure from the tumor causes fluid to flow into the lymph nodes, thus increasing swelling and causing edema [81]. This flow changes proliferation, increases invasion, activates stromal cells, and reorganizes components of the extracellular matrix [77]. However, the classical lymphatic system is not present in the brain, and as such interstitial flow in the

brain is less studied. Drainage of cerebrospinal fluid is within perivascular spaces, creating a pseudo-lymphatic system for the brain [82]. In the brain, the tumor fluid buildup is not able to flow to other parts of the body, and remains within the brain, causing severe brain edema [60].

Normal interstitial fluid flow distributes nutrients, and thus is able to redistribute chemokine gradients. Therefore, migration of cells along these gradient paths are also affected by interstitial flow [83]. Previous studies in our lab have elucidated the effects of interstitial flow on glioma invasion via activation of the CXCR4 receptor and formation of autologous pericellular gradients of CXCL12-dependent mechanisms, as well as through CD44-mechanotransduction [78, 79]. Furthermore, standard of care radiation therapy increased flow-stimulated invasion of glioma stem cells, indicating not only the role and contribution of interstitial flow to cancer cell invasion, but also the detrimental effects to therapeutic efficacy [78, 79].

1.3.5 Chemokines

There are several soluble factors abundant in the tumor microenvironment that create pro-inflammatory environments to promote cancer malignancy. Glioblastoma cells themselves secrete several autocrine factors to support motility. Epidermal growth factor receptor (EGFR) signaling is one of the most prevalent contributors to glioma proliferation, and can also increase glioma invasion [84]. In fact, one of the most common alterations of glioblastoma is abnormal EGF/EGFR signaling, which will be discussed further in Section 1.4.2 of this dissertation. Dysregulation in signaling of Platelet-derived Growth Factor

(PDGF) and its receptor, PDGFR, is another hallmark of glioblastoma, and has also been linked to proliferation, angiogenesis, and invasion *in vitro* [85].

Tumor cells signal and recruit nonmalignant cells through paracrine signaling to assist in tumor progression. Both astrocytes and microglia been observed to secrete the inactive form of matrix metalloproteinase 2, proMMP2, which glioblastoma cells can then activate to break down ECM allowing the cancer cells to invade [38]. Microglia are also the primary source of interleukin 1β which enhances expression and transcription of TGFβ, thus suppressing inflammatory responses to prevent glioblastoma growth [86]. CXCL12, which can be secreted by glioma cells as well as astrocytes and microglia in the microenvironment, can cause increased glioblastoma invasion by interacting with its receptor CXCR4 [87, 88].

Glioblastoma tumor cells also cross-talk with and recruit endothelial cells to promote angiogenesis through paracrine signaling and secretion of angiogenic factors such as VEGF [89, 90]. Other paracrine factors, such as BDNF and PEDF, are secreted by endothelial cells to promote neural stem cell proliferation [91, 92], and can likely also promote glioblastoma stem cell proliferation. Many other cytokines, such as EGF and TNFα have each been shown to increase GBM cell survival and proliferation [84, 93]. While cancer cells certainly have the capability of promoting their own malignant behaviors, studying this sole population misses this valuable crosstalk with glial and other support cells that further creates a pro-tumorigenic niche.

Current chemotherapeutic agents developed to target specific signaling pathways, such as bevacizumab for VEGF [94] and imatinib for PDGFR [95], have not increased

glioblastoma patient survival in clinical trials, but there are many more autocrine and paracrine signaling systems involved in glioblastoma malignancy. As the understanding of glioblastoma pathology expands with the development of robust experimental models, these signaling systems will continue to be exposed and the beneficial chemotherapeutics targeting will hopefully be developed soon after.

1.3.6 Cancer stem cells

A highly malignant subpopulation of cancer cells with properties similar to traditional stem cells were hypothesized and discovered initially in acute myeloid leukemia [96]. Since then, this population has also been identified in a host of other cancer types, including breast, bone, colon, pancreas, melanoma, and liver cancers [97]. Due to their ability to initiate tumors, self-renew and differentiate into all cell types found in a tumor, these cells have been referred to as "tumor propagating cells", "tumor initiating cells", "cancer stem-like cells", and "cancer stem cells" [98, 99]. For simplicity, this population of cells will be referred to as "cancer stem cells" in this dissertation. The exact origins of cancer stem cells are debated: some believe they arise stochastically, from DNA mutations in normal stem cells, while others believe they arise hierarchically, through clonal development and selection from cancer cells [100]. Regardless of their origins, studies have shown these cancer stem cells are highly resistant to therapies, allowing them to persist in tumors post-therapy and give rise to new tumors and metastases. Many studies have identified and isolated the cancer stem cell population from traditional cancer cells via markers previously used to identify non-malignant stem cells. This effort is to not only be able to study and characterize the

population further, but also to translate into identifying specific therapeutic targets against the cancer stem cells to eliminate this highly malignant population.

Glioblastoma stem cells (GSCs) themselves were discovered just over a decade ago [101] and have been correlated with poor prognosis and invasion [36, 102, 103]. GSC resistance to therapies has been studied thoroughly, with results indicating standard of care radiation therapy selects for GSC survival [104]. Surface and intracellular markers shown to select for the cancer stem cell population in other cancers as well neural stem cell markers, have been used to identify glioma cells. The expression of markers can vary drastically within a single patient tumor. CD133, a cell surface marker also known as Prominin1, is the most frequently used marker for GSCs. CD133-positive glioma cells have been shown as more radiation and chemotherapeutic-resistant than their corresponding CD133-negative populations, through activation of cell cycle check point, DNA repair mechanisms, and anti-apoptotic processes [104, 105]. However, later studies have shown CD133-negative glioma cells are still able to clonally expand and grow from single cells, as well as develop into tumors in vivo [106, 107], thus challenging CD133 as a definitive marker for glioblastoma stem cells.

A recent study from Jeremy Rich's group determined that glioma stem cells preferentially require two core iron regulators, transferrin receptor and ferritin, to develop tumors in vivo [108]. Previous studies have shown upregulation of transferrin receptor complex in many cancers, including glioma [109]. Ferritin, or stored excess iron to minimize free radical production, has been shown to contribute to invasion, restore angiogenesis, and

to generate tumors via autocrine growth factor signaling [110, 111]. These studies taken as whole, indicate transferrin receptor complex, also known as the CD71 surface marker, as a potential new marker for identifying stemness in glioblastoma cells.

1.4 Glioblastoma malignancy

1.4.1 Cell growth and death

Many of the hallmarks of cancer, as seminally described by Hanahan and Weinberg, [51, 112] contribute to the ability of cancer cells to grow and proliferate unchecked. Specifically, cancer cells are self-sufficient in growth signals, insensitive to anti-growth signals, and are able to evade apoptosis [51]. Many assays are available to assess cell viability and proliferation, including basic live/dead staining to cell cycle assays with fluorescent dyes, such as propidium iodide and DRAQ5, that intercalate with DNA to proliferation-specific markers such as Ki67.

A distinct pathological feature of glioblastoma is pseudopalisading necrosis, when the cells proliferate rapidly but are unable to maintain nutrient supply and thus necrose. Cells proliferate to grow, but cells die via two primary mechanisms: apoptosis or necrosis [113]. Apoptosis is biochemically regulated and programmed cell death, and is characterized by cell shrinkage, nuclear fragmentation, chromatin condensation and nucleic acid decay. On the other hand, necrosis is premature cell death, typically caused by external factors such as toxins or trauma. An apoptotic cell will eventually become necrotic. Because there

are different pathways for a cell to undergo apoptosis or necrosis, there are also different markers that are identifiable to differentiate the two processes.

Methods for distinguishing the two phenomena were developed using traditional microscopy for qualitative visual assessment, and flow cytometry for specific quantitative assessment [114]. Caspase activation and activity were thought to be necessary for apoptosis and were the traditional markers for assessing apoptosis, but eventually development of annexin V staining expanded assessment of cell death. Cell surface markers such as phosphatidylserine exposure can also be identified via flow cytometry [115]. Flow cytometry, though complex in setup and analysis, is a particularly powerful technique for quantitatively assessing multiple outcomes simultaneously.

Therapeutic strategies aim to halt the uncontrollable growth of cancer cells to stop tumors from growing and recurring. Taxanes aimed to inhibit cell division, and thus halt cell proliferation and growth. Alkylating agents, such as the GBM standard of care temozolomide as well as secondary therapy BCNU, are the oldest type of chemotherapeutic. The main mechanism is to covalently bind their alkyl group to DNA, thus causing DNA strands to break and the cell undergoes apoptosis [116]. Another type of chemotherapeutic is topoisomerase inhibitors, which include drugs such as irinotecan (topoisomerase I inhibitor) and etoposide (topoisomerase II inhibitor). Topoisomerase inhibitors prevent either one of the topoisomerase enzymes from controlling DNA structure, thus causing DNA breaks and leadimg to apoptosis [117, 118]. Platinum agents, such as carboplatin, interfere

with DNA replication by displacing chloride atoms with water via aquation, leading DNA to crosslink and the cell to undergo apoptosis [119].

1.4.2 Alterations and abnormalities

Over the past decade, many different molecular alterations, genetic abnormalities and mutations have been identified as leading to glioblastoma development. The most frequent (70%) gene alteration is loss of heterozygosity on chromosome arm 10q [120]. This mutation is specific to glioblastoma, and is rarely found in other brain tumor grades. It is associated with poor survival. Deletions or alterations in the tumor suppressor gene, p53, appear in 25-40% of glioblastomas, and tend to be associated with tumors in younger patients [120]. Overexpression, as well as truncations of the epidermal growth factor receptor (EGFR) are also frequent [121]. Both of these mutations lead to increased activity of EGFR. One variant, EGFRvIII has shown some promise as a target for kinase inhibitors. Overexpression of MDM2 is an alternative mechanism for escaping p53-regulated cell growth, and is associated with poor prognosis [122]. PTEN mutations, which have been found in 20% of glioblastomas, leads to loss of cellular phosphatase functions, thus activating signaling pathways and resulting in excessive proliferation [123]. Mutations in the isocitrate dehydrogenase enzyme isoform 1 and 2 (IDH1 and IDH2) are common in lower grade gliomas, and are found in glioblastomas that evolved from lower grade gliomas [124]. IDH1 mutations are associated with improved survival for glioblastoma patients.

Some of these characteristics are identifiable via immunohistochemical staining of patient tumor resections. Briefly, after resection of the tumor bulk, a small sample is fixed

in formalin, and embedded in paraffin before it is sectioned into thin (typically 6-8μm) slices and mounted on glass slides. Traditionally, the basic hematoxylin and eosin (H&E) staining will suffice for identifying the cell nuclei and proteins to detect pathological structures and features for diagnosis. Mutations, such as IDH1, are detectable using chromogenic antibody-based staining techniques, and already clinically used to predict patient survival. In other cancers, markers such as Ki67 for proliferation, are regularly used to identify the presence of cancer cells as well.

1.4.3 Invasion

While invasion is considered a hallmark of all cancers [51], it is a distinct and defining feature of glioblastoma. Glioblastoma is characterized by diffuse invasion from the primary tumor bulk into the surrounding healthy tissue. "Pseudopalisading" necrosis is a histopathological feature unique to GBM that connects multiple features of GBM – invasion, hypoxia, and angiogenesis, as cancer cells proliferate, necrose, invade, and recruit blood vessels [58]. Unlike other malignant cancers, glioblastoma tumors rarely metastasize outside the brain, and cancer cells are readily capable of invading throughout the structures of the brain, such as interstitial spaces, white matter tracts, and blood vessels [125, 126]. Invasion is distinct from regular cell migration due to the involvement of the extracellular matrix [127]. A cell is stimulated to invade via extracellular and intracellular cues from the cell itself, surrounding cells, and the microenvironment as well. Cells adhere to the ECM and to other cells via receptor binding. This adhesion is important to cell survival, as cells will undergo anoikis, or programmed cell death upon detachment from the surrounding ECM.

Cells maintain binding through focal adhesions linking the actin cytoskeleton with the cell membrane.

In order for cancer cells to move through the matrix, they need to manipulate the environment. Cancer cells degrade and alter the environment through matrix metalloproteinases (MMPs), calcium-dependent zinc-containing proteases that degrade matrix proteins [150]. MMPs in general are upregulated in all cancers, but in brain cancers specifically, MMP2 and MMP9, which both degrade collagen type IV, are particularly upregulated [128, 129]. These enzymes can be induced by intracellular and extracellular signaling mechanisms and interactions of the glioma cells, as well as glial cells [45]. In addition to MMPs, hyaluronidases, the enzyme to degrade hyaluronan, and cathepsin B, for degrading laminin, are also overexpressed in gliomas [65, 130]. In order to inhibit invasion, therapeutics targeted at MMPs have been developed and tested. Marimastat, an MMP2 inhibitor, was initially promising through preclinical studies, but ultimately was unsuccessful at improving glioblastoma patient outcomes [131, 132].

In addition to degradation of the matrix, cells protrude forward and move via cytoskeleton activation and rearrangement to migrate and invade through tissues. Actin polymerizes and depolymerizes, myosin contracts, and microtubules and intermediate filaments maintain the internal cell structure as the cell body moves forward. Since these processes are fundamentally important to cell viability, chemotherapeutics targeting the cytoskeleton can drastically affect cell survival. Paclitaxel targets microtubules by stabilizing them and preventing mitosis [133]. Vinblastine also targets microtubules in order to prevent

polymerization [134]. However, all cells, not just cancer cells, require cytoskeletal rearrangement for motility, and so compounds targeting this will have toxic side effects on any motile cell.

There are many methods for assessing migration and invasion, and these methods will be discussed further during the description of experimental models for studying glioblastoma in Section 1.5.

1.4.4 Subtypes

When the molecular subtypes for breast cancer were found to be clinically significant and lead to highly successful subtype-specific treatment regimens [135], researchers attempted to identify similar subtype distinctions for other cancers, including glioblastoma, using gene expression data. In 2010, Verhaak, et al. published four subtypes of glioblastoma – classical, mesenchymal, proneural, and neural – discovered through robust gene expression-based catalogs via The Cancer Genome Atlas [136]. These subtypes varied in response to aggressive therapy, which in this study was defined as more than three rounds of the standard-of-care radiation and temozolomide chemotherapy [136].

Classical glioblastoma tumors are characterized by upregulation of epidermal growth factor receptor (EGFR) [136]. Proneural tumors most commonly have mutations in TP53, as well as IDH1 mutations, and PDGFRA mutations [136]. Clinically, patients in the proneural subtype are significantly younger in age, and so they tend to have better overall survival, although there is no significant difference in overall survival for proneural patients who receive aggressive treatment compared to those who do not. The mesenchymal subtype

is enriched for patients with NF1 tumor suppressor gene mutation, as well as PTEN and TP53 mutations [136]. Mesenchymal subtype patients had significant increases in survival after aggressive treatment, compared to those who did not receive aggressive treatment. The neural subtype is characterized by gene expression patterns similar normal neurons in the brain, and patients were the oldest of the cohort [136]. Later studies eventually eliminated the neural subtype as tumor samples were primarily normal brain tissue.

For breast cancer patients, subtype-specific therapeutic regimens have moved therapy towards more personalized medicine. Genetic screenings are done for breast cancer patients in clinic to identify one of five genetic subtype (luminal A, luminal B, triple-negative/basal-like, HER2-enriched, and normal-like) [135] to identify the best course of treatment for patients. Luminal A and luminal B subtypes are estrogen receptor-positive and are associated with the best prognosis. Although HER2-enriched breast cancer grows quickly and aggressively, HER2 protein targeted therapies, such as Herceptin ® (trastuzumab) have been significantly successful in treating patients and improving overall survival [137].

However, in glioblastoma, subtyping has not been successfully translated to the clinic. The extremely heterogeneous nature of glioblastoma was reflected when studies showed multiple subtypes within a single patient [138]. Furthermore, studies have shown subtypes within a patient could change with recurrent tumors [139]. Therefore, although these subtypes help generate and facilitate experimental hypotheses, other avenues for developing more personalized medicine approaches for glioblastoma need to be explored. The

subtypes described by Verhaak, et al. focused on the tumor cells to define the subtypes, but as discussed earlier, the tumor microenvironment is integral to progression and therapeutic response of tumors. As such, subtyping may be more useful and translatable to clinic if it was expanded to look at the tumor as a whole, including the microenvironment, and not just focused on the cancer cells. With the push for personalized medicine continuing, it is important for researchers to study cancer in the context of the tissue and microenvironment.

1.5 Experimental models of glioblastoma

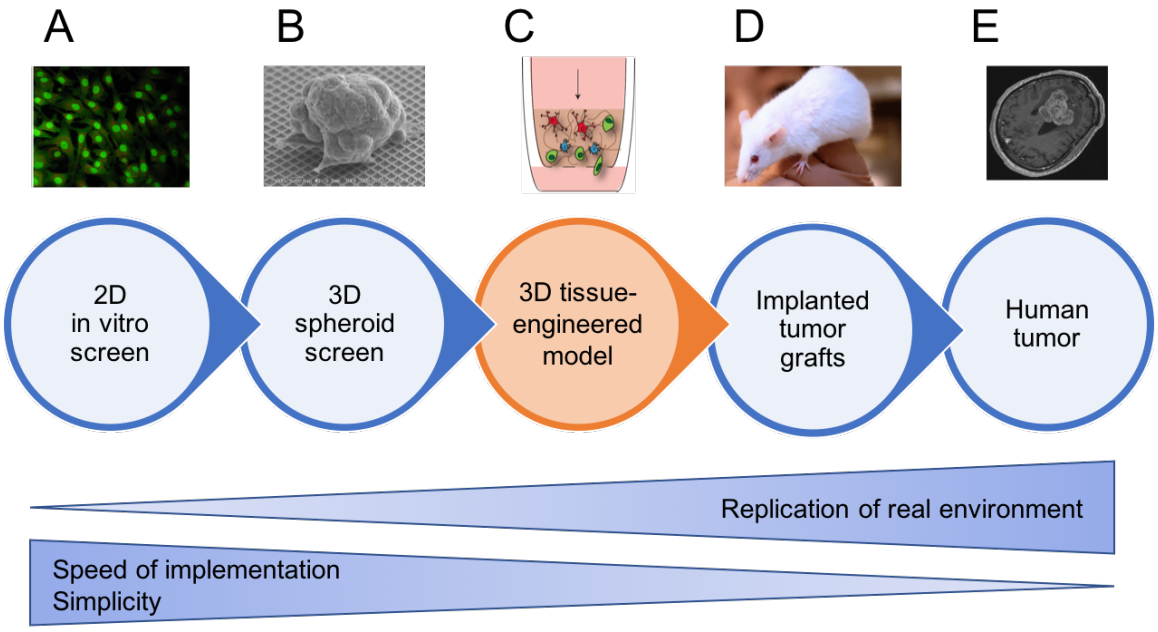

Figure 1.2: Experimental models of glioblastoma span in ease of use as well as replication of native environment. A) Traditional 2D *in vitro* screens are quick and simple. B) *In vitro* spheroid screens add in a 3-dimensional aspect. C) 3D *in vitro* tissue-engineered models can incorporate multiple cell types in a biomaterial matrix to balance representative environment with the ease of *in vitro* experimentation and control. D) Tumors implanted into *in vivo* animal models are costly and time-consuming but more representative of the E) human tumors in the native tissue environment.

1.5.1 2D in vitro cell lines

For over 50 years, serum-based 2D monolayer cultures of cell established from rat, mouse, and human tumors have been used to study glioblastoma *in vitro* (**Figure 1.2A**) [140]. The main advantage of these cell lines is the ease and speed of growing a monolayer of cells in tissue culture vessels. Furthermore, these cells can reliably generate tumors when implanted as tumors in vivo. The U87 human glioblastoma cell line is the most commonly used cell line, but the translation to clinical relevance is limited by lack of heterogeneity, as well as mutations from the original isolation of the cells [141]. Furthermore *in vivo* environments are 3D and as such, the cell behavior upon the traditional tissue culture plastic does not accurately mimic 3D *in vivo* physiology (**Figure 1.2E**) [142, 143]. Cells isolated from tissue undergo changes in metabolism and gene expression when adapting from their accustomed 3D growing environment to 2D culture [142]. Despite these pitfalls, 2D culture is still useful for basic experiments to quickly and easily identify responses.

With 2D experiments are basic methods for studying migration. Since these cells are in 2D, and are not moving through a matrix, these methods cannot be used to specifically examine invasion. In the past, scratch assays to examine fibroblast migration were popular as a simple and inexpensive method for mimicking wound healing. The basic steps involved "scratching" through a cell monolayer and capturing images to assess the rate at which cells migrate to close the scratch [144]. Cancer cells invade differently than normal cells migrate, and as such, this type of assay has been less popular over time. More advanced methods for

studying methods include incorporating an agarose gel, or more physiologically-relevant ECM coating for cells to migrate out.

1.5.2 Simple 3D in vitro models

Tumor spheroids add in a 3-dimensional aspect as these single tumor cell suspensions will cluster and self-assemble to form multicellular masses within a tissue culture vessel (**Figure 1.2B**). These spheroids can mimic some properties associated with in vivo tumors, such as, intercellular interactions, and diffusional limits for mass transport of nutrients and drugs [145–147]. Spheroids are commonly cultured without serum, a necessary ingredient to successful and fruitful 2D culture, in order to preserve the stemness characteristics when culturing cancer stem cells. Cells aggregate to form spheroids through a variety of techniques including spinner flask culture, liquid overlay over agar-coated plates, hanging drops, and microfluid chips [145, 148–150]. While these cell spheroids will eventually make and deposit their own ECM to maintain the 3D architecture, the lack of ECM structure at the beginning detracts from the relevance of native tissues, making spheroids more of a pseudo-3D model without the ability to assess cell-ECM interactions.

To study the important cell-ECM interactions present within tumors, researchers may coat various tissue culture vessels with ECM proteins. However, not only does the process of adsorbing to these substrates significantly alter the original ECM protein, cells are still seeded in a 2D culture fashion on top of the matrix, and thus these experiments are not representative of original *in vivo* environments. Distributing cells within an ECM

hydrogel brought the first technology for studying cells in a true 3D environment [151]. This will be discussed further in later sections.

These more advanced models have also led to more advanced techniques for assessing malignant outcomes. Boyden chamber assays are an extremely popular tool, utilizing a simple platform of tissue culture inserts with a permeable membrane for cells to pass through to mimic and quantify invasion in *in vitro* experiments [152, 153]. Boyden chambers are highly adaptable, and can be used in a simple 2D manner with cells seeded on top of the porous membrane, or can be expanded for utilization in 3D culture, with ECM protein coatings and/or combinations of multiple cell types, or as chemokine attractant assays.

1.5.3 In vivo models

Animal models are considered the gold standard for experimental and preclinical research but are complex, expensive, and less controllable than *in vitro* models (**Figure 1.2D**) [154–156]. There are many categories of animal models: how the tumor develops (implanted, induced, or naturally occurring), where the tumor grows (orthotopic or flank), and type of immune system (immunocompromised for human xenografts or syngeneic and transgenic with intact immune systems) [157]. These categories are not exclusive since animal models can overlap across these categories, for example a syngeneic mouse with a flank implanted tumor. Although orthotopic implants are overall ideal for modeling glioblastoma, there is not a general consensus for the best model, as each type has benefits and drawbacks.

Implanted tumors tend to have consistent growth in the implanted location, but their quick growing nature is not representative of normal tumor development. Induced

tumors, through transgenic or transfected animals, more closely mimic the tumor development but can take long time periods for the tumor to develop, and may grow in random areas. Naturally occurring brain tumors in animals most closely mimic normal tumor development as well as human GBM physiology, but only occur in non-human primates, dogs, and cats, and as such are difficult to acquire and control. Orthotopic models are when the tumor grows in its original tissue space, but for brain tumors this can limit the tumor size as well as limit ability to image the tumor. Flank tumors are easily imageable, and can grow largely, but lose the structure and environment associated with the original tissue space that these tumors would typically grow.

Xenograft models are the gold standard for patient-specific models, with the ability to grow human tumors in an immunocompromised animal, but these models can have difficulty with penetrance and successful tumor growth [158]. Furthermore, the lack of immune system necessary for implanted human cells to grow in the environment mean a significant loss of information from a key contributor of the tumor microenvironment. Syngeneic models have an intact immune system and can generate tumors efficiently, but since they are purely animal, they may not accurately translate to humans [159]. Genetically modified, or transgenic, models are typically utilized to study specific genetic manipulations, such as oncogenes and knockouts to turn on or off or control tumor growth [160, 161]. These models are advantageous since the cancer development and progression more closely resembles humans, but not only are the models labor and time-intensive to develop, the tumors can establish and grow in unpredictable locations and at un-synchronized time scales,

making large cohorts difficult [160]. Furthermore, primary analysis of animal models is via MRI and histology, which are both time consuming and can be difficult to optimize.

Although pre-clinical trials using animal models is a key component to the pathway for drugs to reach FDA approval, there is a high fail rate [162]. Animal models are particularly useful for providing whole body information such as toxicology information [163]. However, since these models are much smaller than humans and certainly have a different biology, it can be difficult to accurately translate successful studies in animals to humans. Patient-derived xenograft models utilize immunocompromised mice in order to grow the human tumors, but there is the loss of adaptive immune responses that are important for glioblastoma defenses [154]. Humanized *in vitro* models bring the benefit of cells directly derived from humans, and as such are more biologically similar to patients than murine studies.

1.5.4 Organotypic models

Brains harvested from animal models can be sectioned and cultured in an *in vitro* environment to combine the benefits of physiologically-relevant tissue microenvironment and ECM structure from *in vivo* studies with the control and visualization benefits of *in vitro* studies [164]. In glioblastoma, these models have been useful for interrogating invasion patterns [165, 166]. Since each brain can be sectioned into 100-400µm thick slices, a single animal can be used to consistently screen through multiple conditions, and thus reduce the number of animals necessary to test hypotheses. However, these experiments are time intensive, as the slices take weeks to equilibrate in specific buffer and media solutions [167].

During this time, the brain slices flatten down [164], and thus are more 2D than their original 3D beginning. Many cells within the tissue will also die during this equilibration time, particularly if the brains are from older rodents. These negatives significantly detract from the physiological relevance of these models.

1.5.5 Complex 3D models

As the understanding of cancer pathology expands, there is a growing need for more complex models to better represent and study the physiology. Several types of complex and unique 3D models have been developed, and are described below.

1.5.5.1 Organoids

As discussed previously, mouse models have played a crucial role in our understanding of tumor biology. However, the limitations of translating mouse phenomenon to human, has necessitated the development of humanized technologies. Organoids are miniature simplified 3D *in vitro* versions of organs [168]. They are typically derived from cells from the tissue of interest, embryonic stem cells, or induced pluripotent stem cells that can self-organize in 3D culture medium and ECM proteins, such as Matrigel, to renew and differentiate into a structure [169]. Organoids can be generated from mouse and human stem cells, but those developed from human cells are more capable of mimicking human organ development *in vitro* [170]. A variety of organs have been developed into organoids, including pancreas, gut, intestines, lung, and kidney, and have also been adapted to study as preclinical cancer model [171].

In 2013, Lancaster et al. developed a method to grow “mini-brains”, a human pluripotent stem-cell derived 3D organoid culture with discrete and independent brain regions [170]. These mini-brains were able to mimic specific and fundamental human cortical development features such as neuronal development, progenitor zone organization and outer radial glial stem cells [170]. While these models have yet to be translated to glioblastoma research, the technology is new and promising, so it will only be a matter of time before researchers are publishing adaptations and findings to study brain tumors using mini brain organoids [172].

1.5.5.2 Tissue-engineered models

The complexity of the tumor microenvironment, as previously discussed, makes studying it with precise control difficult. Basic *in vitro* tissue engineered models were first developed to examine the dynamics of cells within 3D microenvironments, offering one element of tissue-level complexity. It has been shown across multiple cell and tissue types that cells respond differently when moved from traditional 2D tissue culture to 3D culture with some sort of extracellular matrix [173, 174]. Cellular exposure to chemical and physical cues in three dimensions has been linked to altered chemoresistance in tumor cells, differential changes to migration and invasion of normal and malignant cell types, altered cytokine expression, differentiation changes, and viability[175–177]. Tissue engineering provides a simplified platform for incorporating multiple cell types to study complex mechanisms. This platform has recently been applied to cancer research to study the complex tumor microenvironment, or tissue surrounding the cancer. Recent studies indicate the tumor microenvironment is

important in promoting treatment resistance by increasing apoptosis resistance, proliferation, and invasion as well as reducing drug transport to tumor cells [26, 27]. Tissue-engineered models can be an effective platform for simply incorporating multiple microenvironmental components to more accurately represent complex tumors and study therapeutic response of tumor cells (**Figure 1.2C**).

A wide variety of 3D culture scaffolds ranging from natural biomaterials such as various collagen types, hyaluronan mixtures, alginate, and synthetic biomaterials, such as poly-ethylene-glycol (PEG) and poly-lactic acid, have been developed to study GBM cell behavior in 3-dimensions [178–184]. While these studies have been instrumental in furthering the understanding of glioblastoma cell behaviors, a number of factors limit the true relevance of these studies. Many of these studies utilize the traditional 2D culture cell lines U87, U251, U373, etc. which are not the best representation of the heterogenous nature of cells in GBM tumors. While some of these models have utilized advanced biomaterial technologies, to create gradients of stiffness or complex networks [178, 185], the majority of these models are collagen-based, which is not physiologically relevant to the native brain tissue as there is no collagen present. Models using hyaluronan as the primary ECM component, like what is found in the brain, as well as glioblastoma stem cells derived from patients would make a more realistic 3D *in vitro* model of glioblastoma.

Use of tissue-engineered models has also allowed replacement of animal models and have offered not only the advantages of reduced animal use, but also many other benefits [186]. These include the ability to use human cells and patient-derived primary cells, instead

of murine cells and traditional cell lines long grown in culture, to more accurately represent human tissue without confounding species interactions[187]. Furthermore, inclusion of patient-derived primary cells technologically paves the way toward personalized medicine with the ability to incorporate patient cells into tissues recreated outside the patient body [188]. This leads to innovative drug screening platforms that can hopefully identify therapeutic regimens that can be truly successful for patients since they are identified using the patient's own cells.

1.5.5.3 Microfluidic models

In the past decade, microfluidic models composed of small channels have emerged as a platform for studying the cellular, biochemical, and physical microenvironment. Microfluidic devices utilize small channels and chambers with cross-sectional areas smaller than 1mm to manipulate liquids and particles at very small volumes, and allow for precise control of flow, thus establishing complex physical or chemical gradients [189, 190]. While 2D cells can certainly be used with microfluidic devices, combining tissue-engineered models with microfluidic devices creates a precisely tuned *in vitro* model for studying tumor biology and phenomenon with human cells in a physiologically-relevant manner [182]. The highly heterogenous and dynamic nature of the tumor microenvironment lends itself well to the development of microfluidic platforms to closely control and study phenomenon. Microfluidic models have been particularly useful for studying angiogenesis and chemotaxis [183, 191]. However, these models are often limited to the lab in which they were developed due to the complexity and nuance of dealing with these types of specialized systems.

1.5.6 Precision Medicine

Precision medicine is gaining speed in development and clinical use. The use of screening technologies to assess therapeutic responses or predict outcomes in patient samples is important to developing new therapies and using appropriate and effective therapies in the clinic[25]. The ability to assess the response of a patient is crucial to increasing survival in diseases including fibrosis, cancer, and heart disease [192–194]. As discussed previously, re-creation of tissues outside the patient body using tissue engineering methods offers the ability to potentially examine a patient's own tissues in a controlled setting [143, 195]. Several research groups are aiming to utilize the principles and techniques from tissue engineering to build clinically accurate *ex vivo* models of tumors [196]. These systems combine the benefits of mimicking tissue-level structures and interactions with the ease and manipulability of higher throughput screening platforms. Tissue-engineered models of a patient's tumor, in particular, create a platform for systematically testing various therapeutic regimens, without subjecting the patient to the pain and side effects of these drugs. Aside from personalized screening applications, precisely engineered *ex vivo* models of tumors can also be used to test important scientific hypotheses related to disease related to the complex interactions that arise in a complete tissue and thus offer opportunities for drug discovery and development [78, 197].

1.6 Motivation and conclusion

With evidence in many other cancers demonstrating the tumor microenvironment is important in promoting tumor growth and treatment resistance, it is clear the unknown paradigms of the glioblastoma tumor microenvironment must be explored. Understanding this complexity will be essential to discovery and development of successful therapeutic strategies to increase patient survival. Not only is it important to study glioblastoma patient pathology to determine the role of the microenvironment in contributing to this highly malignant cancer, there is a need for robust models of the glioblastoma tumor microenvironment that accurately mimic the biology of the human glioblastoma tumor in order to elucidate the complex interactions. Therefore, in this dissertation, we will demonstrate the design and development of a human 3D *in vitro* model of the glioblastoma tumor microenvironment, composed of patient-derived glioblastoma stem cells with human astrocytes and microglia in a hyaluronan-based matrix, built from quantitative analyses of patient tumor resections that demonstrated the cellular microenvironment composition is predictive of patient survival. This *in vitro* model will examine not only cell death, but also cell proliferation, stemness, and invasion to provide more information on the malignancy of glioblastoma across multiple outcome measures. We will utilize the model to examine how the cellular microenvironment affects different patients, and further demonstrate this model as a platform to study intercellular microenvironment signaling and to assess multiparametric *in vitro* therapeutic response to standard of care treatment, as well as with a panel of clinically-relevant chemotherapeutics.

Chapter 2: Quantitative analysis of the glioblastoma cellular microenvironment to develop predictive statistical models of overall survival

This work was done in conjunction with Fahad Bafakih, M.D. and James Mandell, M.D., Ph.D., who acquired and identified pathological features of patient glioblastoma tumor resections, and Bethany Horton, Ph.D., who developed the statistical models. It was previously published in the *Journal of Neuropathology and Experimental Neurology* in November 2016.

Citation:

Yuan JX, Bafakih FF, Mandell JW, Horton BJ, Munson JM. Quantitative analysis of the cellular microenvironment of glioblastoma to develop predictive statistical models of overall survival. *Journal of Neuropathology & Experimental Neurology.* 2016 Nov 2:nlw090.

2.1 Summary

Glioblastoma, the most common and deadly primary brain tumor, possesses a unique tissue microenvironment compared to other cancers. Though experimental research has shown contributions of non-neoplastic cells to glioblastoma progression, very few quantitative

studies have shown the effect of tumor microenvironmental influences on patient survival. Here we examine the contribution of the cellular microenvironment, including astrocytes, microglia, oligodendrocytes, and blood vessels, to survival in glioblastoma patients. Using histological staining and quantitative image analysis to examine the tumor-associated parenchyma of 33 patients, we developed statistical models to predict patient outcomes based on the complete cellular picture of the tumor parenchyma, showing that blood vessel density predicts poorer prognosis. We further examined unique patient profiles of the cellular microenvironment showing prediction of poorer or better survival based on higher staining for certain glial cells. To examine the role of adjacent parenchymal versus higher tumor cell density bulk parenchymal tissue, we specifically examined the glial components in these regions, which showed high variability within and between patients. Comparison of bulk and adjacent astrocytes and microglia in tissue yielded the strongest prediction of survival, with high levels of adjacent astrocytes predicting poor prognosis and high levels of microglia showing better prognosis. These results indicate the parenchymal make-up of patient tumors predicts survival in glioblastoma and particularly, the balance between reactive glial populations is important for patient prognosis.

2.2 Introduction

Glioblastoma (GBM) claims 12-14,000 lives annually in the United States alone [198]. Standard of care treatment includes immediate surgical resection post-diagnosis, followed by multiple rounds of radiation therapy and temozolomide (TMZ) chemotherapy for all GBM

patients. In spite of this aggressive treatment approach, median survival is less than 16 months after diagnosis [198]. The poor prognosis of GBM has been partially attributed to its ability to invade into the surrounding brain parenchyma, thus making it a "moving target" and difficult to access with treatment approaches [199]. This invasive edge is often missed by bulk targeted treatment such as surgical resection and radiation therapy. In previous work, there has been a benefit to inhibiting invasion of glioma cells in therapeutic outcomes [200]. However, the mechanisms underlying glioma invasion are still unclear with multiple explanations including extracellular matrix heterogeneity [61], vascular and neuronal architecture [201], and interactions with the cellular and cytokine microenvironment [202] being experimentally demonstrated and clinically observed. Nonetheless, the invasion of cancer cells into surrounding brain parenchyma is a hallmark of GBM, and thus a better understanding of this parenchyma with which cancer cells interact is important to disease recurrence and progression in patients.

In GBM, several prognostic indicators have shown success in predicting patient survival and treatment outcomes [203]. There is strong negative correlation between increasing age and postoperative survival in GBM patients [204]. Patients with methylation of the methyl-guanine-O-methyl transferase (MGMT) promoter have been shown to respond more favorably to TMZ [15]. Patients with Isocitrate Dehydrogenase (IDH)1/2 mutation show double the median overall survival compared wild type IDH1 [124, 203, 205, 206]. Overexpression of epidermal growth factor receptor (EGFR) vIII, the mutant form of EGFR, in the presence of EGFR amplification results in shorter overall survival [207]. Many of these

prognostic indicators have led to therapeutic development and changes in treatment regimens, however, survival is still poor with these strategies indicating a need for new targets and therapies [208, 209].

Recent evidence in multiple cancers suggests the tumor microenvironment, or tissue surrounding the cancer, is important to the progression of cancer [26, 210]. Tumors have diverse microenvironments with distinct stromal cell populations that contribute to tumor growth and invasion [211]. The tumor stroma, which can account for over 80% of the tumor bulk, is composed of non-malignant cells and connective tissues, such as blood and lymphatic vessels, extracellular matrix, fibroblasts, and inflammatory cells [212]. Many clinical studies have focused on two major components of the tumor stroma: macrophages and fibroblasts, as the primary support cells of cancer progression. In breast cancer, both tumor-associated macrophages and cancer-associated fibroblasts have been correlated with poor prognosis [63, 213–216]. Though individually many of these elements have been identified in patient populations, no study has yet examined multiple microenvironmental elements simultaneously as they relate to patient outcomes.

Due to the unique microenvironment of the brain, the associated "stroma" contains cell types distinct from non-central nervous system cancers, including oligodendrocytes, microglia, and astrocytes, in addition to blood vessels and macrophages [217]. RNA-sequencing and histological analysis of biopsies from various areas in a GBM tumor have revealed different cellular and molecular compositions in the tumor bulk than in the margins [218]. Though we know this, there have been few studies to quantitatively describe the

parenchymal cellular microenvironment of GBM and relate it to patient outcomes in a comprehensive fashion. Links between patient survival and microenvironmental components of GBM have found that features such as hypoxia, vascularization, cytokines, and immune infiltrates are associated with prognosis [54, 219–221]. Blood vessel density has been correlated with better progression-free and overall survival in patients treated with anti-angiogenic therapies [54, 221]. Increased numbers of microglia/macrophages are found in higher grade versus lower grade gliomas, indicating a positive correlation between microglia concentrations and glioma grade [222]. Experimentally, glial cells, including astrocytes and microglia, have been shown to play a promoting role in glioma progression and invasion [37, 42, 45]. Though individual components of the tumor microenvironment in glioma and other cancers have been studied, there has not been a comprehensive analysis to examine the overall cellular microenvironment, nor an effort to use it predictively of survival, in any cancer.

Based on the preclinical and histopathological evidence that multiple parenchymal cells may contribute to glioma progression, coupled with evidence in other cancers that the stroma plays a role in prognosis, we aimed to more thoroughly and quantitatively examine the cellular components of the glioblastoma microenvironment in patient samples. GBM being inherently infiltrative in nature, we examined not only the entire sample but also specific higher cancer cell density “bulk” and higher parenchymal cell density “adjacent” regions. Then, to test the hypothesis that a holistic view of the tumor microenvironment

may predict patient outcomes, we built several predictive statistical models based on our patient data.

2.3 Materials and Methods

2.3.1 Patient identification

Patient samples were accessed through the University of Virginia Biorepository and Tissue Research Facility. Patient samples were selected by a neuropathologist (JWM) based on a definitive diagnosis of glioblastoma (astrocytoma, WHO grade IV) who had completed tumor resections at the University of Virginia between 2010 and 2013. Samples were de-identified and processed to identify tumors that included a portion of adjacent higher ratio of parenchyma with infiltrating GBM cells (referred to as adjacent tissue). In total, 33 patient samples were identified to be used in our sample from an initial sample size of 68. Descriptive statistics and survival information by traditional prognostic indicators four the patient cohort are included in Table 2.1.

Table 2.1: Descriptive statistics of the patient population used in analysis

Total	N = 33
Sex	54% male
Median age at diagnosis	62.5 years
Median survival	11 months
MGMT hypermethylation	29%
IDH1 positive	9%
Region of tumor	19% Frontal
	52% Temporal
	14% Parietal
	14% Occipital

2.3.2 Immunohistochemistry

Formalin fixed paraffin embedded 8µm sections were deparaffinized with xylene and rehydrated in graded ethanols. Antigen retrieval was performed using high pH antigen unmaking solution (Vector Labs) using microwave heating. After washing twice with permeabilization solution (TBS + 0.01% Triton-X), samples were incubated at room temperature with blocking solution (2.5% horse serum + permeabilization solution). Samples incubated overnight in 4°C with primary antibodies diluted in blocking solution. Detailed information on antibodies used are included in Table 2.2. Antibodies were used at dilutions recommended by the manufacturer (Mfr.), found in previously published literature or tested further and shown in Figure 2.1.

Table 2.2: Antibodies used for immunohistochemical staining with concentrations

Antibody (anti-)	Mfr	Cat#	Host	Concen-tration (µg/mL)	Target	Sensitivity
ALDH1L1	Abcam	ab56777	Mouse	1.05	Astrocytes	Fig. 2.1
ALDH1A1	Abcam	ab23375	Rabbit	5.0	Astrocytes	[223]
Iba1	Abcam	ab5076	Goat	$2.5x10^3$	Microglia	[224]
Oligodendrocyte Specific Protein1	Abcam	ab53041	Rabbit	2.0	Oligoden-drocytes	Mfr's rec
CD31	Abcam	ab28364	Rabbit	5.0	Blood vessels	[225]
Podoplanin	R&D	AF3670	Sheep	1.0	Neoplastic cells	
GFAP	Abcam	Ab7260	Rabbit		Activated astrocytes	

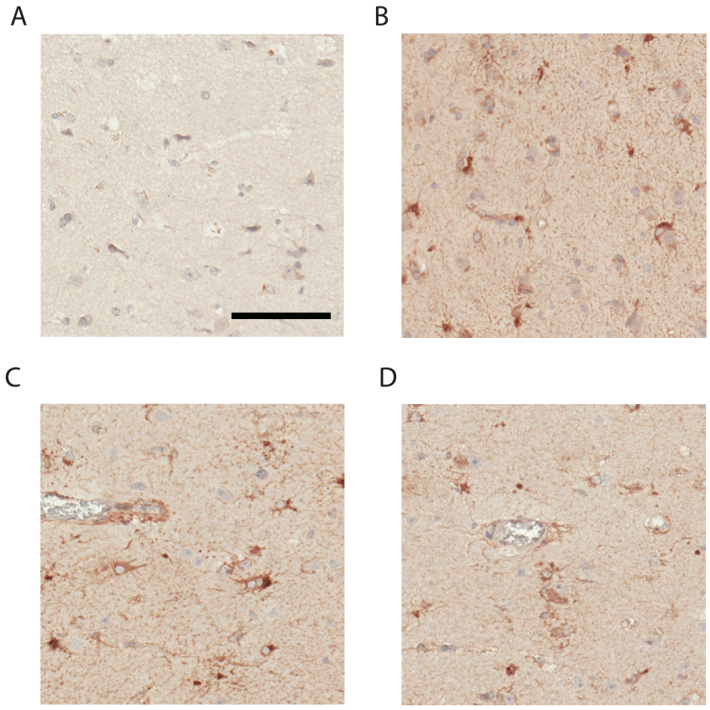

Figure 2.1: Dilutions of anti-ALDH1L1 for immunohistochemical identification of astrocytes. A) Negative control, B) 1:70 dilution from stock, C) 1:200 dilution from

stock, and D) 1:400 dilution from stock. 1:200 dilution was used for staining and analysis due to optimal positive staining of cell body and processes with minimizing background. Scale bar=100μm.

Detection of each primary antibody was carried out with the appropriate universal (rabbit/mouse) or goat ImmPRESS polymer reagent (Vector Labs) according to manufacturer protocol. Samples were developed with DAB substrate (Vector Labs) and counterstained with hematoxylin (Thermo Scientific). Slides were then dehydrated with 100% ethanol and xylene, and mounted using Histochoice Mounting Media (Amresco). Hematoxylin and eosin staining was performed by the University of Virginia Biorepository and Tissue Research Facility following standard protocols.

Specificity of ALDH1L1 to non-neoplastic astrocytes was confirmed by co-immunostaining with podoplanin and GFAP with secondary fluorescence staining in tumor-bearing and non-tumor bearing patient samples (**Figure 2.2**). Further specificity was confirmed by pathologist (**Figure 2.3**). Overall, there was an average 2.6% co-immunostaining between ALDH1L1 and podoplanin in tumor-bearing samples indicating a selectivity of ALDH1L1 for non-neoplastic astrocytes. All other antibodies have proven specificity for their cell types as provided by the manufacturer or through publications [223–226].

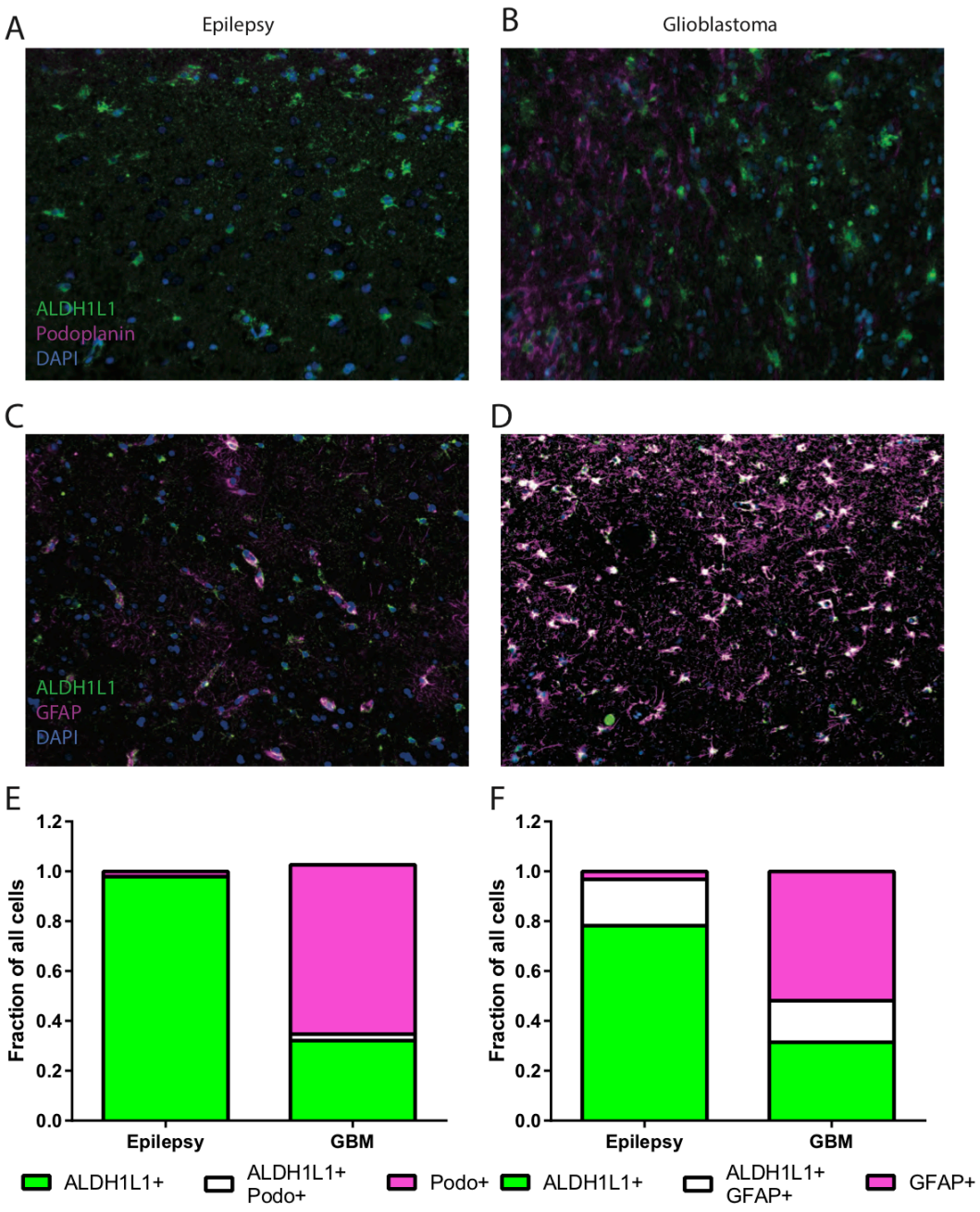

Figure 2.2: Representative images for ALDH1L1 specificity. Left side: epilepsy brain sections, Right side: glioblastoma brain sections. A and B) ALDH1L1 and podoplanin staining. C and D) ALDH1L1 and GFAP staining. E and F) Quantification of stainings indicates ALDH1L1 staining identifies non-neoplastic astrocytes. A minimum of 150 cells were counted for glioblastoma sections, and 50cells for epilepsy sections.

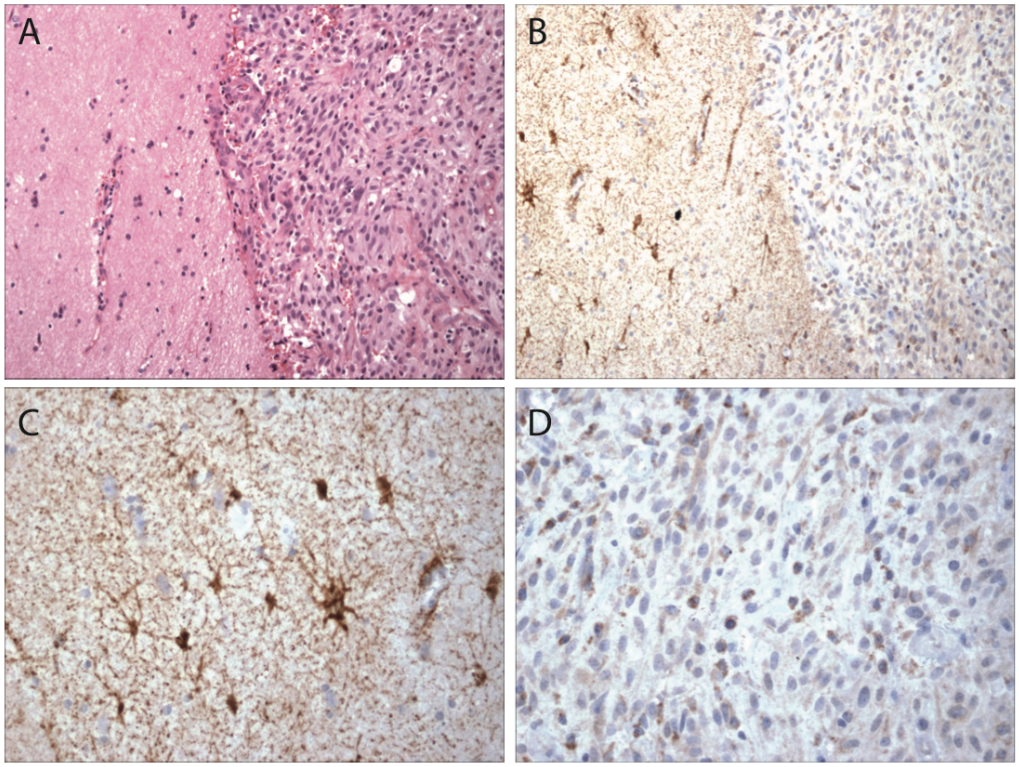

Figure 2.3: ALDH1L1 is a selective, but not specific marker of non-neoplastic reactive astrocytes in glioblastoma resection samples. A) Hematoxylin and eosin staining, and B) anti-ALDH1L1 staining in Patient 51 shows more astrocyte-like cells in adjacent areas compared with tumor bulk. Closer images in C) in adjacent area and D) tumor bulk.

2.3.3 Image analysis

Stained slides were scanned with Aperio Scanscope (Leica Biosystems) and analyzed using ImageJ (National Institutes of Health). 3-5 random non-overlapping 856x476µm (407,465µm^2) regions throughout the tumor sections were selected using Image ScanScope (Leica). Number of regions varied analyzed depended on size of whole patient resection sample. Astrocytes, identified by anti-ALDH1L1 or anti-ALDH1A1 staining, microglia, identified by anti-Iba1 staining, and oligodendrocytes, identified by anti-OSP1, were quantified for percent coverage. In ImageJ, the Threshold_Colour plugin was used to remove

purple color from hematoxylin stained nuclei, leaving brown from DAB staining. Each image was then converted to 8bit and then processed using settings from pre-loaded ImageJ threshold filters (Huang, MaxEntropy, RenyiEntropy, or Yen) so only DAB-stained portions were included in the threshold. Pre-loaded threshold filters were used for consistent threshold settings and the appropriate filter was selected based on best threshold coverage of the positive DAB stain without including background in measurement (**Figure 2.4**). The same threshold filter was used for all regions within one patient sample. Percent area for the whole was then measured based on the threshold to determine percent coverage for each stain. Percent coverage for multiple regions within each sample was averaged for one percent coverage measurement per patient. Individual blood vessels, identified by positive anti-CD31 staining, were counted across five random areas and averaged for vascular density (number per mm^2).

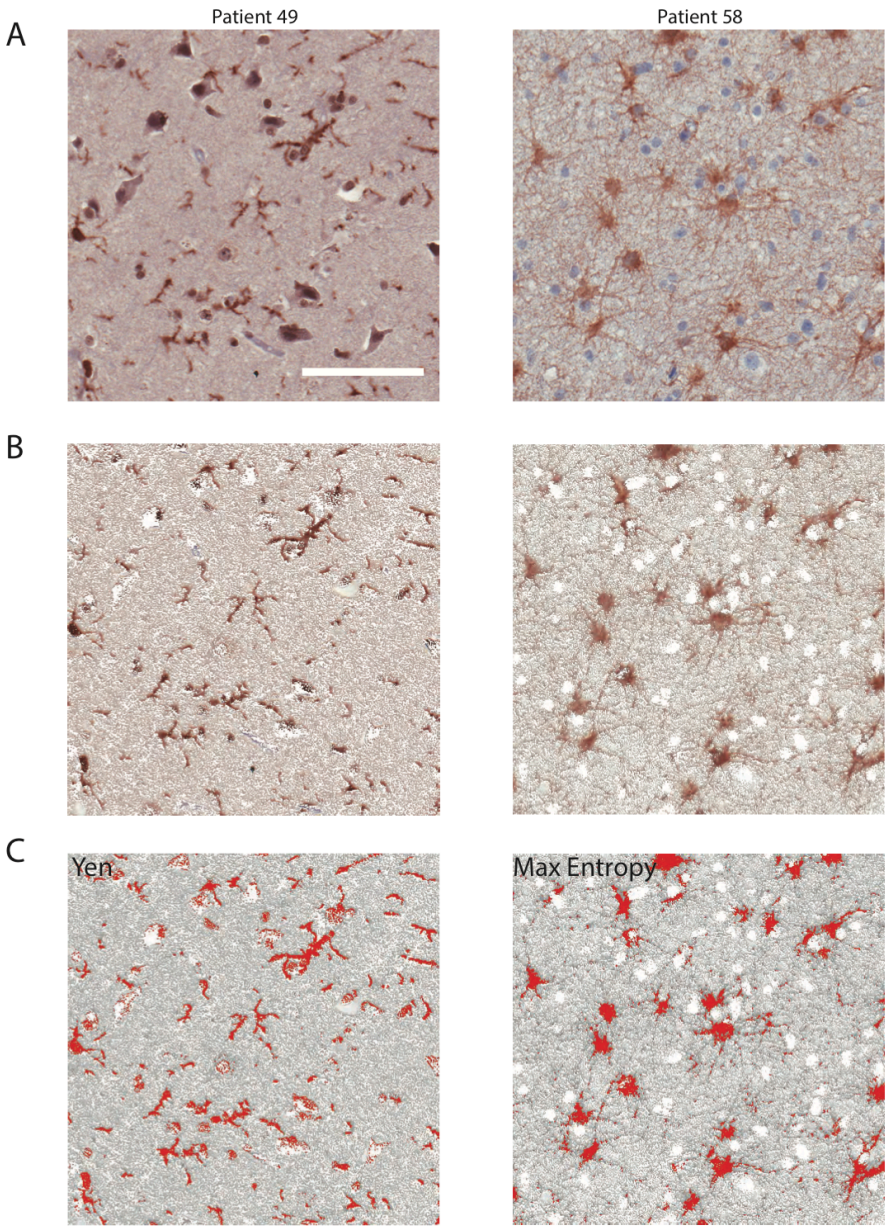

Figure 2.4: Representative images for how coverage was quantified. Left side: anti-ALDH1L1 for Patient 49, Right side: anti-Iba1 for Patient 58 A) Original image B) Color threshold to remove nuclei C) Resulting threshold with corresponding default ImageJ thresholds indicated. Scale bar = 100µm.

2.3.4 Adjacent area definition and analysis

Adjacent and bulk regions of tumor tissue samples were identified by neuropathologists (JWM and FFB) using H&E samples. Though GBM infiltrates brain tissue, there are regions of higher density GBM cells and regions of lower density infiltration into surrounding parenchyma. Adjacent regions are defined as regions where <25% of cells were neoplastic, thus primarily being composed of reactive glia and neural tissues. These regions tended to be away from the tumor bulk but did contain infiltrating tumor cells as determined from aberrant nuclei. Tumor bulk regions were defined as regions with >50% of cells as neoplastic and contained densely packed cells compared to surrounding tissues. Only samples that contained both adjacent and bulk regions were used for our analyses and comprised the 33 patient samples used here. 2-3 non-overlapping 856x476μm (407,465μm^2) regions within the adjacent areas were selected using Image ScanScope (Leica) depending on the size of this region. Image analysis in the adjacent area was performed as described above.

2.3.5 Statistical analyses for basic parameters

Correlations between cellular components were fit with a straight line and analyzed for good of fit, or R. Differences between slopes and y-intercepts were tested for significance. Frequency distribution histograms were generated and fit with a Gaussian curve distribution. Group comparisons were conducted using paired t-tests. Survival curve comparisons were conducted using Log-Rank (Mantel-Cox) test and Log-Rank hazard ratios are given as HR=A/B (95% Confidence Interval). Analysis of variability of measurements within each individual was conducted by calculating the standard deviation of all

representative images from a single patient. Graphs and analyses were completed with GraphPad Prism software.

2.3.6 Development of survival prediction model

A proportional hazards model was used to model overall survival. Additional tests were performed to ensure appropriateness of the proportional hazards assumption. Survival modeling and testing the proportional hazards assumption were performed using the "phreg" procedure in SAS (version 9.4).

2.4 Results

2.4.1 Description of the patient cohort

We examined the overall survival of our cohort of 33 patients in relation to traditional prognostic indicators (**Table 2.3**). In our total cohort, we saw a median overall survival of 11 months. Within this cohort, patients with MGMT hypermethylation had a median overall survival of 18 months, compared to 11 months for those without MGMT hypermethylation ($p<0.05$). Our cohort had only two patients with IDH1 mutation with a median overall survival of 11 months. Patients with tumor in the parietal lobe had a median overall survival of 6 months, frontal 11.5 months, temporal 11 months, and occipital 10 months. As has been seen in other studies, age was negatively correlated with survival time. In our cohort, patients under the age of 50 years had a median overall survival of 13 months, while over 50 years had a median overall survival of 8 months.

Table 2.3: Description of patient cohort survival

	Median survival	# of patients	HR(95% CI)	p-value
IDH1+	11 months	2	1.143 (0.2589, 5.311)	ns
IDH1-	11months	31		
MGMT hypermethylated	18months	6	0.5444 (0.2570, 1.021)	*0.0399
MGMT non-hypermethylated	10months	27		
Age (under 50yrs)	13months	7	0.8787 (0.4172, 1.751)	ns
Age (over 50yrs)	8months	26		
Parietal lobe	6months	5		ns
Frontal lobe	11.5months	4		
Temporal lobe	11months	9		
Occipital lobe	10months	4		

2.4.2 Cellular components vary by patient

We used four antibodies to examine the cellular microenvironment of glioblastoma samples (**Table 2.2**): CD31 for blood vessels, OSP-1 for oligodendrocytes, ALDH1L1/A1 for non-neoplastic astrocytes (Supplemental Figure 3), and Iba-1 for microglia/macrophages. Comparing across patients, at multiple locations throughout the sample, we saw a range in the percentage of area coverage between patient samples for each cell type (**Figure 2.5**).

For example, when looking at just two of our patients, Patient 58 had higher percentage of area coverage for ALDH1L1 and Iba1 (**Figure 2.5A, B**), lower percentage of area coverage for OSP1 (**Figure 2.5C**), and higher number of blood vessels/mm^2 (**Figure 2.5D**) than Patient 63. There is patient-to-patient heterogeneity for astrocyte, microglia, and oligodendrocyte coverage, as well as blood vessel density (**Figure 2.5E**). Distribution of blood vessel density for each patient fit a normal distribution best (R=0.912) while patient survival did not (R=0.178) (**Figure 2.6** histograms).

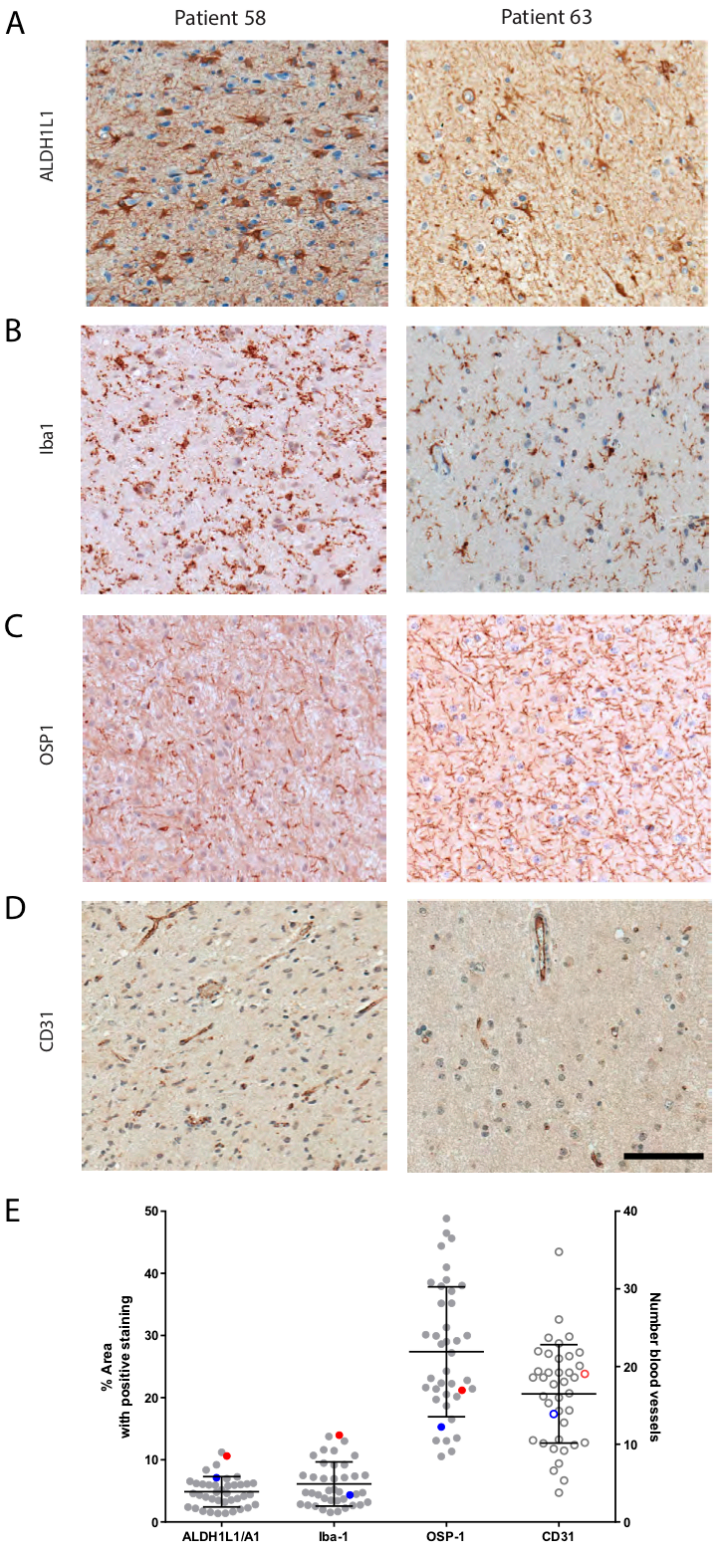

Figure 2.5: Representative images for immunohistochemical staining for cellular components across tumors in two patients. A) ALDH1L1 identification of astrocytes

(brown). B) Iba-1 identification of microglia. C) Oligodendrocyte Specific Protein-1 (OSP-1) identification of oligodendrocytes and processes. D) CD31identification of blood vessels. E) Quantification of components was conducted to determine the percent of tissue area occupied by positive staining for ALDH1L1/A1+ astrocytes, Iba-1+ microglia, and OSP-1+ oligodendrocytes (left axis). CD31+ vessels were quantified as number per tissue area (right axis). Patient 58 indicated in red, Patient 63 in blue. n=33. Scale bar=100µm.

2.4.3 Astrocytes and blood vessel density correlate, but not with survival in our sample

Since we saw a high degree of variability among the cellular components, we were interested to understand how the different components related to each other across the cohort and how these elements related to overall survival time. We compared our quantified measurements of area percentage for each cellular component to each other and identified some interesting relationships. The negative correlation between ALDH1L1/A1 percent area coverage and blood vessel (CD31+) density was found to be statistically significant ($p<0.05$). All other correlations between cellular components were not found statistically significant. Furthermore, when we correlated patient survival to each individual component, we did not find a significant correlation (**Figure 2.6A**).

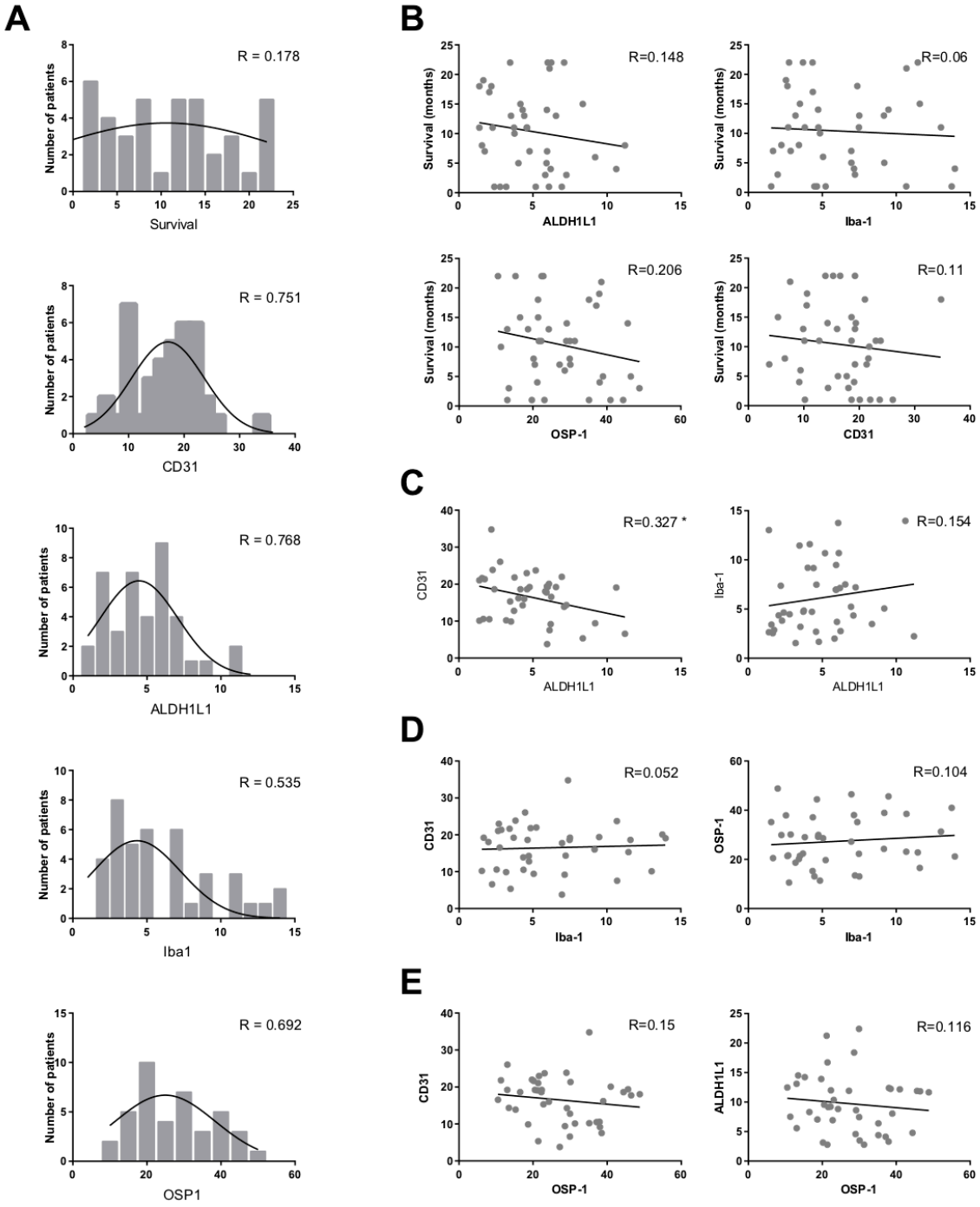

Figure 2.6: Correlations between and distributions of cellular components across patients. A) Individual components correlated with survival (in months) from diagnosis. B) Correlations and distribution of astrocyte area coverage as assessed by ALDH1L1/A1. C) Microglia (Iba-1) correlations with other components. D) Oligodendrocyte (OSP-1) correlations with all components. E) CD31+ vessel density correlated with cellular

components. Correlation of vessels with ALDH1L1/A1 staining ($p<0.05$). All r values are displayed and are significantly different from 0 where indicated. *$p<0.05$.

2.4.4 When we develop a predictive statistical model from the cellular components combined, blood vessel density is predictive of survival

In order to determine if the components together may be useful in predicting patient outcomes, we created a proportional hazards model based on our dataset. Blood vessel density and astrocyte, microglia, and oligodendrocyte area coverage were considered in modeling overall survival. Models considered include univariate survival models for each component and a model with the four components, of which the latter was the most promising. These components were not statistically significant in the univariate models but blood vessel density was statistically significant when modeling in the presence of the other components. No adjustment was made for considering multiple models due to the exploratory nature of this research. In this model, only blood vessel density was statistically significant, where one unit increase in blood vessel density was associated with 0.6% increase in hazard. Figure 2.7A shows the predicted survival curves in four patient profiles for this model. Although blood vessel density is statistically significant in the survival model, its impact on hazard is minimal (**Figure 2.7A**, **Table 2.4**).

We then created a predictive model for five phenotypes of patients based on interesting observations from our patient cohort concerning patterns for blood vessels, oligodendrocytes, astrocytes, and microglia as compared to the average case (**Figure 2.7B**). These phenotypes were selected when at least two patients in our cohort exhibited this

phenotype. The different components were set as high (being above the 75th percentile) or low (25th percentile). Figure 2.7B shows the predicted survival curves of these five hypothetical patients. We found Patient Profile 4 (low blood vessels, high oligodendrocytes, low astrocytes, high microglia) predicted the best overall survival while Patient Profile 3 (high blood vessels, high oligodendrocytes, high astrocytes, low microglia) predicted the worst overall survival (**Figure 2.7B**, **Table 2.4**).

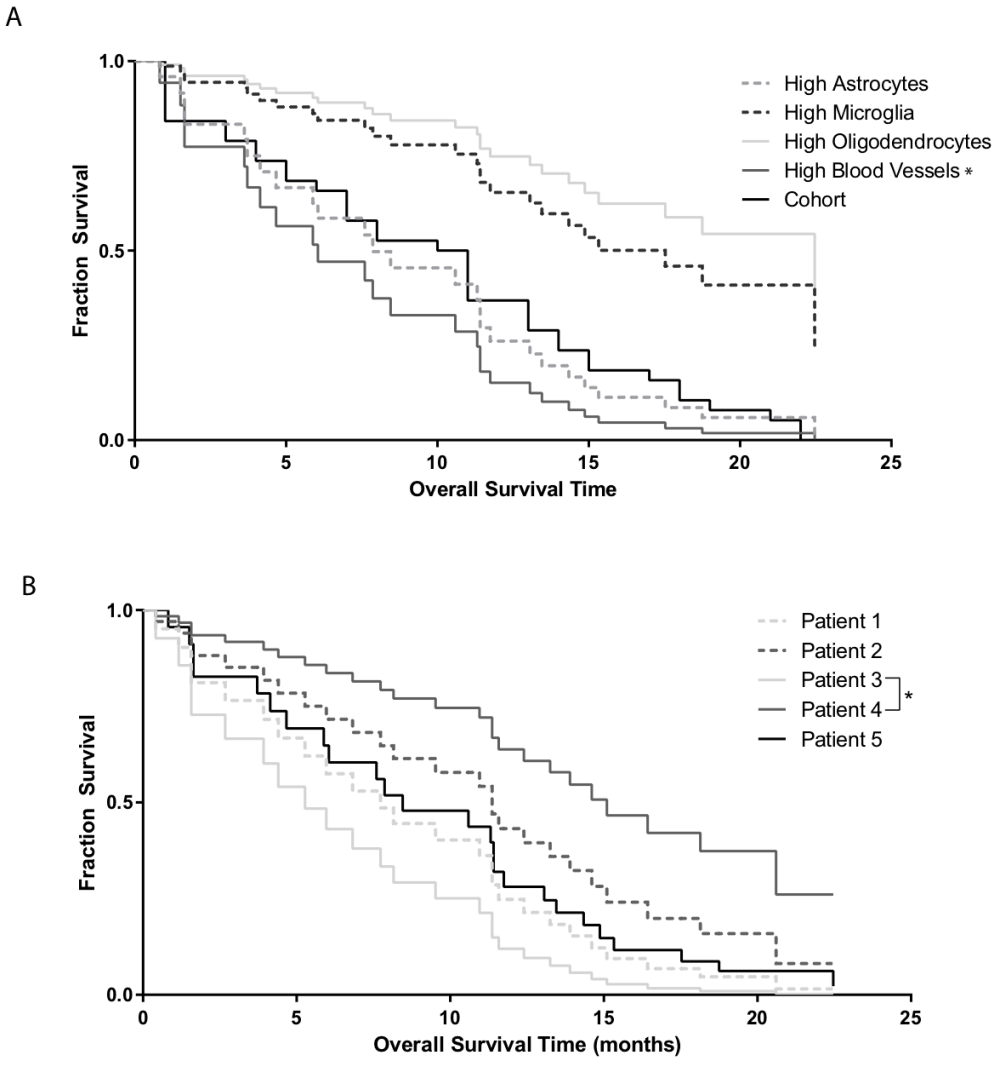

Figure 2.7: A predictive model incorporating cellular components was developed to study contributions of microenvironmental components to survival. A) Kaplan-

Meier plots of predicted survival times based on high levels of individual cellular components in the tumor microenvironment based on a model incorporating all components simultaneously. Blood vessel density yielded a statistically significant ($p<0.05$) yet small increase in hazard to overall survival time. B) Kaplan-Meier plots of predicted survival times for hypothetical patients created based on patterns within our cohort. Patient profile 4 has the best overall survival while Patient 3 has the worst ($p=0.0403$). The following pattern was tested for blood vessels, oligodendrocytes, astrocyte, and microglia to represent each patient: 1-high, high, low, low. 2-high, low, high, high. 3- high, high, high, low. 4-high, low, high, low.

Table 2.4: Hazard ratios from proportional hazards model incorporating combined cellular components

	Minimum	Maximum	HR (95% CI)*	p-value
Blood vessel density	48.0	355.5	1.43 (1.01, 2.01)	0.043
Astrocyte area coverage	1.4	11.2	1.27 (0.87, 1.85)	0.209
Microglia area coverage	1.5	14.0	0.84 (0.61, 1.15)	0.264
Oligodendrocyte area coverage	11.4	48.8	1.28 (0.93,1.76)	0.126

*Hazard ratio for a 20% increase of the total range of the variable of interest

2.4.5 Single patients show great diversity in cellular coverage

We hypothesized one potential reason that individual components are not predictive of survival is the inherent diversity in cellular constituents in single patient samples in our analysis. When we examined our quantifications of the individual fields of view within single samples (**Figure 2.8**), we noticed there is diversity in the measurements of the tissue. Within each patient, we see different percent area coverage of astrocytes (**Figure 2.8A**), microglia (**Figure 2.8B**), and oligodendrocytes (**Figure 2.8C**), and blood vessel density (**Figure 2.8D**) within the regions indicating intratumoral heterogeneity.

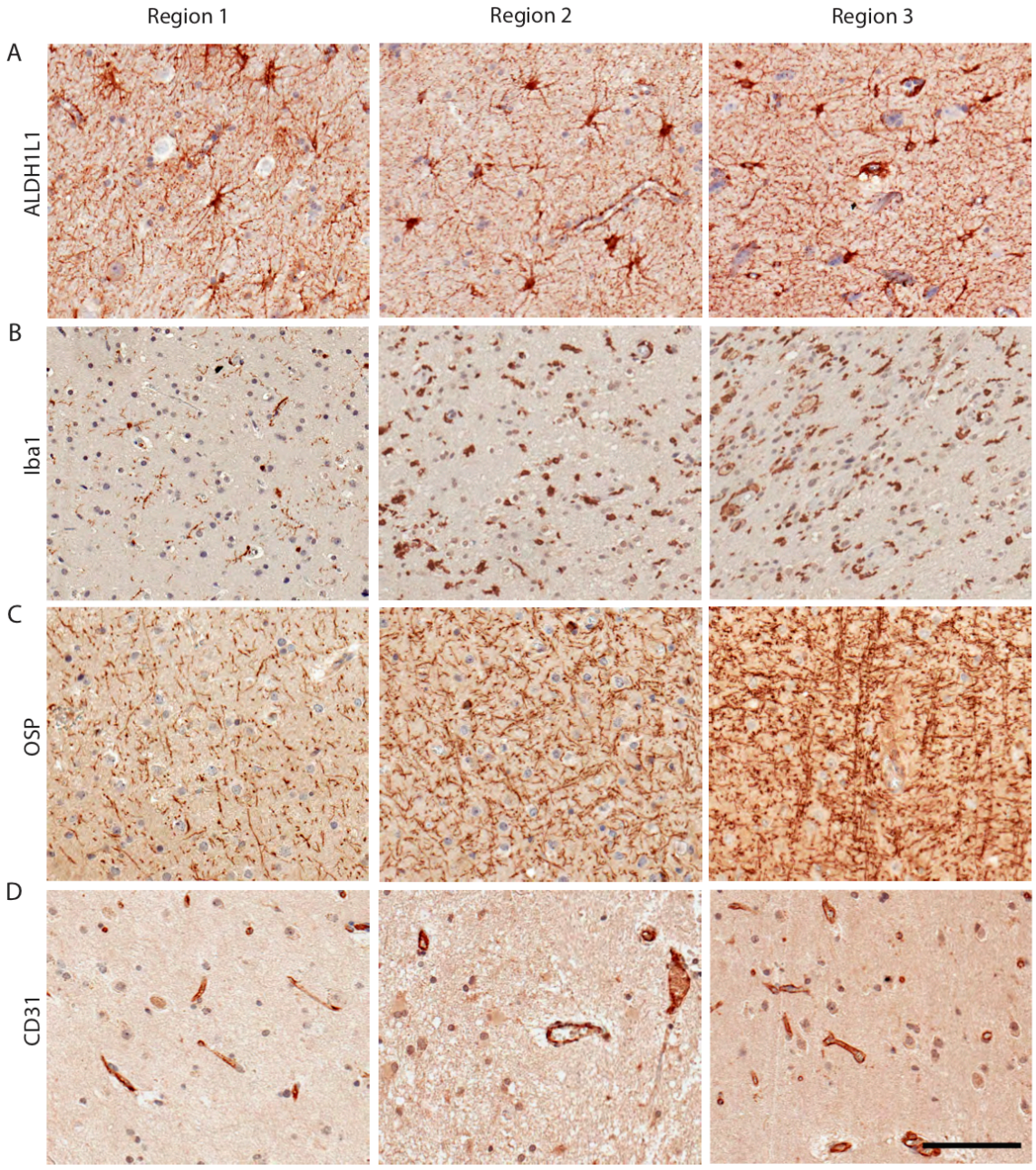

Figure 2.8: **Quantified regions within single patients show diversity of cellular density and morphology** A) ALDH1L1+ astrocytes B) Iba-1+ microglia C) OSP-1+ oligodendrocytes and processes, D) CD31+ blood vessels across three different regions of parenchymal tissue adjacent to tumor bulk in a single patient. Scale bar= 100µm.

We analyzed our individual regional quantifications by calculating the standard deviation of each measurement across the five quantified regions per patient (**Figure 2.9A**). We determined there are a number of patients with high diversity in measurements within the same sample but in different regions. The standard deviation of measurements per patient did not correlate with survival for any metric (**Figure 2.9B**). Additionally, patients with standard deviation greater than the overall standard deviation for the entire cohort did not show significantly different hazard of death compared to patients with lower standard deviations for ALDH1L1 (χ^2=0.2046, p=0.651; HR=1.185 (0.5672, 2.477)), Iba-1 (χ^2=0.0027, p=0.959; HR=1.019 (0.4925, 2.110)), nor OSP1 (χ^2=0.1744, p=0.676; HR=1.442 (0.2584, 8.052)).

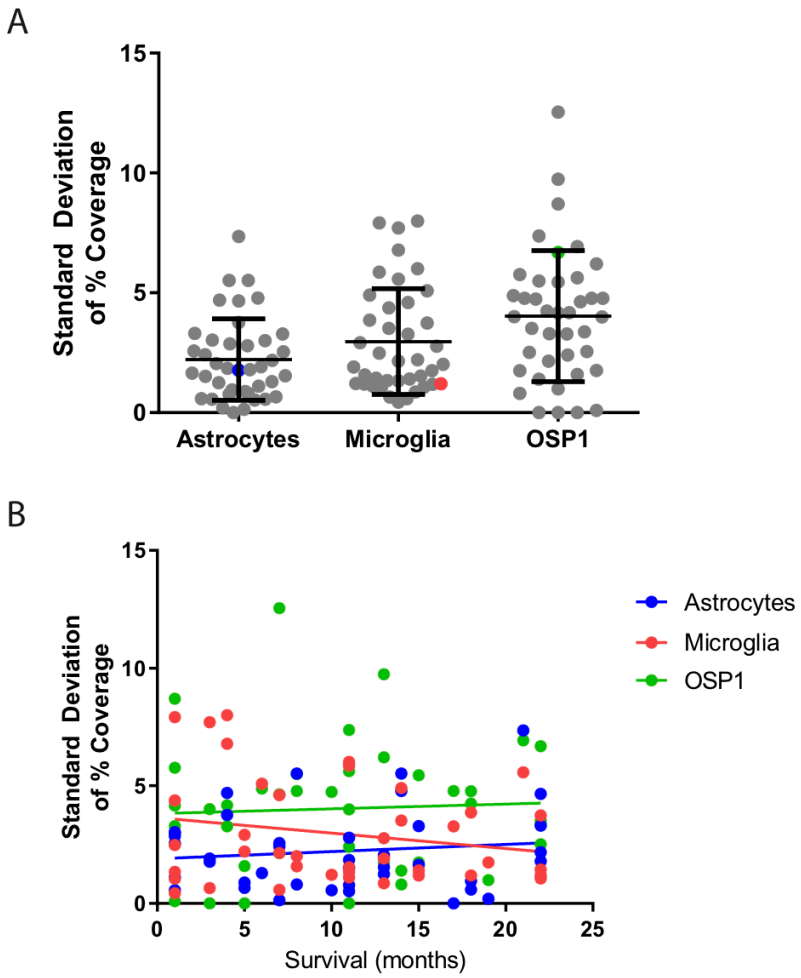

Figure 2.9: Single patients show diversity in cellular coverage. A) Standard deviation of each measurement across the five quantified regions per patient. Colored dots represent patients shown in Figure 3.4. B) Standard deviation of measurements per patient did not correlate with survival for any metric.

2.4.6 The adjacent tissue microenvironment differs from that in bulk tumor

We wanted to compare the separate defined regions adjacent to (higher parenchymal cell density) and within the bulk (higher tumor cell density) (**Figure 2.10A, B**). We saw differences in area coverage, of astrocytes (**Figure 2.10C**), microglia (**Figure 2.10D**), oligodendrocytes (**Figure 2.10E**), and blood vessel density (**Figure 2.10F**) in the tumor

bulk as compared to the adjacent areas. We focused our analysis on astrocytes and microglia because of previous literature indicating their importance in glioma progression. We found a lower percent area coverage for astrocytes and microglia in the adjacent regions than in the tumor bulk and there is larger range in measures within the tumor bulk across patients (**Figure 2.11A**). Percent area coverage for both microglia (**Figure 2.11B**) and astrocytes (**Figure 2.11C**) were positively correlated between the adjacent and bulk areas. We see the ratio of percent area coverage of adjacent regions to tumor bulk is more widespread for astrocytes than microglia (**Figure 2.11D**). All correlations were found to be statistically significant.

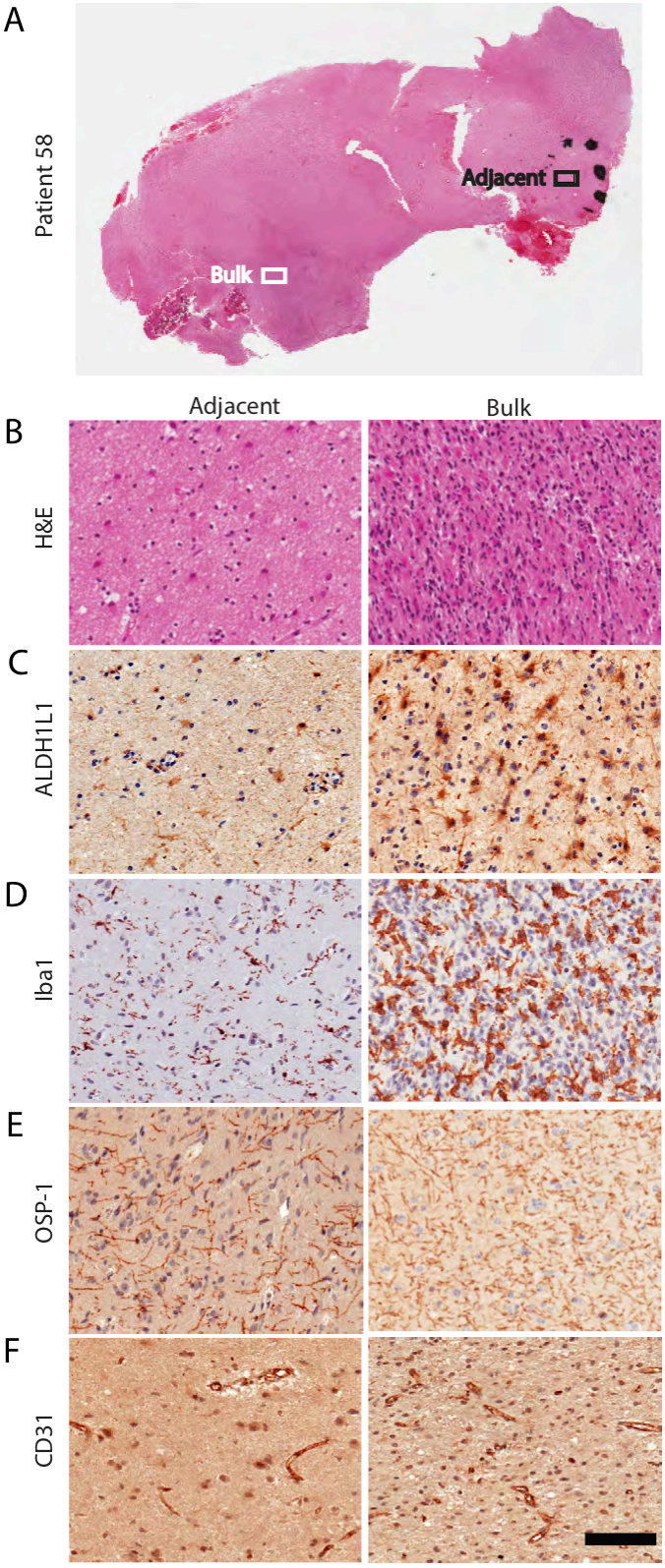

Figure 2.10: **Comparison of bulk and adjacent regions reveals contrasting infiltration of astrocytes and microglia.** A) Whole tumor sample from Patient 58 with

adjacent (black) and bulk (white) areas indicated. B) Hematoxylin and eosin staining. C) ALDH1L1+ cells D) Iba-1+ cells, E) OSP-1+ staining, and F) CD31+ blood vessels in adjacent and bulk tissue. Scale bar= 100µm.

2.4.7 The contrast between the tumor bulk and adjacent tissue is predictive of survival

When considering astrocyte and microglia area coverage, both within and adjacent to the tumor, the most significant survival model incorporated the four components: astrocyte and microglia area coverage, within and adjacent to the tumor bulk (**Figure 2.11E**). Other proportional hazards models considered in this exploratory analysis include univariate models for each of these measurements, as well as bivariate models. These components were not statistically significant in the univariate models but several components were statistically significant when modeling in the presence of the set of four components. No adjustment was made for considering multiple models due to the exploratory nature of this research. Of the four covariates in the model, astrocyte area adjacent tumor and microglia area adjacent and within tumor bulk were statistically significant in the model (p-values = 0.040, 0.026, and 0.043, respectively, **Table 2.5**). Astrocyte area adjacent to the tumor and microglia area within the tumor bulk were associated with increased hazard of death, where a 20% increase in the range of the component is associated with an increase in hazard of 81% and 41%, respectively. A 20% increase in the range of microglia area adjacent the tumor was associated with a 45% decrease in hazard (**Table 2.5**).

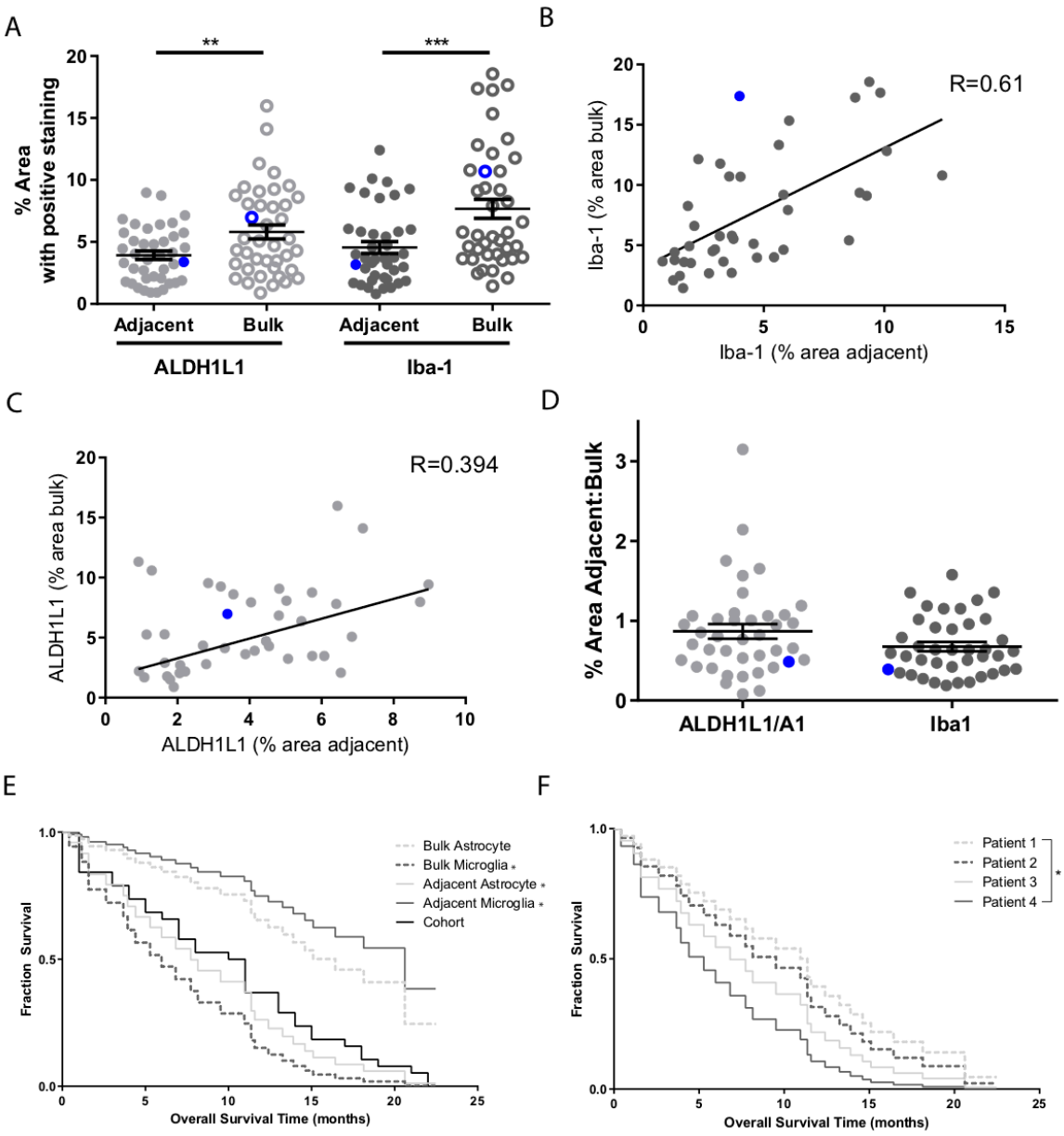

Figure 2.11: **Comparison of adjacent and bulk astrocyte and microglia populations is predictive of survival.** A) Quantified area coverages of ALDH1L1+ and Iba-1+ in adjacent and bulk tumor tissue, *p<0.05, ***p<0.001. B) Correlation between area coverage for astrocytes (ALDH1L1/A1+ cells) in bulk and adjacent regions of tissue samples, **p<0.01. C) Correlation between area coverage for microglia (Iba-1+ cells) in the bulk and adjacent regions of tissue samples, **p<0.01. D) Ratio of %positive area staining between the adjacent regions and bulk regions of tumors for each patient. Blue points indicate Patient 58 (shown in Figure 5). E) Predictive survival curves from model incorporating information about bulk and adjacent glial populations. Shown data is for high (upper quartile) populations for each of the markers, with high bulk microglia (p=0.043),

high adjacent astrocytes (p=0.040), and high adjacent microglia (p=0.026) showing significant effects on survival. F) Predictive survival curves for hypothetical patients created based on patterns within our cohort. Patient profile 1 has better overall survival while Patient 4 had worse overall survival (p=0.026). The following pattern was tested for astrocyte bulk, astrocyte adjacent, and microglia bulk, microglia adjacent to represent each patient: 1-high, high, high, high. 2-high, low, high, low. 3-low, high, high, high.4-high, high, high, low.

Table 2.5: Hazard ratios from proportional hazards model incorporating components of the sample tumor bulk and adjacent tissue

	Minimum	Maximum	HR (95% CI)*	p-value
Adjacent Astrocyte	0.9	9.0	1.81 (1.03, 3.19)	0.040
Bulk Astrocyte	1.5	16.0	0.88 (0.71, 1.08)	0.211
Adjacent Microglia	0.8	12.4	0.45 (0.22, 0.91)	0.026
Bulk Microglia	1.4	18.6	1.41 (1.01, 1.98)	0.043

*Hazard ratio for a 20% increase of the total range of the variable of interest

We then created patients with unique profiles of astrocyte and microglia coverage based on patterns observed in our patient cohort. Figure 3.6F displays the predicted survival curves in four patient profiles and our model development cohort, where all components have a value of the 25th percentile of the data except for the component that is high, given by the 75th percentile of the data. This allows us to observe the impact a high measurement is predicted to have on survival when the other components are relatively low. In this analysis, Patient Profile 1 (high astrocyte bulk, high astrocyte adjacent, high microglia bulk, high microglia adjacent) has the best predicted overall survival while Patient Profile 4 (high astrocyte bulk, high astrocyte adjacent, high microglia bulk, low microglia adjacent) had the worst predicted overall survival (**Figure 2.11F**).

2.5 Discussion

2.5.1 The role of multiple cellular components in the glioma microenvironment

Across patients, there was a range of coverage areas for the four histological stains that we used: ALDH1L1/A1, Iba1, CD31, and OSP-1. We assumed these coverage areas correlate to incidence of astrocytes, microglia/macrophages, blood vessels, and oligodendrocytes as their distinctive cellular components. When taken alone, none of the cellular components predicted survival in our cohort, but when combined together, there was a mild effect on hazard of death with high blood vessel staining. High blood vessel and blood microvessel count alone in astrocytoma has previously been correlated with poor prognosis in larger patient cohorts [227, 228]. Here we examined both intratumoral and peritumoral vasculature, but due to our sample size, we only saw an effect on hazard of death when we incorporated it with our additional microenvironmental components into our overall statistical model. Our lack of effect of blood vessels alone may be due to the smaller cohort or to our differential analysis method by analyzing not only within tumor tissue but within adjacent parenchyma, leading to increased variability.

Since patient samples have been grouped based on genomic analyses [136], stromal-specific transcriptional analyses [229], and particular histological markers [177] in other cancers, we examined how patients grouped by microenvironmental signatures could predict survival outcomes. We found combination effects of multiple high or low populations alter hazard ratios in survival predictions. This analysis indicates the potential for patient survival to be predicted based on microenvironment composition. By selecting a few “signatures” as

representative patients, we found that the difference between our "best" survivor and "worst" survivor was the increased staining for OSP1, indicative of increased oligodendrocytes, in our worse survivor. Oligodendrocytes have not been linked to changes in glioblastoma survival to date, however, they are known interactors with astrocytes and microglia in ways that contribute to reactivity. Studies suggest activated microglia can be detrimental as well as necessary for growth of oligodendrocytes while oligodendrocytes interact with microglia through multiple cytokines [230]. These changes could be indicative of an interaction of these cells with other glial populations that in total, alter survival, and may be worth further study in the preclinical setting.

2.5.2 The role of astrocytes and microglia in survival prediction

Reactive astrocytes and microglia make up a large percentage of the area of the tumor and adjacent regions of the brain, lending credence to the idea that they are involved in invasion of cancer cells into healthy parenchyma and promotion of disease. We found the percentage of the area covered by microglia or astrocyte staining was not predictive of survival unless we compared specifically these percentages in regions adjacent, or high parenchymal cell density, and in the bulk, or high tumor cell density, areas. Interestingly, higher coverage of astrocytes in adjacent tissue regions increased the hazard of death, whereas positive staining within the tumor had no effect on survival. Previous studies using the ALDH1A1 antibody to identify populations of cells within bulk tumor regions indicated a positive correlation of staining with survival, but we did not see this effect [231]. This marker has been used in other cancers to potentially identify cancer stem cell populations,

but was not found to specifically identify these cells in glioma (based on Nestin, CD133, or CD15 expression), and rather co-localized primarily with Glial Fibrillary Acidic Protein, a marker of astrocytes, and particularly activated astrocytes [231]. In our hands, we saw staining of non-neoplastic astrocytes of the antibodies and thus believe that our staining is indicative of changes to astrocytes specifically, as opposed to cancer cells, in line with the second study of this marker (**Figure 2.2, 2.3**).

Increased coverage of microglia adjacent to the tumor actually decreased the hazard of death while microglia in the tumor increased the hazard of death. Microglia have primarily been seen to increase invasion of glioma cells *in vitro*, but *in vivo*, have a much more duplicitous relationship. This may be due to the complex identification of these cells in the brain and the complex relationship of myeloid cells with glioma [232]. We noticed Iba1+ cells, which includes both microglia and macrophages, within the tumor displayed a more amoeboid phenotype consistent with reactive cells, whereas adjacent microglia displayed a more ramified phenotype indicative of a less reactive environment. Interestingly, the adjacent microglia/macrophages were detrimental to survival consistent with previous studies showing intratumoral microglia/macrophages to correlate with poor prognosis [233, 234]. The role, identity, and pathological markers of specific subpopulations of microglia and macrophages is still controversial [232], and thus we chose to only look at the whole population in our sections, without differentiating. It is possible we are identifying these differential populations by examining the bulk infiltrates, which could include macrophages

due to the compromised vasculature, and microglia in the adjacent regions where macrophages would have a harder time accessing tissue [235].

Glioma cell invasion is a central reason for poor prognosis, and multiple parenchymal cell types have experimentally been shown to contribute to invasion. Specifically, astrocytes increase invasion and proliferation of glioma cells *in vitro* [45] and tumor infiltration *in vivo* [236]. We found that astrocytes adjacent to tissues increased the hazard of death, potentially indicating their role in promoting invasion away from the tumor bulk and into the brain parenchyma. Interestingly, comparing our predictive patient profiles, we saw the difference between the "best" survivor and "worst" survivor was the high levels of adjacent microglia being predictive of worse prognosis when all other cellular populations were high. This differs from our first adjacent/bulk model where high microglia adjacent was beneficial to survival when all other factors were low. Thus, there is a more complex relationship between the differential populations that is affected by the overall cellular profile of the patient. Since this difference specifically centers around microglia, this may be indicative of their complex role in glioblastoma progression in general, and their multifunctional interactions with all elements of the brain parenchyma.

2.5.3 Potential as prognostic indicators and intratumoral heterogeneity

Here we describe four potential histological markers for glioblastoma that specifically target the tumor microenvironment: ALDH1L1/A1, Iba-1, CD31, and OSP-1. The variability in these markers across and within patients indicates the need to use quantitative tools to better characterize patient samples. Intratumor heterogeneity is an emerging concept

in cancer prognosis and experimental study [237]. From our patient profiles, we found specific combinations of expression both throughout the tumor sample and when specifically comparing the adjacent and bulk tissue regions, could predict poorer or better survival. Interestingly, the differences between the worst responders and best responders in our predicted patients were usually a single change to one cellular population, as opposed to a completely different cellular profile. Thus, using multiple markers to indicate prognosis may lead to better assessment of patient outcomes and may lead to better combinatorial therapeutic targets in preclinical studies and clinical therapeutic strategies.

Chapter 3: Rational design of a 3D brain tumor model

3.1 Summary

The most common and deadly brain cancer, glioblastoma, is characterized by diffuse invasion of tumor cells from the primary bulk into the surrounding tissue, and it is these invading cancer cells that remain post-therapy to cause cancer recurrence. Many researchers focus solely on the invading cancer cells; yet, it is an emerging theme that the tumor microenvironment, or tissue surrounding the cancer, is important in promoting cancer malignancy via multiple mechanisms. The understudied glioblastoma microenvironment is uniquely complex and includes many different components: glial cells, extracellular matrix, soluble factors and biophysical forces. Because this complexity can be difficult and costly to study *in vivo*, tissue-engineered models can provide a platform for incorporating defined populations of parenchymal cells as well as extracellular matrix to more realistically recapitulate the tumor microenvironment *in vitro*. We designed and built a patient-defined 3D *in vitro* human brain tumor microenvironment model that specifically recreates the tissue left behind post-resection. This hyaluronan-based model incorporates human astrocytes and microglia with patient-derived glioma stem cells to more accurately mimic the complex and aggressive glioblastoma microenvironment.

3.2 Introduction

Glioblastoma is the most common and deadly form of brain cancer in adults, claiming 12-14,000 lives annually in the United States [3]. Standard of care treatment is immediate surgical resection, followed by multiple rounds of radiation therapy and oral temozolomide chemotherapy [238]. Despite this aggressive treatment plan, glioblastoma always recurs and patient survival after diagnosis is very low, at less than 2 years [3]. This disease is characterized by diffuse invasion of the cancer cells from the primary tumor bulk into the surrounding brain tissue, and it is these invading cancer cells that remain post-therapy, leading to inevitable cancer recurrence [5, 6]. The highly infiltrative nature of glioblastoma has been repeatedly cited as a reason for poor prognosis [6–8, 239, 240].

While the limited therapeutic access from the blood-brain barrier makes glioblastoma difficult to treat, there are also distinct support cells in the brain that can promote cancer proliferation and growth [21]. It is an emerging theme that the tumor microenvironment (TME), or tissue surround the cancer, is important in promoting treatment resistance via multiple mechanisms – enriching cancer stem cells, increasing apoptosis resistance, proliferation, and invasion, and reducing drug transport to tumor cells [26, 27]. The brain tumor microenvironment is particularly unique – the support cells here are called glial cells and are not found in other parts of the body. These glial cells include astrocytes, the most abundant cell in the brain, as well as microglia, the primary immune cell of the brain. The primary extracellular matrix component of the brain is hyaluronan, and while collagen is abundant in other tissues throughout the body, there is none in the brain.

Because the complexity of the tumor microenvironment can be difficult and costly to study *in vivo*, many researchers focus solely on the cancer cells themselves. However, the contribution of the tumor microenvironment is crucial, particularly when assessing therapeutic outcomes, to accurately understand and represent the cancer in the native human brain environment. Tissue-engineered models of cancer are gaining a lot of attention as they provide a more realistic look at the microenvironment in a higher throughput and easily tunable manner compared to animal models [241]. Tissue-engineered models can incorporate relevant parenchymal cells and extracellular matrices to more realistically mimic the complex tumor microenvironment than standard 2D cell culture [143, 195, 241]. Since contribution of the tumor microenvironment is essential to predicting therapeutic outcomes, we believe developing tissue-engineered model of the glioblastoma microenvironment that incorporates important glial cells in the native extracellular matrix can be used to screen and identify therapeutics that are more likely to succeed in the clinic.

When building 3D *in vitro* models for studying the tumor microenvironment in other cancers, current literature uses arbitrarily chosen ratios of cancer cells to parenchymal cells [242, 243]. However, these arbitrary ratios are not necessarily representative of the tissue environment seen in patients. While *in vitro* models of the tumor microenvironment in other cancers, such as breast, ovarian, and pancreatic, have begun incorporating multiple parenchymal cells, current research on the cellular glioblastoma tumor microenvironment focuses only on single glial population [32, 42, 244, 245]. Incorporating multiple glial cells, such as both astrocytes and microglia, into a tissue-engineered model will not only be more

physiologically-relevant, but also provide a platform to study the possible synergistic effects of glioblastoma from these two stromal cell types.

Furthermore, although invasion is a defining hallmark of glioblastoma, it is not the only contributor to the highly malignant nature of glioblastoma. The cells remaining post-therapy have stem-like capabilities of self-renewal, proliferation and differentiation to form new tumors [6, 246]. This highly malignant subpopulation of cancer cells are termed cancer stem cells. Cancer stem cells have the ability to self-renew and differentiate into multiple lineages, similar to traditional stem cells [247, 248]. In glioblastoma, they are referred to as glioblastoma stem cells, or GSCs. GSCs are highly resistant to therapies and have been attributed to glioblastoma growth and recurrence [99, 104, 249]. These malignant outcomes should not be overlooked when studying glioblastoma.

In this chapter, we present our design rationale for building a multicellular 3D *in vitro* model of the cellular glioblastoma microenvironment incorporating human astrocytes and microglia in addition to patient-derived glioblastoma stem cells. We designed our model based on analyses from patient samples to more realistically represent native patient physiology. The three cell populations are integrated into a hyaluronan-based matrix to mimic the primary extracellular matrix component of the brain. Furthermore, our model has been optimized to examine not just invasion, but also maintenance of stem nature and proliferation, to better understand the many factors contributing to glioblastoma growth and malignancy.

3.3 Material and methods

3.3.1 Immunohistochemistry and image analysis

Patient samples were accessed through the University of Virginia Biorepository and Tissue Research Facility. Patient samples were selected by a neuropathologist (J. Mandell, University of Virginia) based on a definitive diagnosis of glioblastoma (astrocytoma, WHO grade IV) who had completed tumor resections at the University of Virginia between 2010 and 2013. Samples were de-identified and processed to select tumor sections that included a portion of adjacent non-bulk tumor tissue (here referred to as the parenchyma interface) as identified by a neuropathologist (F. Bafakih, University of Virginia).

Formalin fixed paraffin embedded 8µm sections were deparaffinized with xylene and rehydrated in graded ethanols, antigen retrieved using high pH antigen unmasking solution (Vector Labs), and stained with anti-ALDH1L1 (Abcam) and anti-Iba1 (Abcam), followed by DAB substrate (Vector) according to manufacturer suggested protocols and counterstained with hematoxylin (Thermo Scientific). Hematoxylin and eosin staining was performed by the University of Virginia Biorepository and Tissue Research Facility following standard protocols. Areas at the tumor-parenchyma invasive front of tumor recetions were imaged using wide-field microscopy with EVOS FL Auto (Life technologies) and Aperio Scanscope (Leica Biosystems) and quantified using ImageJ (National Institutes of Health). Cell populations are reported as a percentage of total cells identified by the nuclear counterstain.

3.3.2 Cell lines and culture

Patient-derived G2, G34, and G528 human glioblastoma stem cells (GSCs) (generously provided by the Purow lab at the University of Virginia, who obtained them from Jakub Godlewski and Ichiro Nakano, who derived them while at Ohio State University) were maintained in non-treated culture flasks in Neurobasal media (Life Technologies) supplemented with 1% B27, 0.5% N2, 0.01% FGF, 0.1% EGF, 0.3% L-Glutamine, and 1% penicillin-streptomycin. Human primary cortical astrocytes were purchased from Sciencell and cultured according to manufacturer's suggested protocol. Human SV40-immortalized microglia were purchased from Applied Biological Materials, Inc and cultured in Dulbecco's Modified Eagle's Medium (DMEM; Life technologies) supplemented with 10% fetal bovine serum (FBS). All cell lines were maintained at 37°C in a humidified incubator containing 5% CO_2 and 21% O_2. Cell lines were tested annually for mycoplasma (last test date: 12/2015, negative) and all experiments were completed afterwards.

3.3.3 Cell tracker and media viability optimization

Cells were fluorescently labeled with a range of concentrations of various CellTracker dyes (Life technologies) and Vybrant dyes (Life technologies) according to manufacturer's suggested protocol and maintained in respective medias described above. Growth of labeled cells was measured after 18 hr, 48hr, and 72 hr with the Cell Counting Kit-8 (CCK-8) cell proliferation and cytotoxicity (Dojindo) according to manufacturer's suggested protocol. After 72 hr, cells were also assessed for viability using Live and Dead ReadyProbes Reagents

(Life technologies) and imaged using wide-field microscopy with EVOS FL Auto (Life technologies) and quantified using ImageJ (National Institutes of Health).

Cells were also tested in varying media compositions to determine optimal viability using the previously described assays. Media compositions tested include basal astrocyte medium (Sciencell), supplemented with 1% B27 and 0.5% N2, and/or 0.01% FGF and 0.1% EGF.

3.3.4 Three-dimensional cell assays

Experiments were carried out with 8µm pore size tissue culture inserts (Sigma Aldrich). Cells were fluorescently labeled with CellTracker dyes (Life technologies) and Vybrant dyes (Life technologies) according to manufacturer suggested protocol. Glioblastoma cells ($5.0x10^5$), astrocytes ($8.0x10^4$), and microglia ($8.0x10^4$) were seeded in 75 µL gel (0.2% hyaluronan; ESI Bio) and 0.12% rat tail collagen I (Corning) based on ratios quantified from human sections. Gels solidified at 37°C in a humidified incubator containing 5% CO_2 and 21% O_2 for 2 hr, then experimental media was added to the top and bottom of each tissue culture insert such that media was level inside and outside of the insert.

3.3.5 Invasion assay and flow cytometry

After 18hr, gels were removed from tissue culture inserts and digested using Roche Liberase DL (Sigma Aldrich). Cells migrating through the porous membrane were identified by staining with DAPI (Invitrogen), counting five representative fields per insert, and reported as total cells invaded/total cells seeded x 100 (%) for each insert. Cells remaining post-gel digestion were stained for Live/dead (Life technologies), CD71 (eBioscience), and Ki-67

(eBioscience) according to manufacturer's suggested protocol. Flow cytometry was performed using Guava easyCyte 8HT (Millipore) and analyzed using guavaSoft 2.7 (Millipore).

3.4 Results

3.4.1 Analysis of patient samples to determine baseline ratio of cellular components

Our results from Chapter 2 not only indicate the importance of glial populations to glioblastoma prognosis, but particularly the populations within the infiltrative tumor-parenchymal interface. In order to specifically test how these glial cell populations in the infiltrative zone contribute to glioblastoma malignancy, our goal was to build a patient-defined 3D *in vitro* model of the cellular glioblastoma microenvironment. We re-quantified each of the 33 patient samples (**Figure 3.1A**) used in Chapter 3 at the tumor-parenchyma interface (**Figure 3.1B, C**) for specific astrocyte (ALDH1L1+, **Figure 3.2A**) and microglia (Iba1+, **Figure 3.2B**) population counts (**Figure 3.2C**) to define the ratios of cells to incorporate into the 3D *in vitro* model. Based off the analysis across our entire patient cohort, an average ratio of cancer cells to parenchymal cells for our entire patient cohort was determined to be 6:1:1 Glioblastoma cells to Astrocyte to Microglia.

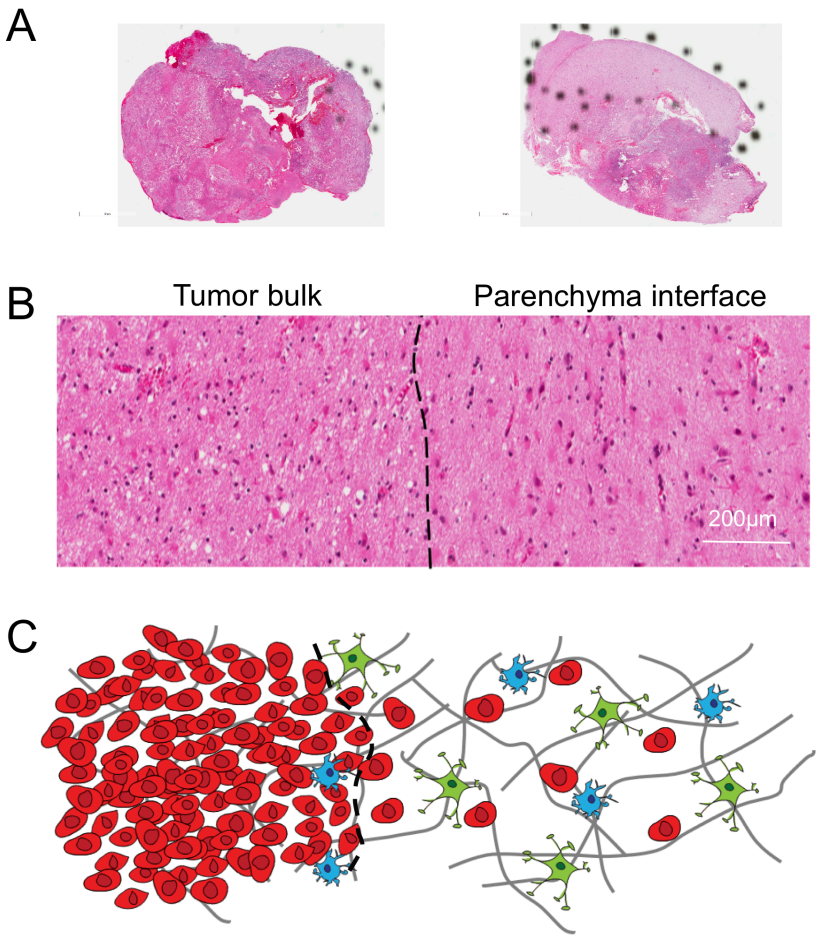

Figure 3.1: Patient tumor resections with reactive tissue areas were selected to study the tumor-parenchyma interface. A) From our whole patient cohort of 64 samples, 33 patient samples were identified by collaborating neuropathologists as containing reactive tissue, outlined in the dotted region. B) With this hematoxylin and eosin image, the tumor bulk region (left side), making most of the tumor resection is characterized by high nuclei (purple) from cancer cells, while the parenchyma interface (right side) has fewer nuclei, representing healthy tissue with infiltrative cancer cells. C) Graphical schematic of tumor bulk containing predominantly cancer cells (red) while the parenchyma interface is comprised of infiltrative cancer cells amongst healthy astrocytes (green) and microglia (blue).

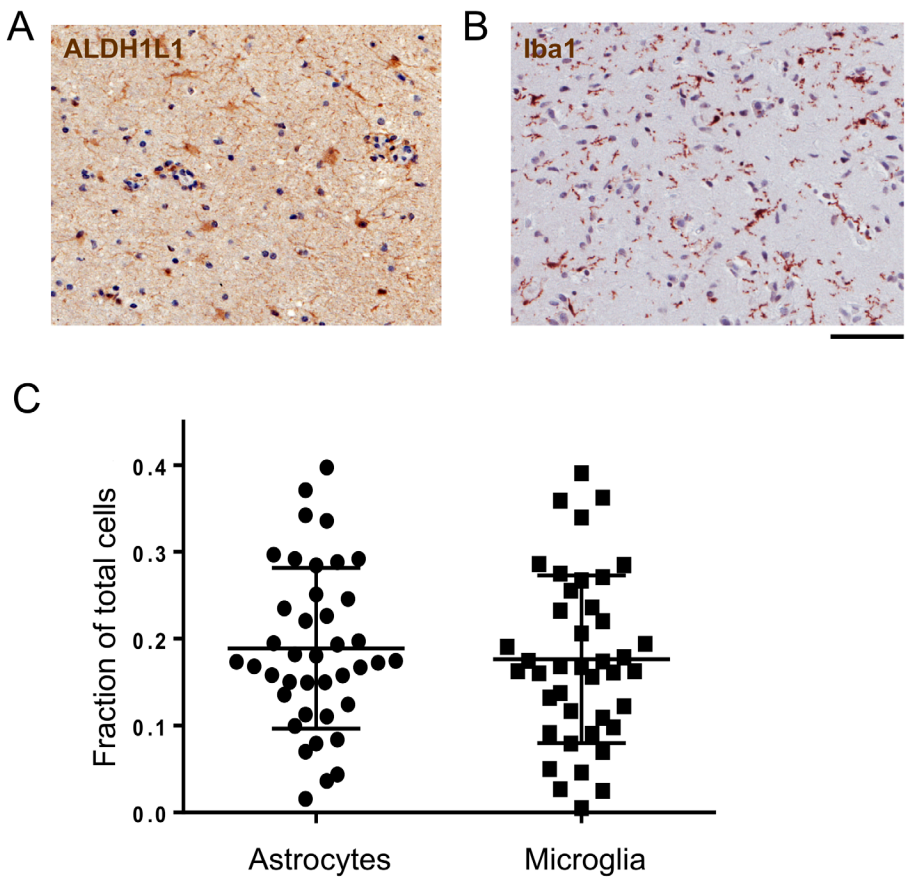

Figure 3.2: Quantification of astrocytes and microglia populations at the tumor-parenchyma interface. Chromogenic immunohistochemistry identified populations of A) ALDH1L1+ astrocytes and B) Iba1+ microglia within patient tumor resections. C) Astrocyte (circle) and microglia (square) populations were quantified for each of the 33 patients. Scale bar = 100μm.

3.4.2 Development of model components

Many studies use adherent glioma cell lines, such as U87 and GL261, to study glioblastoma due to their ease of culture, accessibility, and ability to reliably generate tumors in vivo [250–252]. However, traditional 2D culture is not physiologically relevant and growth in three dimensions is more representative of native human tissue [143, 253, 254]. Glioblastoma stem cells (GSCs) not only grow into spheroids to add in a dimensionality missed with

adherent lines, but also have inherent heterogeneities within the cultures that make them more similar to native glioblastoma tumors [247, 255, 256].

Because hyaluronan is the primary extracellular matrix component of the brain, we wanted our 3D *in vitro* model to also be primarily hyaluronan to accurately mimic the native brain tissue. Our lab has previously published a 0.2% polyethylene glycol-diacrylate crosslinkable hyaluronan with 0.12% rat tail collagen I matrix [78, 79], which we expanded here to better mimic the human glioblastoma microenvironment. We built our *in vitro* model with patient-derived glioblastoma stem cells as these are the population of malignant cancer cells which remain post-therapy and lead to recurrence. Glioblastoma stem cells derived from multiple different patients (G2, G34, G528), are each incorporated into the model, and standard adherent glioma cell lines (U251) could also be incorporated [257]. In addition to glioblastoma cells, we incorporated primary human cortical astrocytes and SV40-transduced human microglia to include within the 3D matrix to form a fully humanized *in vitro* model of the cellular glioblastoma microenvironment. The cell-matrix solution can be pipetted into multiple different culture vessels (cell culture well plates, tissue culture inserts, etc.) and solidifies at 37°C for 60minutes to form a cohesive gel, with cells uniformly distributed throughout, with an elastic modulus of 500-800Pa, comparable to brain tissue.

3.4.3 Optimization of model components for viability

Since our model incorporates multiple cell types, we needed to be able to distinguish the separate cell populations in order to study the individual contributions of each of our three cell types. We chose to use cell tracker dyes to label individual cell populations because these

fluorescent organic dyes pass freely into cell membranes where they are enzymatically transformed and unable to leave, thus retaining the dye through several generations of daughter cells. Labeling concentrations and conditions of the cell tracker dyes were optimized to maximize viability or cell types while still maintaining fluorescence intensity observable via fluorescence microscopy, as well as flow cytometry (**Figure 3.3 A, B**). After testing a range of doses, it was determined all Cell Tracker dyes at 2µM dose were non-toxic (>95% viability) and did not impede proliferation (n.s. change in growth curves) in all cell types (**Figure 3.3 C, D**). A hybrid media recipe of astrocyte medium supplemented with N2 and B27 resulted in >90% viability across all cell types (**Figure 3.4A**). Other media recipes were mildly toxic over time (50-70% viability) or showed altered growth curves as compared to the cell-specific media ($p<0.05$ curve comparison). Once optimized for individual components, we applied our labeled cells into our systems and cultured for multiple days and showed high viability over the entire time period.

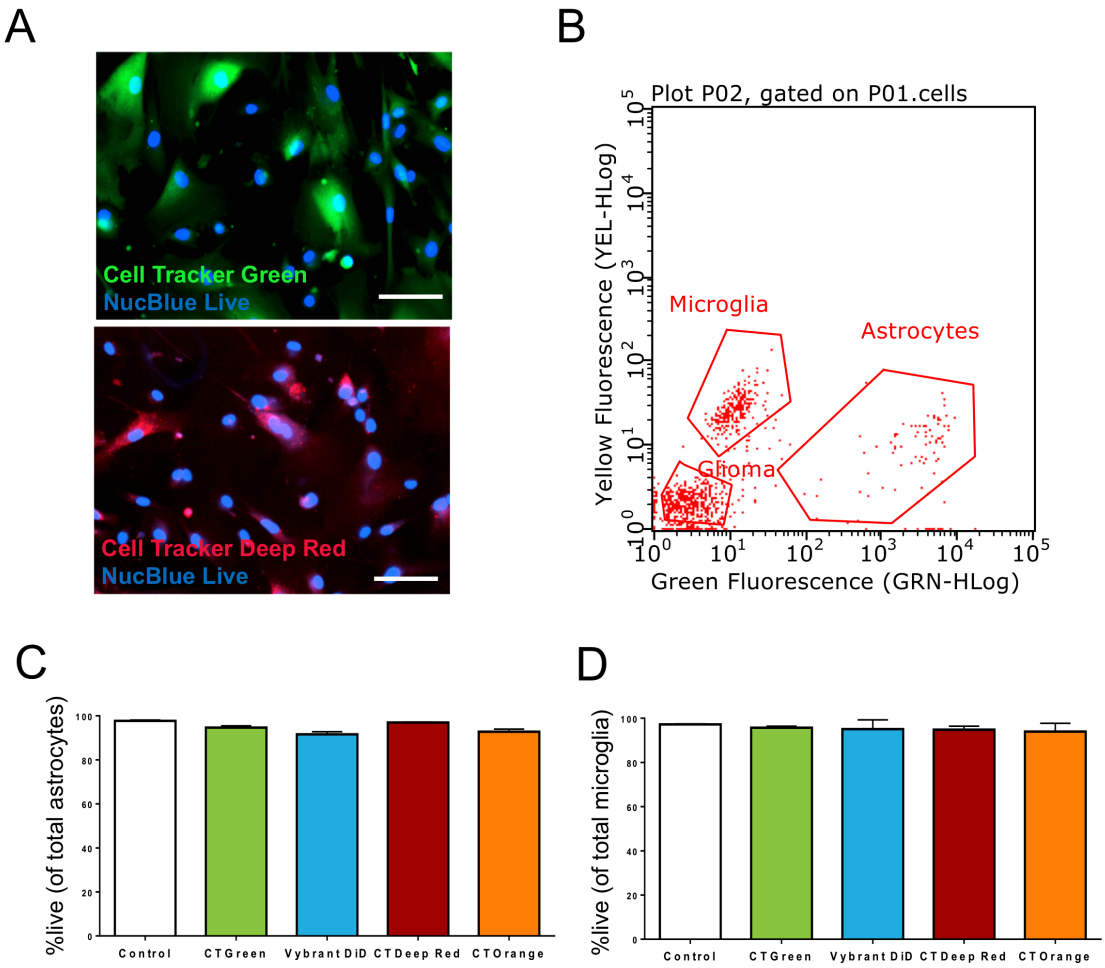

Figure 3.3: Optimization of cell tracker stains for identifying individual cell components. A) Human primary astrocytes labeled with cell tracker green (top) and human SV40-microglia labeled with cell tracker deep red (bottom) with Nuclear Blue Live counterstain labeling all live cells in the tissue culture dish. B) Each cell population is distinguishable using flow cytometry. All Cell Tracker dyes at 2µM dose were non-toxic for C) human primary astrocytes and D) human SV40-microglia. Scale bar = 100µm.

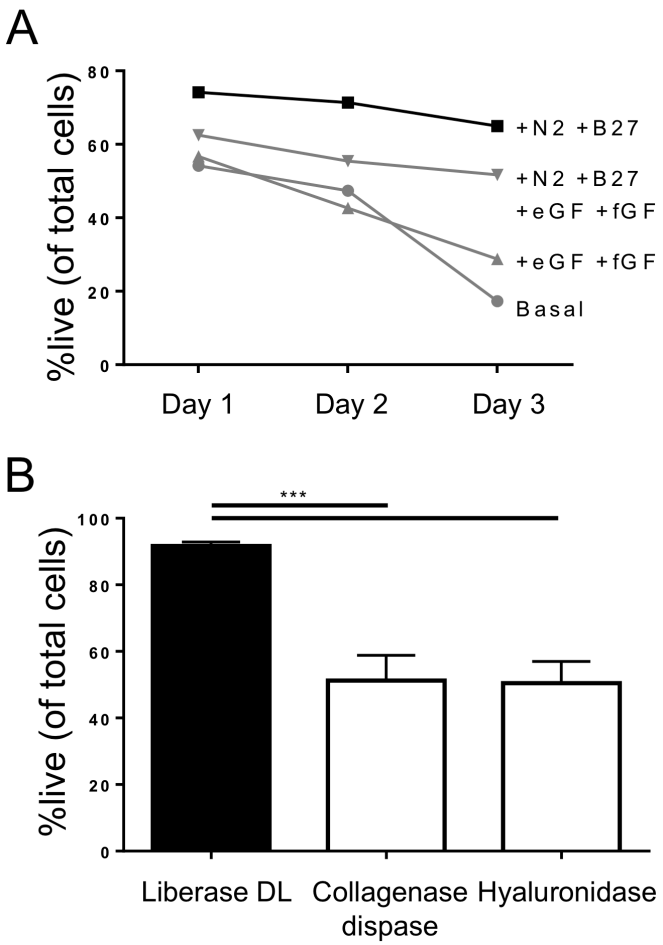

Figure 3.4: Optimization of viability for multi-day culture and outcome assessment. A) Multiple media recipes were tested to determine the optimal recipe for viability of all cell types across three days of culture, with a hybrid media recipe of astrocyte medium supplemented with N2 and B27 resulting in >90% viability across all cell types. B) A variety of enzymes were tested to degrade the hyaluronan-collagen matrix, with Liberase DL resulting in >95% viability. *** $p<0.001$.

3.4.4 Optimization of outcome measures for 3D system

Our model is incorporated into tissue culture inserts with an 8μm porous membrane at the bottom (**Figure 3.5**). Cells within the gel matrix are able to move through the matrix and travel through the porous membrane to mimic invasion. We use fluorescence microscopy

to image the bottom of the porous membrane and quantify invasion of the cells (**Figure 3.5**, bottom panel).

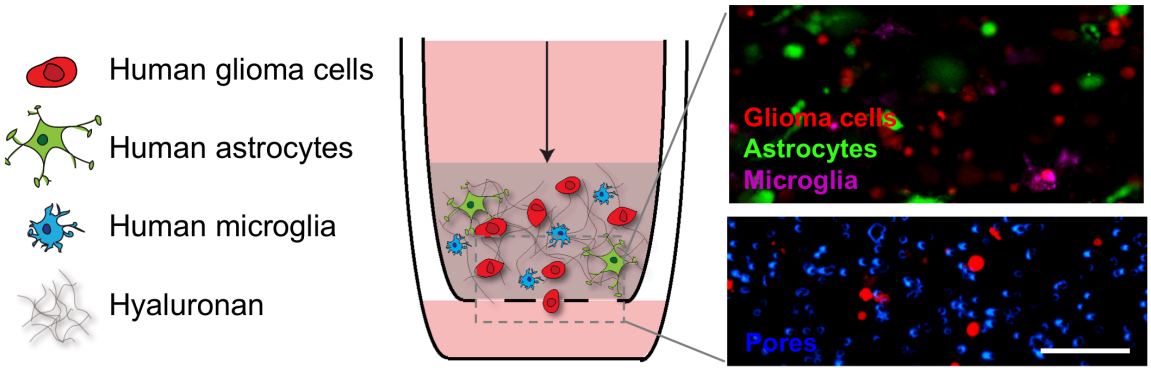

Figure 3.5: Schematic overview of 3D in vitro model of the brain tumor microenvironment. Human glioblastoma cells, such as patient-derived glioblastoma stem cells, (red), human astrocytes (green), and human microglia (blue/purple) are incorporated into a hyaluronan matrix and seeded into a tissue-culture insert with a porous membrane through which cells can migrate for quantification of invasion (bottom panel). Scale bar = 100μm.

Most studies focus on invasion of glioma cells, but glioblastoma tumors recur not only when the cells have invaded, but also because the remaining malignant cells are stem-like, capable of proliferating and differentiating to create new tumors [6, 246]. Therefore, it is important to assess multiple malignant measures other than invasion, such as proliferation and stemness, in order to understand why glioblastoma recurs.

Our goal was to assess multiple outcomes simultaneously, so we optimized our model for analysis via flow cytometry to quantitatively measure multiple parameters on each of our cell populations concurrently. In order to run flow cytometry on our cell populations, we needed to degrade our 3D matrix fully, without affecting the cell viability. Since our

matrix is a combination of hyaluronan and collagen, a variety of enzymes were tested to degrade the matrix, with Liberase DL resulting in >95% viability (**Figure 3.4B**).

While there are a variety of markers and measurement techniques for proliferation, stem populations, and cell death, we optimized our flow cytometry panel to include Ki67+ proliferation (**Figure 3.6A**), CD71+ stemness (**Figure 3.6B**) [108], and death (**Figure 3.6C**) for our benchtop flow cytometer, Guava easyCyte 8HT (Millipore). This panel is in addition to our human primary astrocytes labeled with Cell Tracker Green, SV40-immortalized microglia with Cell Tracker Deep Red and glioma cells with Cell Tracker Orange (**Figure 3.5**, top panel).

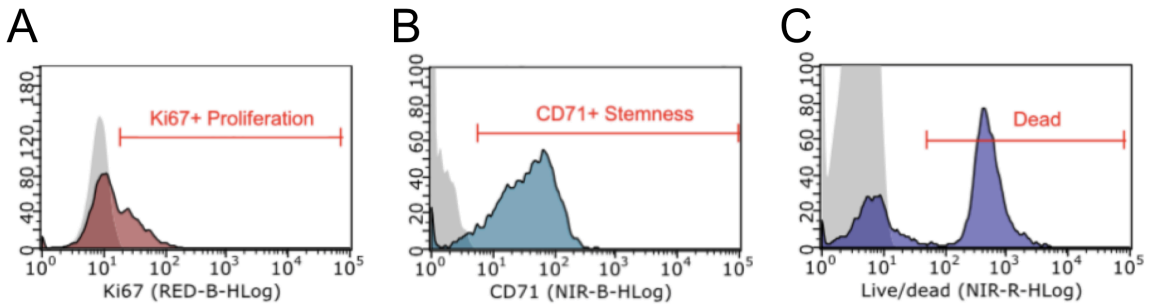

Figure 3.6: Flow cytometry plots for multiple malignant outcome assessment. Our 3D *in vitro* system is optimized for simultaneous assessment of multiple parameters, such as A) Ki67+ proliferation, B) CD71+ stemness, and C) death via live/dead staining via flow cytometry.

3.4.5 Assessment of relevant mimicking of patient samples

We have seen our *in vitro* model recapitulates percentages of activated astrocytes seen in the adjacent infiltrative regions of glioblastoma. Specifically, we see ~30% of neoplastic astrocytes (Podoplanin+ ALDH1L1+) are activated (GFAP+) in both our *in vitro* model

(**Figure 3.7A**) and within patient samples, as well as ~20% of non-neoplastic astrocytes (ALDH1L1+) are activated (GFAP+) in both (**Figure 3.7B**).

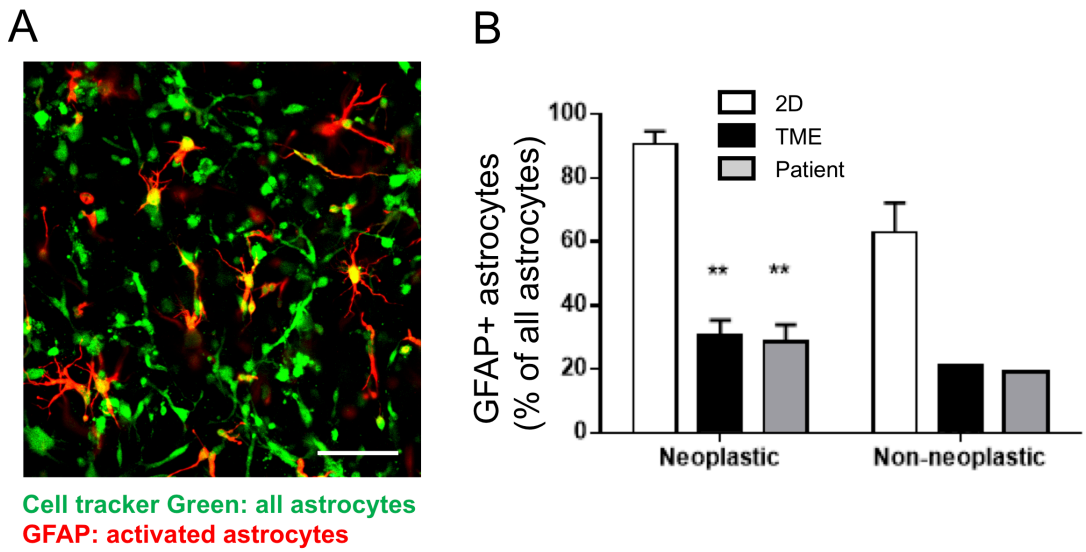

Figure 3.7: Comparison of *in vitro* model with patient samples. A) Image of astrocytes (green) in 3D culture with GFAP (red) staining for activation. B) Quantification of percent activated astrocytes in our model compared with standard 2D culture in patients for neoplastic and non-neoplastic conditions. Scale bar = 50μm.

3.5 Discussion

In this chapter, we present a robust patient-defined tissue-engineered model of the cellular glioblastoma microenvironment at the invasive front. This model is easily tunable, with the ability to add or remove components, as well as the ability to assess many outcome measures via flow cytometry. Here, we present a panel of various malignant outcomes – invasion, stemness, and proliferation – that contribute to glioblastoma recurrence but other measures, such as apoptosis, activation, drug uptake, and more could also be adapted for analysis.

While our system specifically models the cellular microenvironment at the invasive interface of the tumor, this can be adapted to model tumor bulk and therefore assess other

microenvironmental influences on drug response such as hypoxia and pH fluctuations seen at the tumor core [258]. Furthermore, our system utilizes tissue culture inserts to model and quantify invasion, but due to the pipettable liquid form of the cell-gel solution prior to gelation, it is easily adaptable to other vessels such as microfluidic devices to study other disease-related phenomenon such as pressure and chemical gradient changes [259, 260].

The use of tissue-engineered models of disease is rapidly increasing in multiple pathologies, including neurodegeneration, cancer, fibrosis, cardiac, and other toxicities. Our model differentiates from many other tumor models by inclusion of multiple cell types and physiologically relevant fluid flow. These aspects create a more tissue-relevant disease phenotype for cancer. Regardless of the model, the technique of flow cytometry can be used to interrogate multiple parameters. The ability to assess multiple factors is a key advantage to better understanding the multiple mechanisms that contribute to ultimate patient survival. In cancer specifically, tumors relapse and regrow not only because the tumor cells do not die in response to therapy, but also because they migrate to other regions, proliferate to generate new resistant tumor cells, and have stem-like properties. Therefore, the ability to simultaneously examine multiple factors will greatly benefit the understanding of the complexities contributing to cancer growth and recurrence.

The ease of manipulation and relative simplicity of 2D cell culture has had a profound impact on clinical and translational research, especially in drug discovery initiatives. With thousands of tumor cells lines now available, high-throughput drug screening platforms are emerging with the aim to discover novel drug targets and effective compounds against cancer

[261, 262]. However, many of these efforts fail to translate to clinical efficacy in patients [263]. One possible contributor to this disconnect between bench and bedside may be the lack of microenvironmental components such as extracellular matrix, stromal cells, and biophysical forces like fluid flow, that are naturally inherent to a tissue but absent in a 2D unicellular system [264]. The ability to incorporate these factors into a multicellular 3D tissue engineered system [242] and scale this model from individual tissue culture inserts into a 96-well plate format transforms current drug screening capabilities. We will demonstrate the potential for utilizing this system for these purposes in Chapter 6 of this dissertation.

Given the emerging critical role the tumor microenvironment plays in cancer progression and drug resistance [26, 265], strategies are in development to identify new compounds that target key microenvironmental components [266]. These strategies may include inhibiting angiogenesis and lymphangiogenesis, quelling chronic inflammation, reducing activity of cancer-associated fibroblasts, stimulating infiltration of antitumor immune cells, or even targeting noncellular microenvironment components such as extracellular matrix, pH, fluid flow, and interstitial pressure [267]. However, drug screening initiatives to identify compounds that target the microenvironment to increase cancer susceptibility to treatment necessitates the inclusion of these components in high-throughput screening models. Tissue-engineered models, such as the one presented in this chapter, offer such a tool to expand drug screening strategies to examine microenvironment-targeted therapies.

Chapter 4: Elucidating microenvironmental contributions to measures of glioblastoma malignancy

4.1 Summary

Using our optimized patient-defined 3D *in vitro* human brain tumor microenvironment model described in the previous chapter, we studied the contributions of cellular microenvironment components to multiple measures of glioblastoma malignancy, including invasion, stemness, and proliferation using glioblastoma stem cells derived from three different patients. We found glioblastoma stem cells derived from patient G528 appeared more malignant than those from mesenchymal subtype patients G2 and G34 when cultured alone in the 3D matrix, while incorporating the glioblastoma stem cells with astrocytes and microglia led to patients G2 and G34 exhibiting the more malignant phenotype. Implanting these glioblastoma stem cells in murine orthotopic xenografts resulted in a median overall survival of 25.5 days for G528, and 13 days for G34, indicating G34 glioblastoma stem cells were more malignant, as seen when we incorporated these cells with a physiologically-relevant cellular microenvironment. Design of experiment analyses indicate the main contributor was different for each outcome measure, indicating the importance of studying multiple outcomes to gain a better understanding of glioblastoma.

4.2 Introduction

The most common and malignant form of brain cancer, glioblastoma, is also one of the most invasive types of cancer. Characterized by diffuse invasion of tumor cells from the primary tumor bulk in the surrounding healthy brain tissue, these invading cells persist after surgical resection, and are considered the primary cause for inevitable recurrence [6–8]. Glioblastoma is a cancer that simultaneously grows and invades, making it highly integrated and difficult to completely surgically resect from surrounding brain tissue. These tumor cells heavily interact with the surrounding brain tissue to create a tumor microenvironment (TME). It is increasingly apparent in many cancers that the tumor microenvironment plays a major role in the development and progression of tumors, including enrichment of cancer stem cells, apoptosis resistance, increasing proliferation, promoting invasion, and limited drug transport to tumor cells [26, 27].

The glioblastoma microenvironment is uniquely complex and includes many different components: glial cells, extracellular matrix, soluble factors and biophysical factors. Brain tumor growth and recurrence is likely mediated by multiple factors from the complex microenvironment, but in particular, glial cells have been implicated [32, 34, 245]. Current research on the cellular glioblastoma tumor microenvironment focuses only on the contributions of either astrocytes or microglia [32, 42, 244, 245] to glioma cell invasion, as well as glioblastoma patient survival. However, little is known about how these cellular microenvironment components contribute to other aspects of glioblastoma malignancy, as well as how the microenvironment affects different patients. Furthermore, recent studies in

our lab and others have characterized and elucidated the biophysical factor of interstitial flow in the tumor microenvironment as increasing invasion of glioblastoma cells *in vitro* and *in vivo* [77, 78]. It is currently unclear how interstitial flow affects proliferation and stemness of glioblastoma stem cells, as well as how this phenomenon plays a role when incorporated with glial components of the tumor microenvironment.

In this chapter, we used the 3D *in vitro* human glioblastoma microenvironment model developed in Chapter 3 to specifically test how cellular microenvironment components individually and synergistically affect malignancy of glioblastoma stem cells derived from three different patients. We then compared our *in vitro* findings with the gold standard pre-clinical model of murine xenografts to assess the physiological relevance. Finally, we incorporated physiologically-relevant interstitial flow into our *in vitro* model to assess how this overlooked phenomenon can further contribute to glioblastoma.

4.3 Materials and methods

4.3.1 Cell lines and culture

Patient-derived G2, G34, and G528 human glioblastoma stem cells (GSCs) were maintained in non-treated culture flasks in Neurobasal media (Life Technologies) supplemented with 1% B27, 0.5% N2, 0.01% FGF, 0.1% EGF, 0.3% L-Glutamine, and 1% penicillin-streptomycin. Human primary cortical astrocytes were purchased from Sciencell and cultured according to manufacturer's suggested protocol. Human SV40-immortalized microglia were purchased from Applied Biological Materials, Inc and cultured in Dulbecco's Modified Eagle's Medium

(DMEM; Life technologies) with 10% FBS. All cell lines were maintained at 37°C in a humidified incubator containing 5% CO_2 and 21% O_2.

4.3.2 Three-dimensional cell assays

Experiments were carried out with 8µm pore size tissue culture inserts (Sigma Aldrich). Cells were fluorescently labeled with CellTracker dyes (Life technologies) and Vybrant dyes (Life technologies) according to manufacturer's suggested protocol. Glioblastoma stem cells ($5.0x10^5$), astrocytes ($8.0x10^4$), and microglia ($8.0x10^4$) were seeded in 75 µL gel (0.2% hyaluronan; ESI Bio) and 0.12% rat tail collagen I (Corning) based on ratios quantified from human sections. Gels solidified at 37°C in a humidified incubator containing 5% CO_2 and 21% O_2 for 2 hr. For static conditions, experimental media was added to the top and bottom of each tissue culture insert such that media was level inside and outside of the insert. For flow conditions, an experimental media pressure head of 1 cm was created between the top and bottom of each tissue culture insert, leading to an average velocity of 0.7 µm/s through the cell/gel compartment.

4.3.3 Invasion assay and flow cytometry

After 18hr, gels were removed from tissue culture inserts and digested using Roche Liberase DL (Sigma Aldrich). Cells migrating through the porous membrane were identified by staining with DAPI (Invitrogen), counting five representative fields per insert, and reported as total cells invaded/total cells seeded x 100 (%) for each insert. Cells remaining post-gel digestion were stained for Live/dead (Life technologies), CD71 (eBioscience), and Ki-67 (eBioscience) according to manufacturer's suggested protocol. Flow cytometry was

performed using Guava easyCyte 8HT (Millipore) and analyzed using guavaSoft 2.7 (Millipore).

4.3.4 Tumor inoculation in animal studies

8-10week old male NOD-SCID mice were inoculated with 10,000 glioma stem cells derived from patient G34 (n=7) or 400,000 glioblastoma stem cells derived from patient G528 (n=6) in 10μL of neurobasal media supplemented with N2, B27 without vitamin A, glutamax, and penicillin-streptomycin 2mm lateral and posterior to bregma at a depth of 2.6mm. Animals were assessed daily for signs of distress, and euthanized accordingly. All animal procedures were conducted in accordance with the University of Virginia Institutional Animal Care and Use Committee (Charlottesville, VA).

4.3.5 Immunostaining in vivo

Brains were collected, soaked in sucrose, cryoembedded, and sectioned at 12μm. Three sections at varying depths within the tumor were immunostained with mouse anti-human nuclei (clone 235-1, Millipore) followed by secondary Dylight 488 horse anti-mouse (Vector), rat Ki67 conjugated to eFluor570 (SolA15, eBioscience), and rabbit Sox2 (Millipore) followed by secondary AlexaFluor 660 goat anti-rabbit (Life technologies).

4.3.6 Design of experiments

JMP software (SAS) was used to identify key differences among experimental conditions. Independent variables included patient from which the glioblastoma stem cell is derived from (GSC), addition of each of the glial cell microenvironmental conditions (cells), and interstitial flow (flow). Dependent variables were outcome measures of invasion,

proliferation, and stemness. The classical screening design was fit for standard least squares to determine which factors have the main effect, and the resulting effects were summarized. $p<0.05$ is considered statistically significant.

4.3.7 Statistics

Experiments are repeated at least three times to yield biological replicates (based on power analyses). All data are presented as mean ± standard error of the mean (SEM). Independent, unpaired *t* tests and two-way ANOVA was used for statistical analysis of unmatched groups. Statistical analyses were run using Graphpad Prism software. $p<0.05$ is considered statistically significant. Graphs were generated using Graphpad Prism software.

4.4 Results

4.4.1 Contributions of cellular microenvironment to invasion

After optimizing the design of 3D *in vitro* model describe in Chapter 3, the model was then used to probe contributions of the cellular tumor microenvironment to glioblastoma malignancy. Since the model is tunable, the individual and combined contributions of astrocytes and microglia on glioblastoma stem cell invasion, proliferation and maintenance of stem can be examined using fluorescence microscopy and flow cytometry. We examined patient-specific differences by incorporating glioblastoma stem cells derived from three different patients into our model, and assessed the resulting malignant changes to each patient with the addition of astrocytes, microglia, or both.

We began with studying invasion, by determining the effects of astrocytes, microglia, or both on invasion of each of our patient-derived glioblastoma stem cell (GSC). Using fluorescence microscopy, we quantify the number of cells migrated through the porous membrane at the bottom of the tissue culture insert to determine a percentage of the original cell population seeded into the matrix have invaded. For GSCs derived from patient G2, we found addition of astrocytes, and addition of microglia increased invasion of G2 cells compared to invasion of these cells alone in the matrix. When incorporating both astrocytes and microglia with G2 cells, we found a significant increase in invasion of G2 cells compared to the cells alone in the matrix (**Figure 4.1A**). For GSCs derived from patient G34, we found addition of astrocytes, and addition of microglia increased invasion of G34 cells compared to invasion of these cells alone in the matrix. When adding both astrocytes and microglia to G34 cells, we found a significant increase in invasion of G34 cells compared to the cells alone in the matrix (**Figure 4.1A**). On the other hand, for GSCs derived from patient G528, we found addition of astrocytes, and addition of microglia did not significantly change invasion of G528 cells compared to invasion of these cells alone in the matrix. When adding both astrocytes and microglia to G528 cells, we found a trend towards decreased invasion of G528 cells compared to the cells alone in the matrix (**Figure 4.1A**).

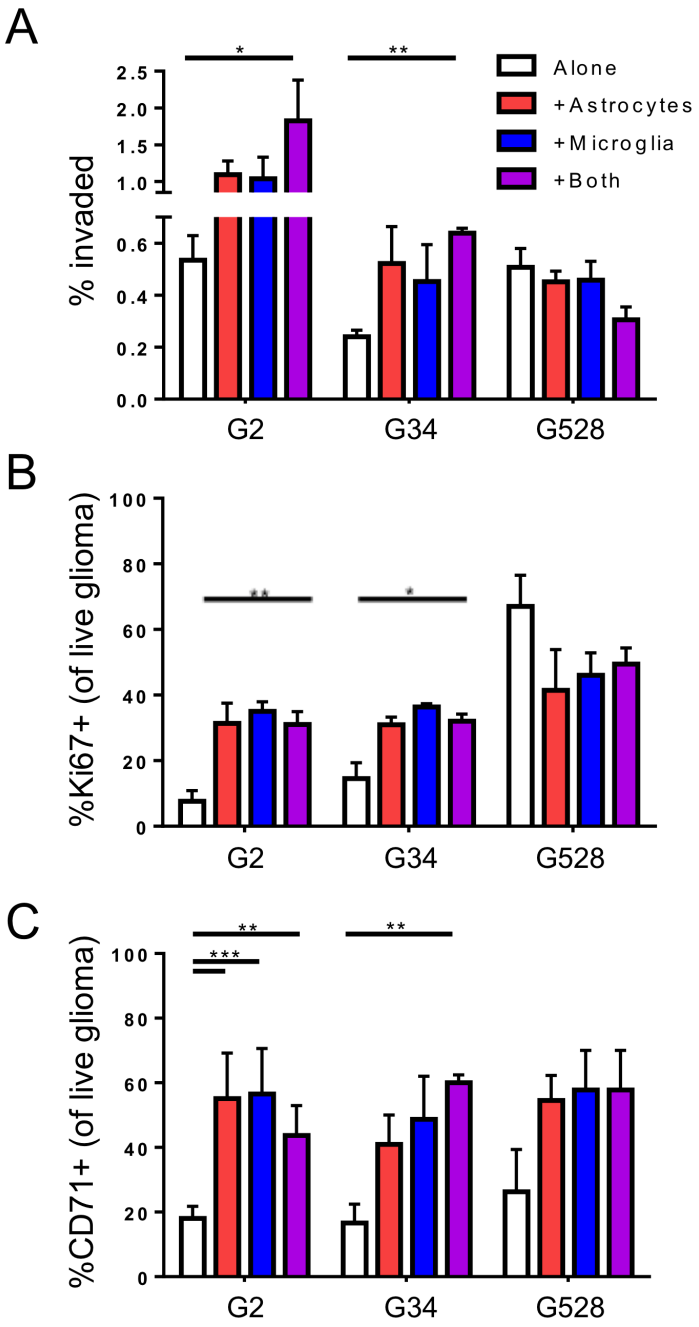

Figure 4.1: Contributions of cellular microenvironmental components to measures of glioblastoma malignancy across glioblastoma stem cells derived from three different patients. Addition of astrocytes (red bars), microglia (blue bars), or both (purple bars) increased A) % invaded glioblastoma stem cells (GSCs) from patients G2 and G34, but decreased for G528 compared to GSCs alone, B) %Ki67+ proliferating GSCs from patients G2 and G34, but decreased for G528 compared to GSCs alone, and C) %CD71+ stem cells from all three patients. *p<0.05, **p<0.01, ***p<0.001.

4.4.2 Contributions of the cellular microenvironment to proliferation

Although invasion is a major hallmark of glioblastoma malignancy, we wanted to gain a fuller understanding of how the cellular microenvironment affects glioblastoma by studying other aggressive cancer cell behaviors, such as proliferation. After removing the cell-gel matrix from the tissue culture insert, we degraded the matrix, leaving only our cells, and performed flow cytometry to quantitatively assess effect of the cellular microenvironment on proliferation via the Ki67 marker of glioblastoma stem cells derived from multiple patients.

We found addition of astrocytes, and addition of microglia each increase Ki67+ proliferation of glioblastoma stem cells derived from patient G2 compared to G2 cells alone in the matrix (**Figure 4.1B**). Addition of both astrocytes and microglia significantly increased Ki67+ proliferation of G2 cells compared to G2 cells alone, with no glial cell additions (**Figure 4.1B**). Similar trends were found with G34 patient-derived glioblastoma stem cells – addition of astrocytes, and addition of microglia each increase Ki67+ proliferation of glioblastoma stem cells derived from patient G34 compared to G34 cells alone in the matrix, and addition of both astrocytes and microglia significantly increased Ki67+ proliferation of G34 cells compared to with no glial cell additions (**Figure 4.1B**). Interestingly, glioblastoma stem cells derived from patient G528 exhibited the highest Ki67+ proliferation alone in the matrix, compared to the G2 and G34 cells alone in the matrix. And unlike the GSCs from our other two patients, addition of astrocytes, microglia, and both decreased Ki67+ proliferation of G528 cells compared to G528 cells alone in the matrix (**Figure 4.1B**).

4.4.3 Contribution of cellular microenvironment to stemness

The discovery of cancer stem cells in glioblastoma necessitates better understanding of the environments that support the growth and maintenance of these highly malignant cells. Because studies generally focus on the glioblastoma stem cells alone and little is known about how the microenvironment promotes niches for them, we used our *in vitro* model to determine how the cellular microenvironment affects the stem nature of glioblastoma stem cells derived from three different patients. Since these GSCs were all initially acquired via CD133 sorting and are therefore CD133 positive, we used the CD71 surface marker, or transferrin receptor complex, recently identified by Jeremy Rich's group as a robust marker for glioblastoma stem cells [108], to identify our stem populations via flow cytometry.

For G2 patient-derived glioblastoma stem cells, addition of astrocytes, addition of microglia, and addition of both astrocytes and microglia all significantly increased the CD71+ stem population of G2 glioblastoma stem cells compared to G2 cells alone in the matrix (**Figure 4.1C**). For G34 patient-derived glioblastoma stem cells, addition of astrocytes and addition of microglia increased the CD71+ stem population compared to G34 alone. Addition of both astrocytes and microglia significantly increased the CD71+ stem population of G34 glioblastoma stem cells compared to G34 cells alone in the matrix (**Figure 4.1C**). Addition of astrocytes, addition of microglia, and addition of both astrocytes and microglia trends towards increased CD71+ stem population of G528 glioblastoma stem cells compared to G528 cells alone in the matrix (**Figure 4.1C**). This data together suggests addition of the cellular microenvironment increases CD71+ stemness of glioblastoma stem

cells regardless of the patient from which they are derived, indicating the native environments in which tumors grow are selecting for the malignant stem cell populations.

4.4.4 Comparison of in vitro model to in vivo xenografts

When looking at our various outcome measures across our three different patient-derived cells, we see different behaviors with and without the cellular microenvironment. Comparing the three patient-derived glioblastoma stem cells alone in the matrix (white bars), the cells derived from patient G528 appear the most malignant across our three outcome measures. But when comparing the glioblastoma stem cells within the cellular microenvironment (purple bars), the G2 and G34 cells appear more malignant than G528. In order to compare the relevance of our *in vitro* model, we performed survival studies with murine orthotopic xenografts of each of the patient-derived glioblastoma stem cells. Since patients G2 and G34 are both classified as the mesenchymal subtype (subtypes previously described in Chapter 2) and we observed similar trends across each of our malignant outcome measures for the two patients, we decided to select one of these patients, G34, to inoculate *in vivo* and compare with the glioblastoma stem cells derived from patient G528, who is classified as the classical subtype.

Glioblastoma stem cells were implanted intracranially in the brains of immunocompromised NOD-SCID mice. Seven days after inoculation, tumors were visible via magnetic resonance imaging. Overall survival between each cohort was significantly different, with a median overall survival for G528-inoculated xenografts of 25.5 days, while G34-inoculated xenografts had a median overall survival of 14 days (**Figure 4.2**). This

significant difference between overall survival suggests the glioblastoma stem cells derived from patient G34 are more malignant than G528, as was predicted and represented when we included the cancer cells with the physiologically-relevant cellular microenvironment.

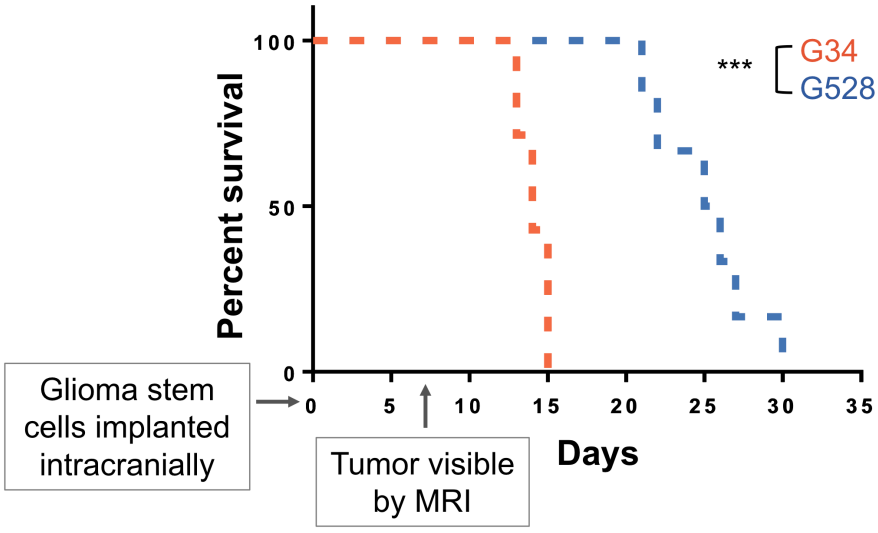

Figure 4.2: Kaplan-Meier survival curves for murine xenografts orthotopically implanted with G34 and G528 patient-derived glioblastoma stem cells. The median overall survival post-tumor implant for G34 (orange line, n = 7) was 14 days, and 25.5 days for G528 (blue line, n=6). *** $p < 0.001$

We then assessed the microenvironment of the xenograft brains to determine how the implanted tumor cells are affected by the microenvironment *in vivo*. Using immunohistochemistry, we identified the human glioblastoma stem cells via Human Nuclear Antigen staining (**Figure 4.3A**), the Ki67+ proliferating cells (**Figure 4.3B**), and the Sox2+ stem cells (**Figure 4.3C**) within the murine xenograft brains. After quantifying each population, we compared this with their respective populations within our *in vitro* tumor microenvironment model, as well as with the traditional spheroid growth of the glioblastoma stem cells. We found significant differences between the Ki67+ proliferating cell population

when the glioblastoma stem cells are cultured in spheroids compared to when they are orthotopically inoculated in murine xenografts (**Figure 4.4A**), as well as the stem populations measured with CD71 for in vitro analyses and Sox2 for *in vivo* (**Figure 4.4B**). The respective populations using our 3D i*n vitro* tumor microenvironment model trended similarly to the *in vivo* results (**Figure 4.4**, black bars), suggesting our 3D *in vitro* model incorporating astrocytes and microglia in a hyaluronan matrix is more physiologically-relevant to *in vivo* models than traditional spheroid culture.

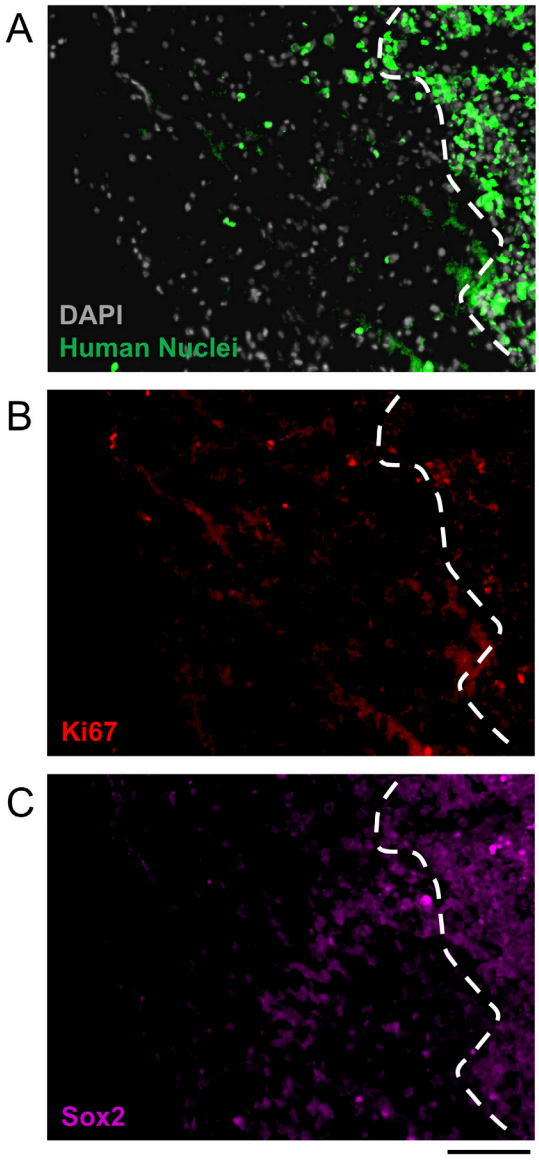

Figure 4.3: Representative staining of murine xenograft brain sections. Cell populations of interest were identified in murine xenograft brain sections via A) DAPI (gray) nuclear staining for all cells and Human nuclear antigen (green) for implanted patient-derived glioblastoma stem cells, B) Ki67+ proliferating cells (red), and C) Sox2+ stem cells (purple). Scale bar = 100μm.

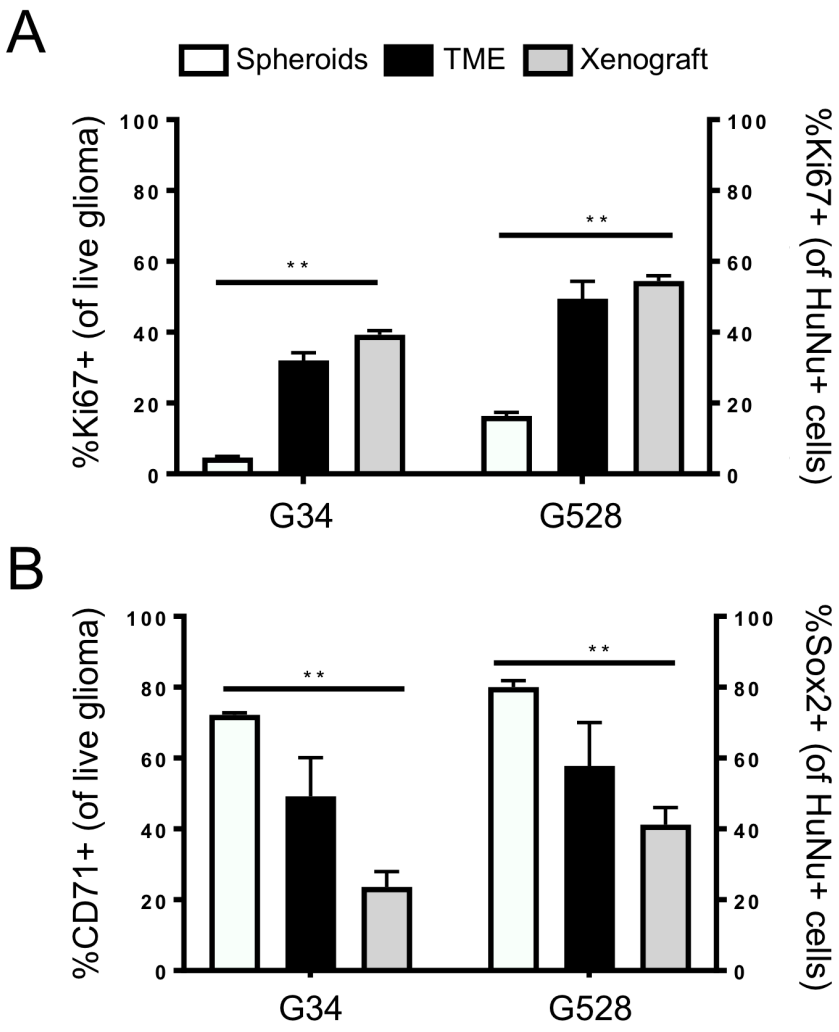

Figure 4.4: Comparison of malignant populations between spheroid culture, 3D *in vitro* microenvironment model, and murine xenografts. A) *In vitro* measurements of %Ki67+ of total live glioma in spheroids (left Y-axis, white bars) was significantly lower than the corresponding %Ki67+ of total Human Nuclear Antigen (HuNu)+ cells quantified in xenograft models (right Y-axis, gray bars), with %Ki67+ of total live glioma within our 3D *in vitro* model (left Y-axis, black bars) trending closer to the populations observed *in vivo*. B) *In vitro* measurements of %CD71+ of total live glioma in spheroids (left Y-axis, white bars) was significantly higher than the corresponding %Sox2+ of total Human Nuclear Antigen (HuNu)+ cells quantified in xenograft models (right Y-axis, gray bars), with %CD71+ of total live glioma within our 3D *in vitro* model (left Y-axis, black bars) trending closer to the populations observed *in vivo*. **$p<0.01$

4.4.5 Determination of greatest effector of each outcome measure

We utilized classical screening design of experiment analyses to determine how the many independent factors within our system are contributing to our multiple outcomes – invasion, CD71+ stemness, and Ki67+ proliferation based on our *in vitro* data. Statistical design of experiment analyzes multi-factor data to yield a consistent and objective conclusions about the involvement of the investigated parameters [268]. In addition to our independent variables previously described – patient from whom the glioblastoma stem cell is derived from (input as GSC), and addition of each of the glial cell microenvironmental conditions (input as cells) – we also included experimental data incorporating the biophysical force of interstitial flow (input as flow). From this analysis, we found different independent variables have more significant effects on our outcome measures. Specifically, for invasion, the patient from whom the glioblastoma stem cell is derived from is the most significant contributor ($p = 0.00933$, **Table 4.1**). For stemness, interstitial flow ($p = 0.00087$) as well as the addition of each of the cellular microenvironmental conditions ($p = 0.04852$) are significant contributors (**Table 4.1**). Lastly, interstitial flow ($p = 0.0003$) as well as the patient from whom the glioblastoma stem cell is derived from ($p = 0.000013$) are significant contributors to proliferation (**Table 4.1**). This analysis indicates the importance of the components of the tumor microenvironment for evaluating glioblastoma malignancy across multiple measures.

Table 4.1: Summary of greatest effector of each malignant glioblastoma outcome measure.

Invasion

Source	LogWorth	PValue
GSC	2.030	0.00933
Flow	0.428	0.37301
Cells	0.285	0.51918

Stemness

Source	LogWorth	PValue
Flow	3.062	0.00087
Cells	1.314	0.04852
GSC	0.333	0.46481

Proliferation

Source	LogWorth	PValue
Flow	4.554	0.00003
GSC	3.871	0.00013
Cells	0.021	0.95206

4.5 Discussion

Our studies indicate the cellular microenvironment has differential effects on the malignancy of glioblastoma stem cells derived from multiple different patients. Specifically, our tunable *in vitro* model suggested that without the cellular microenvironment, glioblastoma stem cells derived from patient G528 were more malignant across multiple outcome measures than the other patient-derived cells. However, with the cellular microenvironment, glioblastoma stem cells derived from patient G34, and patient G2, were more malignant than G528. This malignancy was reflected in *in vivo* xenograft survival studies, when mice inoculated with

G34 cells had a median overall survival significantly lower than mice inoculated with G528 cells.

The trends observed between our three different patient-derived glioblastoma stem cells could be attributed to the experimentally-derived subtypes of each of these patients. We saw similar *in vitro* trends between G2 and G34 patient-derived glioblastoma stem cells, and they are both classified as mesenchymal subtype. On the other hand, our G528 glioblastoma stem cells had significantly different patterns, and these cells could be classified as the classical subtype. Our studies were limited to three patients, so it is difficult to draw a conclusion based on the subtypes. Building tumor models outside the patient body using tissue engineering methods offers the ability to potentially examine a patient's own tumor in a controlled setting [143, 195]. While this is certainly advantageous for understanding the tumor biology and heterogeneity, it is particularly useful for screening therapeutic strategies to identify regimens that may be successful for the patient. Glioblastoma patients have poor prognosis, and typically do not have much time to try multiple therapeutic regimens. As such, recreating glioblastoma tumors *ex vivo* in an *in vitro* setting, provides a platform for testing many therapeutic regimens without subjecting the actual patient.

Furthermore, development and use of physiologically-relevant *in vitro* models via tissue engineering paves the way for eventual replacement of animal models [186]. Although patient-derived xenografts are the gold standard for personalized medicine, animal studies are costly and labor-intensive. *In vitro* modeling greatly minimizes the cost and facility requirements, as well as provides an opportunity to use human cells, as opposed to relying

on non-human models. In this chapter, our studies demonstrate the ability to distinguish malignancy between glioblastoma stem cells derived from patients G34 and G528 *in vitro*, corroborated these differences with *in vivo* xenograft studies of the same cells. While this finding does not definitively prove animal models can be eliminated, it is a promising step towards reducing the animal model burden.

Finally, our design of experiment analyses indicated the elements of the microenvironment – interstitial flow, glial cell components, and patient cells – affect our outcome measures – invasion, proliferation, and stemness differently. The earlier studies did not incorporate interstitial flow, as we aimed to specifically study the contributions of the cellular components. Interstitial flow was then incorporated for the model to be even more physiologically-relevant and was included in this analysis to determine if it was a significant contributor. Had this analysis shown interstitial flow did not have a significant role, the *in vitro* model could remain incorporating only the glial cells as the microenvironment without adding another level of complexity. Since this analysis showed interstitial flow as a significant contributor for multiple outcomes, it will now be included as part of the whole optimized 3D *in vitro* model for continued studies throughout this dissertation. This design of experiment analysis demonstrates the highly heterogenous nature of glioblastoma with patient-to-patient variabilities strongly contributing to malignant behaviors, necessitating engineering of technologies and platforms for higher throughput patient-specific *in vitro* modeling.

Chapter 5: Identifying microenvironment intercellular signals of interest

5.1 Summary

We utilized our 3D *in vitro* microenvironment model comprised of patient-derived glioblastoma stem cells with human astrocytes and human microglia to identify novel intercellular signals as potential therapeutic targets. A Luminex bead array identified three cytokines of interest, CXCL8, CXCL1, and CCL2, as particularly upregulated within the microenvironment, as opposed to the glioblastoma stem cells alone. We performed gain-of-function and loss-of-function experiments to identify the role these cytokines and their receptors have on invasion and stemness of glioblastoma stem cells. We found each of the cytokines themselves and their receptors have differing effects on invasion and CD71+ stemness. Specifically, blocking the receptors reduced invasion and CD71+ stemness in the presence of cellular microenvironment, but blocking the cytokines did not affect invasion. Lastly, we stained patient tumor resections for each cytokine to determine the potential clinical relevance of these cytokines as signals of interest. This chapter demonstrates the potential of a 3D *in vitro* multicellular model as a platform to study paracrine signaling between cancer cells and support cells that are difficult to study *in vivo* and incapable with traditional 2D cell culture.

5.2 Introduction

Drug discoveries and improving understanding of tumor biology has significantly improved overall survival in the last ten years for patients in many cancers [2]. However, in the most common and deadly form of brain cancer, glioblastoma, patient prognosis and survival odds remain quite dismal. Recent advances in the clinical treatment of glioblastoma have only increased the median survival time to 16 months after first diagnosis [3, 4]. Glioblastoma is a highly invasive cancer; the tumor cells readily invade and integrate into surrounding tissue as the tumor develops, making it impossible to target all of the cells with any treatment. The tissue surrounding the tumor is referred to as the tumor microenvironment, and it has been linked to almost every aspect of cancer therapeutic failure including cellular invasion, transport of drugs, stem cell selection, increasing proliferation, resistance to apoptosis, immune evasion, and genomic instability [26, 27]. However, in glioblastoma, where the tumor microenvironment is near impossible to separate from the tumor bulk, little is known about how the microenvironment affects this cancer.

Furthermore, since glioblastoma is a tumor of the brain, the microenvironment is uniquely complex. Glial cells, such as astrocytes and microglia, are the primary stromal cells of the brain, and not only are they not found anywhere else in the body, they have each been implicated in contributing to glioblastoma invasion [32, 34, 245]. Tumor cells communicate and hijack healthy stromal cells in the tumor microenvironment via paracrine signaling of soluble factors to assist in tumor progression. Astrocytes or microglia, or sometimes both glial cells, are known to secrete various proteins that glioblastoma cells can

utilize to invade or resist cell death, such as proMMP2 [38], interleukin 1β, [86], CXCL12 [87, 88], and many more. These signaling networks are complex and affect various malignant outcome measures. Current experimental models are limited in the ability to easily study the direct communication links between glioblastoma cells and glial cells, and require complex shRNA development to knockdown specific cytokines, or time-consuming and costly development of transgenic animal models manipulated to knock out cytokines or upregulate signaling pathways [160, 161].

Multiple chemotherapeutic agents have been developed to target specific signaling pathways in other cancers, such as bevacizumab for VEGF and imatinib for PDGFR, but these chemotherapeutics have not shown improvements in survival in glioblastoma in clinical trials [94, 95]. The glioblastoma microenvironment is complex, and there are many more autocrine and paracrine signaling systems involved in glioblastoma malignancy. Using our model developed in Chapter 3 that incorporates multiple parenchymal cells, we aimed to identify and understand novel intercellular paracrine signaling between the glial cell populations and cancer cells that could have potential therapeutic benefits when translated *in vivo*.

5.3 Materials and methods

5.3.1 Cell lines and culture

Patient-derived G2, G34, and G528 human glioblastoma stem cells (GSCs), a kind gift from the Purow Lab at the University of Virginia (who obtained them from Jakub Godlewski and

Ichiro Nakano--who derived them while at Ohio State University), were maintained in non-treated culture flasks in Neurobasal media (Life Technologies) supplemented with 1% B27, 0.5% N2, 0.01% FGF, 0.1% EGF, 0.3% L-Glutamine, and 1% penicillin-streptomycin. Human cortical astrocytes were purchased from Sciencell and cultured according to manufacturer's suggested protocol. Human SV40-immortalized microglia were purchased from Applied Biological Materials, Inc and cultured in Dulbecco's Modified Eagle's Medium (DMEM; Life technologies) supplemented with 10% FBS. All cell lines were maintained at 37°C in a humidified incubator containing 5% CO_2 and 21% O_2.

5.3.2 Three-dimensional cell assays

Experiments were carried out with 8µm pore size tissue culture inserts (Sigma Aldrich). Cells were fluorescently labeled with Cell Tracker dyes (Life technologies) according to manufacturer suggested protocol. Glioblastoma stem cells ($5.0x10^5$), astrocytes ($8.0x10^4$), and microglia ($8.0x10^4$) were seeded in 75µL gel (0.2% hyaluronan; ESI Bio) and 0.12% rat tail collagen I (Corning) based on ratios quantified from human sections. Gels solidified at 37°C in a humidified incubator containing 5% CO_2 and 21% O_2 for 2hr, then experimental media was added to the top and bottom of each tissue culture insert such that media was level inside and outside of the insert.

5.3.3 Invasion assay and flow cytometry

At the end of time course (18-hr), gels were removed from tissue culture inserts and digested using Roche Liberase DL (Sigma Aldrich). Cells migrating through were identified by staining with DAPI (Invitrogen), counting five representative fields per insert, and reported

as total cells invaded/total cells seeded x 100 (%) for each insert. Cells remaining post-gel digestion were stained for Live/dead (Life technologies) and CD71 (eBioscience) according to manufacturer's suggested protocol. Flow cytometry was performed using Guava easyCyte 8HT (Millipore) and analyzed using guavaSoft2.7 (Millipore).

5.3.4 Luminex and ELISA

Gels were seeded as described above and after 18hr, removed from 96-well plate, homogenized and lysed with TPER (ThermoScientific), and centrifuged to collect supernatant. Luminex assay was performed by the University of Virginia Flow Cytometry Core following standard protocols. For ELISA studies, protein secretion was quantified using IL-8 (CXCL8), MCP-1, (CCL2) and Gro-1 (CXCL1) kits following manufacturer's protocol (eBioscience).

5.3.5 Loss and gain-of-function experiments

For loss-of-function studies, blocking antibodies for CXCL8, (R&D, 0.2µg/mL), CCL2 (R&D 2µg/mL), CXCL1 (R&D 7µg/mL) and their appropriate isotype controls (IgG_1 and IgG_{2b}) were added into the gel solution and media. Similarly, antagonists for receptors CXCR2 (Millipore, 50nM) and CCR2 (Millipore, 10nM) were added into the gel solution and media throughout.

For gain-of-function studies, recombinant human MCP-1 protein (Gibco PHC1014, 10ng/mL) was incorporated into the gel solution and media. 24hr-conditioned media was harvested from simultaneous 2D culture of human cortical astrocytes and human SV40-microglia, and incorporated into the gel solution and media.

5.3.6 Statistics

Experiments are repeated at least three times to yield biological replicates (based on power analyses). All data are presented as mean ± standard error of the mean (SEM). Independent, unpaired *t* tests and two-way ANOVA was used for statistical analysis of unmatched groups. Statistical analyses were run using Graphpad Prism software. $p<0.05$ was considered statistically significant. Graphs were generated using Graphpad Prism software.

5.4 Results

Using our 3D *in vitro* model developed from Chapter 3, we were interested in changes in the system specific to the microenvironment that would otherwise be missed if we focused only on the glioma cells. Our goal was to identify a cytokine target from the microenvironment with the potential for therapeutically benefit. We ran a Luminex bead array on hydrogels containing each of our patient-derived glioblastoma stem cells (GSCs) independently, astrocytes and microglia without glioblastoma cells, as well as each of the GSCs with astrocytes and microglia. This was to specifically identify cytokines particularly upregulated when glial cells are combined with glioblastoma stem cells that are greater than the additive combination of each compartment alone. Since glioblastoma stem cells can secrete cytokines via autocrine signaling that astrocytes and microglia also secrete, we hoped to identify cytokines that are synergistically secreted when all three components are together that is otherwise not significantly increased when each component is alone. We tested all three of our patient-derived glioblastoma stem cell to hopefully identify cytokines that were

upregulated across all three patients that could be utilized as a therapeutic target for all glioblastoma patients.

5.4.1 Identification of cytokines of interest

From our Luminex Cytokine 40 array, we have observed multiple cytokines have increased expression in our full microenvironment model compared to the glioblastoma stem cell alone (**Figure 5.1**). MATLAB was used to generate fold change from raw Luminex data, which was determined based on standards ran simultaneously to experimental conditions. Some cytokines we observed increases in, such as IL-6 and IL-1, have been previously implicated in *in vivo* glioblastoma progression [269–271]. Our analyses revealed novel cytokines – CXCL1, CXCL8, or CCL2 – that have not been previously discussed in the context of the microenvironment in current glioblastoma literature. We then conducted ELISA studies on multiple biological replicates of the same conditions to confirm presence of these cytokines within the 3D *in vitro* model across our three patient-derived glioblastoma stem cells (**Figure 5.2**).

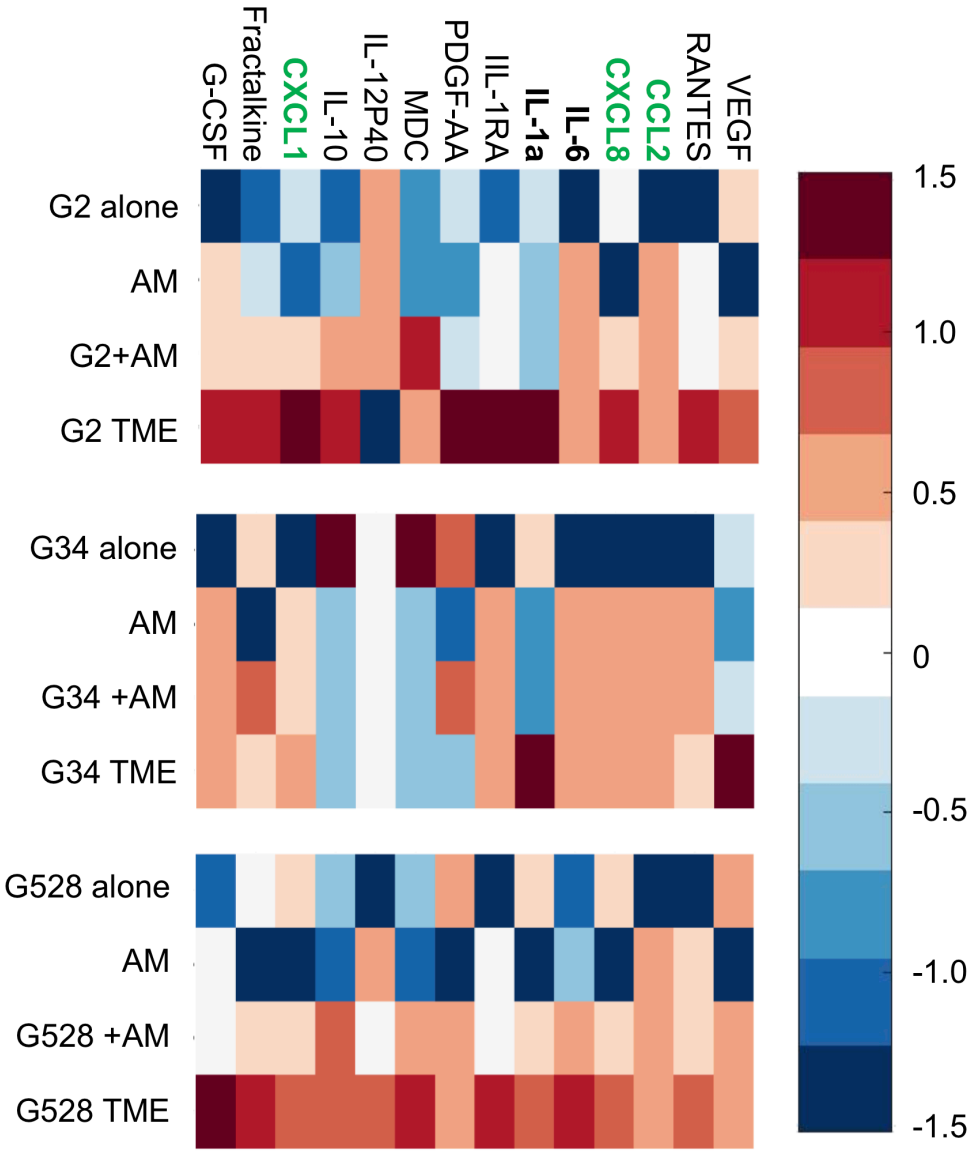

Figure 5.1: Luminex array results. Heat map results of Luminex array on a log scale for GSC alone, astrocytes and microglia (AM) alone, the sum of these two samples (G# +AM) or the full model will all three components (G# TME). Cytokines with increased values compared to the sum of all components are bolded and the three that have not been previously discussed in literature are bolded in green font.

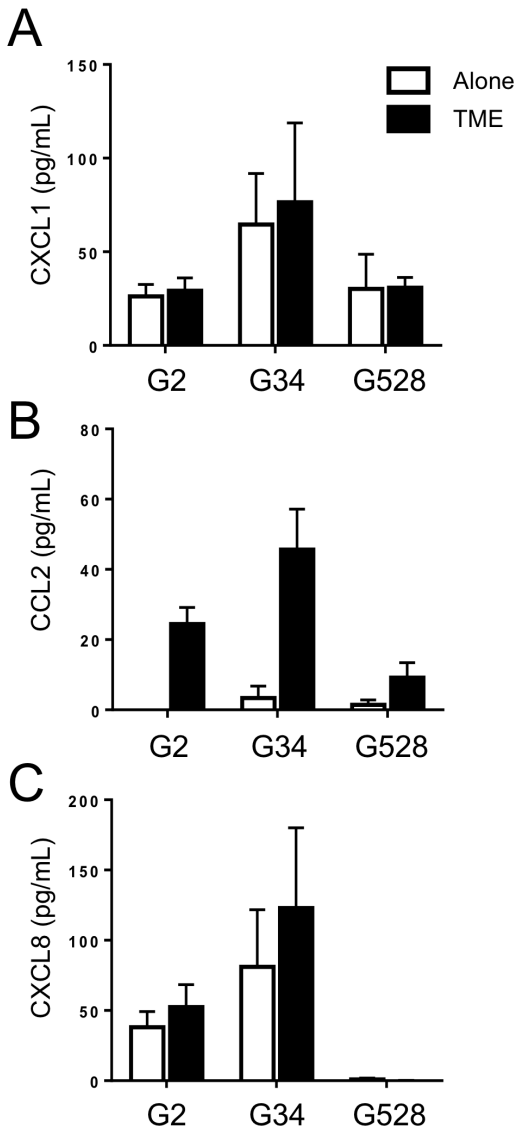

Figure 5.2: ELISA assay results. Patient-derived glioblastoma stem cells G2, G34, and G528 were incorporated into the 3D hyaluronan matrix alone (white bars) and with astrocytes and microglia (TME, black bars) and measured for A) CXCL1, B) CCL2, and C) CXCL8 secretory profiles.

5.4.2 Loss-of-function effects on malignant outcomes within the tumor microenvironment

In order to determine the effects of these cytokines, we used glioblastoma stem cells derived from patient G34 since we observed the most consistent ELISA signal for all three cytokines with these cells. Cytokines CXCL1 and CXCL8 both bind with the CXCR2

receptor, while CCL2 binds with the CCR2 receptor. Using the glioblastoma stem cells derived from patient G34, we found blocking both cytokine receptors with antibodies in the presence of the full cellular microenvironment (including astrocytes and microglia) significantly reduced the invasion of G34 cells compared to no treatment, to similar or reduced invasion percentages as the G34 glioblastoma stem cells alone in the matrix (**Figure 5.3A**). Similarly, antibody blocking of receptors CXCR2 and CCR2 in the presence of the full cellular microenvironment (including astrocytes and microglia) significantly reduced the CD71+ stemness of G34 cells compared to no treatment (**Figure 5.3B**).

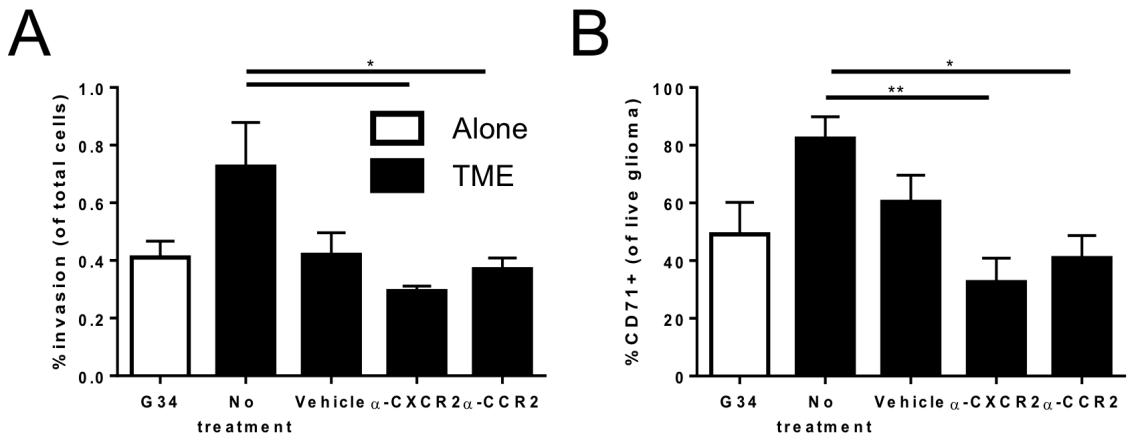

Figure 5.3: Antibody blockade of CXCR2 and CCR2 receptors. Blocking CXCR2 and CCR2 receptors in the presence of the cellular tumor microenvironment (TME, black bars) significantly reduced A) %invaded cells and B) %CD71+ stem cells compared to no treatment. * $p < 0.05$, ** $p < 0.01$.

Blocking the receptors of the cytokines does not directly measure the effects of the cytokines themselves, and multiple cytokines can bind to the same receptor (such as most CXCL8 and CXCL1 binding to CXCR2), so we then tested the effects of inhibition of each cytokine on G34 glioblastoma stem cells in a 3D matrix with or without the cellular

microenvironment. Blocking antibodies against all three cytokines did not yield significant decreases in percent invasion of G34 glioblastoma stem cells compared to no treatment, or to levels similar to the G34 glioblastoma stem cells alone in the 3D matrix (**Figure 5.4A**). This result indicates these cytokines may not play a role in glioblastoma cell invasion. When inhibiting the cytokines through blocking antibodies for each of the cytokines, we found significant reduction in CD71+ stemness of G34 glioblastoma stem cells compared to no treatment, to similar or reduced invasion percentages as the G34 glioblastoma stem cells alone in the matrix (**Figure 5.4B**).

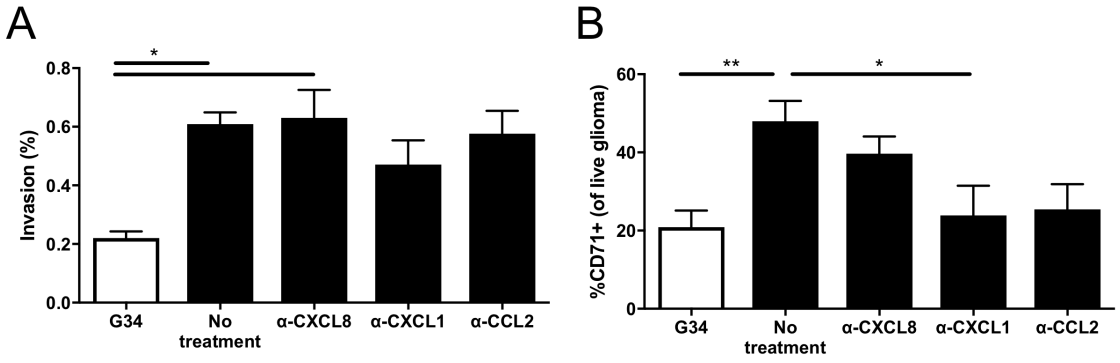

Figure 5.4: Antibody blockade of CXCL8, CXCL1, and CCL2 cytokines. Although A) % invasion was not significantly decreased by blocking CXCL8, CXCL1, or CCL2, in the presence of the tumor microenvironment (black bars), but B) %CD71+ stem cells significantly reduce with blocking CXCL1 in the presence of the tumor microenvironment and trended towards decreasing with blocking CXCL8 and CCL2 compared to no treatment. * $p < 0.05$, ** $p < 0.01$.

5.4.3 Gain-of-function effects with CCL2

We then performed gain-of-function experiments with CCL2 (MCP-1) protein and the G34 patient-derived glioblastoma stem cells to determine if this protein is sufficient for gaining the effects from the cellular microenvironment, or if there are other cytokines that may be

affecting our outcome measures. We incorporated CCL2 protein with G34 glioblastoma stem cells into the 3D matrix, and compared changes to invasion and stemness with G34 glioblastoma stem cells within the cellular tumor microenvironment, as well as G34 cells cultured with conditioned media from 2D co-culture of astrocytes and microglia. Percentage of CD71+ stemness (**Figure 5.5A**) and invasion (**Figure 5.5B**) both significantly increased with the addition of CCL2 protein, as well as with conditioned media from astrocytes and microglia, from G34 glioblastoma stem cells alone in 3D culture.

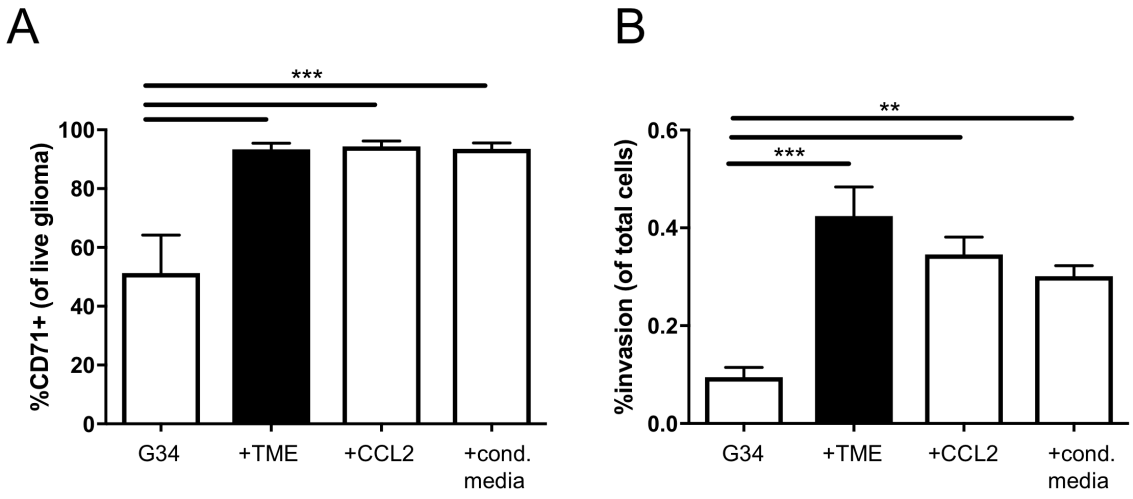

Figure 5.5: Gain of function studies through addition of CCL2 protein and conditioned media. Addition of CCL2 protein and conditioned media from astrocytes and microglia, significantly increased A) %CD71+ stemness and B) % invasion of G34 patient-derived glioblastoma stem cells in a 3D hyaluronan matrix. ** $p < 0.01$, *** $p < 0.001$.

5.4.4 Clinical relevance of cytokines of interest

To determine if the cytokines we identified in our *in vitro* samples are clinically relevant, we used chromogenic immunohistochemistry to identify the presence of the cytokines in our glioblastoma patient resections from Chapter 2, as well as non-cancerous

epileptic brain tissue resections. Collaborating neuropathologist, Dr. Jim Mandell, assessed the staining intensity of these samples and identified regions of interest as well as what cells may be responsible for the cytokines. He observed CXCL1 signal was highest within the cytoplasm of tumor regions, but in the reactive tissue was mostly nuclear (**Figure 5.6A**). There was higher signal of CCL2 in the neurons, as well as some astrocytes away from the tumor-dense regions (**Figure 5.6B**). CXCL8 staining was mostly in the serum of the tumor samples, and not within the tumor cells (**Figure 5.6C**).

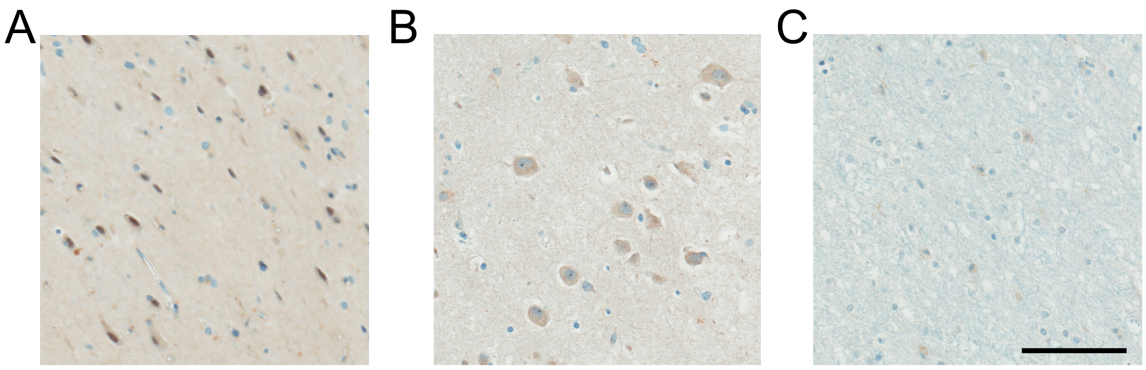

Figure 5.6: Cytokine staining via immunohistochemistry in patient tumor samples. Patient tumor resections were stained for A) CXCL1, B) CCL2, and C) CXCL8 to identify presence and clinical relevance of these cytokines as a novel therapeutic target. Scale bar = 100μm.

5.5 Discussion

It has been shown across multiple cell and tissue types that cells respond differently when moved from traditional 2D tissue culture to 3D culture with some sort of extracellular matrix [173, 174]. Cellular exposure to chemical and physical cues in three dimensions has been linked to altered chemoresistance in tumor cells, differential changes to migration and invasion of normal and malignant cell types, altered cytokine expression, differentiation

changes, and viability [175–177]. Using a novel 3D *in vitro* model, such as the ones we developed in this dissertation, provides a unique platform for studying these phenomena. Here, we demonstrated the ability our 3D *in vitro* model to identify and study novel paracrine signaling networks between glioblastoma stem cells and supporting glial cells. Glial cells in the microenvironment are thought to primarily affect cancer cells through cytokine signaling. Activated astrocytes in particular secrete a number of cytokines that could influence invasion, proliferation, and stemness [272, 273] however the current state of science has limited the ability to specifically test these pathways in a controllable manner.

Using our developed 3D i*n vitro* model, we identified two cytokines, IL-6 and IL-1, that have been previously implicated in *in vivo* glioblastoma progression [269–271], as well as three novel cytokines CXCL1, CXCL8, or CCL2 – that have not been previously discussed in the context of paracrine signaling in glioblastoma. Studies focused on glioblastoma cells alone have shown that upon exposure to radiation therapy, human glioblastoma cells increase production of CXCL8 [274, 275], and that CXCL1 contributes to increased migration [276]. Investigating these cytokines using our 3D *in vitro* model suggests the CCL2 signaling pathway contributes to stem nature, since including this protein significantly increased the %CD71+ population and blocking its receptor, CCR2 significantly decreased the %CD71+ population compared to the G34 glioblastoma stem cells alone in the 3D matrix. We were primarily interested in demonstrating the ability of our system to examine the total effect of microenvironment cytokines, so further studies would be required

to hone in on this signaling mechanism, such as using shRNA to specifically identify which cell population is providing the cytokine signaling.

Although the immunohistochemical staining in patient samples did not corroborate our *in vitro* findings, this study demonstrates not only the potential for utilizing an *in vitro* system to screen for therapeutic targets, but also the importance for returning to patient samples to determine the clinical relevance of findings. There are also many other techniques, although more expensive, that could be implemented to more specifically identify the secretory profiles of patients than immunohistochemistry on tumor resections, such as through serum sampling, Luminex assays, and genomic analyses. Furthermore, our *in vitro* model is specifically design to mimic the invasive front of glioblastoma tumors. Although neurosurgeons typically resent a few extra millimeters of tumor border in an effort to remove the invasive front of the tumor, there is no guarantee that the region has been removed [11]. While we performed staining on samples with the "reactive" regions described in Chapter 2 to represent more of the invasive front, this region is particularly small compared to the majority of the tumor bulk resected from patients. As such, it is difficult to draw conclusions from analyses of this small area of interest, but given the inability to identify and resect the tumor invasive edge, it is currently the best means for studying the invasive edge. Our inability to conclusively identify the presence of our cytokines within patient samples via immunohistochemistry does not mean these cytokines do not play an important role in patients.

Chapter 6: Probing glioblastoma microenvironment contributions to therapeutic response

6.1 Summary

Current therapeutic screening strategies examine only cell death, and dismiss the important microenvironment contributions that are inherent to native human tissue. As such, we used our 3D *in vitro* human microenvironment model to demonstrate therapeutic response in a variety of ways. We replicated the standard-of-care treatment regimen of radiation therapy with temozolomide chemotherapy on varying microenvironment compositions, and found altering the ratios of glial cells with standard of care treatment significantly minimized cell survival and invasion but did not minimize Ki67+ proliferation or CD71+ stemness via design of experiment analyses. We then presented our model as a screening platform by dosing with a panel of six clinically relevant chemotherapeutics – BCNU, carboplatin, etoposide, irinotecan, methotrexate, and temozolomide, and compared our *in vitro* response with *in vivo* murine xenograft survival. We found *in vitro* invasion outcome measurements trended towards correlative with *in vivo* overall survival. This chapter demonstrates the versatility of our tissue-engineered model through assessing and applying diverse therapeutic strategies.

6.2 Introduction

Brain cancers are notoriously difficult to treat, and the most common and deadly type, glioblastoma, is particularly resistant to therapies [3]. Despite large improvements in survival for patients of other cancers, glioblastoma patient survival has not significantly improved in the last decade [2]. The advancement of standard of care glioblastoma treatment to combine rounds of radiation therapy and oral temozolomide chemotherapy after immediate surgical resection of the tumor bulk, has only increased the median survival time after first diagnosis to 16 months [3, 4]. Glioblastoma tumors always recur, and thus this cancer is essentially considered incurable.

Glioblastoma is characterized by diffuse invasion of tumor cells from the primary tumor bulk in the surrounding healthy brain tissue. These invading cells persist after surgical resection, and are considered the cause for inevitable recurrence [6–8]. Furthermore, these tumor cells interact with the surrounding brain tissue to create a tumor microenvironment (TME). The tumor microenvironment has been implicated in multiple aspects of therapeutic failure including enrichment of cancer stem cells, apoptosis resistance, increasing proliferation, promoting invasion, and limited drug transport to tumor cells [26, 27]. Glioblastoma, in particular, is a cancer that simultaneously grows and invades, making it highly integrated and difficult to separate from surrounding brain parenchyma. Current research on the cellular glioblastoma tumor microenvironment focuses only on the contributions of either astrocytes or microglia [32, 42, 244, 245] to glioma cell invasion as well as glioblastoma patient survival. Previous studies in other cancers have indicated the

protective ability of parenchymal cells to treatment on cancer cells [277], indicating the importance of examining the effects of the microenvironment on therapeutic response.

Selection of a therapeutic strategy for recurrent GBM depends solely on physician experience and a trial-and-error approach with the readily available chemotherapeutic drugs. The use of adjuvant chemotherapy is beneficial for about 25% of GBM patients, but even in these cases, there is always recurrence and eventual death [18]. No strategic selection process is in place for brain cancer therapy. In other cancers, several strategies have been experimentally employed to predict patient outcomes prior to treatment – genomic profiling, tissue microarrays with molecular profiling, and therapeutic testing of either single treatment monolayer (2D) cell cultures to examine cell death or patient-derived spheroid cell cultures to assess spheroid shrinkage [25]. These techniques model the tumor bulk and dismiss the critical interactions between the tumor and surrounding stroma; and if applied to glioblastoma, cannot accurately represent the cancer in the native human brain environment. In addition to the lack of microenvironmental stimuli, current screening strategies only examine cell death as a determinant of therapeutic selection. However, glioblastoma recurrence occurs not just because the cancer cells survive after therapy; they can also repopulate or invade into the surrounding tissue to develop new tumors [23]. Therefore, it is important to assess outcomes other than cell death in response to therapy, such as invasion, proliferation, and selection for cancer stem cells, to better understand therapeutic response and glioblastoma progression.

By using our *in vitro* system developed in Chapter 3 that mimics patient GBM microenvironments, we may be able to draw conclusions about the heterogeneity of therapeutic responses to this disease, particularly in regards to the microenvironment. We can use our human 3D *in vitro* microenvironment system to test and screen therapies by identifying multiparametric therapeutic response in an environment more representative on native in vivo tissue. Since we identified it as an important contributor to glioblastoma malignancy in Chapter 4, we will utilize interstitial flow to dose our 3D *in vitro* model in a physiologically-relevant manner. We believe this system as a whole, patient-derived glioblastoma stem cells with human astrocytes and microglia in a 3D hyaluronan matrix with chemotherapeutic dosing via gravity-driven interstitial flow, will be more beneficial than traditional single cell screening assays and animal models for identifying therapies that can be successful when translating to patients in the clinic.

6.3 Materials and methods

6.3.1 Cell lines and culture

Patient-derived G34 and G528 human glioblastoma stem cells (GSCs) were maintained in non-treated culture flasks in Neurobasal media (Life Technologies) supplemented with 1% B27, 0.5% N2, 0.01% FGF, 0.1% EGF, 0.3% L-Glutamine, and 1% penicillin-streptomycin. Human cortical astrocytes were purchased from Sciencell and cultured according to manufacturer's suggested protocol. Human SV40-immortalized microglia were purchased from Applied Biological Materials, Inc and cultured in Dulbecco's Modified Eagle's Medium

(DMEM; Life technologies) with 10% FBS. All cell lines were maintained at 37°C in a humidified incubator containing 5% CO_2 and 21% O_2.

6.3.2 Development of survival prediction model

A proportional hazards model was used to model overall survival. Additional tests were performed to ensure appropriateness of the proportional hazards assumption. Survival modeling and testing the proportional hazards assumption were performed using the "phreg" procedure in SAS (version 9.4).

6.3.3 Three-dimensional cell assays

Experiments were carried out with 8µm pore size tissue culture inserts (Sigma Aldrich). Cells were fluorescently labeled with Cell Tracker dyes (Life technologies) and Vybrant dyes (Life technologies) according to manufacturer suggested protocol. Glioblastoma stem cells ($5.0x10^5$), astrocytes ($8.0x10^4$), and microglia ($8.0x10^4$) were seeded in 75 µL gel (0.2% hyaluronan; ESI Bio) and 0.12% rat tail collagen I (Corning) based on ratios quantified from human sections. Gels solidified at 37°C in a humidified incubator containing 5% CO_2 and 21% O_2 for 2 hr, then experimental media was added to the top and bottom of each tissue culture insert such that media was level inside and outside of the insert.

For studies adjusting the microenvironment ratios, the amount of G528 patient-derived glioblastoma stem cells, astrocytes, and microglia were adjusted based on relevant quartile ratios (**Table 6.1**) identified from our survival curve studies presented in Chapter 3. Specifically, the ratio of one glial population was raised or lowered while the other was

held at the middle with a constant number of glioblastoma stem cells ($5.0x10^5$). The cell populations were seeded in the same gel matrix recipe described above.

Table 6.1: Number of cells incorporated into ratiometric conditions.

	Low (25%)	Mid (50%)	High (75%)
Astrocytes	$6\ x10^4$	$8\ x10^4$	$11\ x10^3$
Microglia	$5.5\ x10^3$	$8\ x10^4$	$11.7\ x10^3$

6.3.4 Invasion assay and flow cytometry

At the end of time course (18-48hr), gels were removed from tissue culture inserts and digested using Roche Liberase DL (Sigma Aldrich). Cells migrating through were identified by staining with DAPI (Invitrogen), counting five representative fields per insert, and reported as total cells invaded/total cells seeded x 100 (%) for each insert. Cells remaining post-gel digestion were stained for Live/dead (Life technologies), CD71 (eBioscience), and Ki-67 (eBioscience) according to manufacturer's suggested protocol. Flow cytometry was performed using Guava easyCyte 8HT (Millipore) and analyzed using guavaSoft2.7 (Millipore).

6.3.5 Therapeutic dosing

To replicate the standard of care treatment regimen, 24hrs after gels were seeded into transwells, the plate was gamma irradiated at a dose of 2Gray via the University of Virginia Radiology department aSARRP device (Xstrahl Life Sciences) with a collimator 137Cs gamma beam irradiator (Mark 1 Model 68A Dual). The following day, 100 μM temozolomide

chemotherapy was flowed through gels with a pressure head of 1 cm leading to an average velocity of 0.7 μm/s through the cell/gel compartment.

For screening studies, 24hrs after gels were seeded into tissue culture inserts, a range of concentrations of BCNU, carboplatin, etoposide, methotrexate, irinotecan, and temozolomide chemotherapies flowed through gels with a pressure head of 1 cm leading to an average velocity of 0.7 μm/s through the cell/gel compartment. Chemotherapeutic-free media was added to the bottom compartment. After 24hours of dosing, media that had flowed through the gel into the bottom compartment was carefully removed, and the same range of concentrations of each drug was added again at the top to reestablish the pressure head for another 18hrs of dosing.

6.3.6 Tumor inoculation in animal studies

8-10week old male NOD-SCID mice were inoculated with 10,000 glioblastoma stem cells derived from patient G34 (n=7 per group), or 400,000 glioblastoma stem cells derived from patient G528 (n=6 per group), in 10μL of neurobasal media supplemented with N2, B27 without vitamin A, glutamax, and penicillin-streptomycin 2mm lateral and posterior to bregma at a depth of 2.6mm. 7 days after inoculation, chemotherapeutics were injected intraperitoneally according to the following table (**Table 6.2**).

Table 6.2: Dosing schedule for murine xenograft survival studies

Drug	*Schedule*	*Dose*	*Citation*
BCNU	Days 7, 10	25mg/kg	[278]
Carboplatin	Days 7, 10	10mg/kg	[279]
Etoposide	Days 7, 8, 9, 10, 11	3 mg/kg	[236]
Irinotecan	Days 7, 8, 9, 10, 11	4 mg/kg	[280]
Methotrexate	Days 7, 10	25 mg/kg	[279]
Temozolomide	Days 7, 8, 9, 10, 11	5 mg/kg	[281]

Animals were assessed daily for signs of distress, and euthanized accordingly. All animal procedures were conducted in accordance with the University of Virginia Institutional Animal Care and Use Committee (Charlottesville, VA).

6.3.7 Statistical analysis and data representation

All experiments were run independently at least three times, and each experiment had three technical replicates per experimental condition averaged to yield the value for a single n used in statistical analyses. Statistical analyses were performed using Graphpad Prism Software. Data were analyzed using one-way or two-way ANOVA tests. Averages of replicates in experiments were used to determine statistical significance. All graphs were generated using Graphpad Prism. For all data, *$p<0.05$, **$p<0.01$, and ***$p<0.001$, and

graphs are given as mean ± standard error of the mean. JMP software (SAS) was used to identify key differences among experimental conditions. The classical screening design was fit for standard least squares to determine which factors have the main effect, and the resulting effects were summarized. $p<0.05$ is considered statistically significant. Figures were generated using Adobe Illustrator.

6.4 Results

6.4.1 Changing the microenvironment affects standard of care therapeutic response

All glioblastoma patients receive standard of care radiation and temozolomide therapies so the varying differences in overall survival for each patient is hardly predictable. Since we found patient-to-patient heterogeneity in cellular microenvironment compositions and specific combinations of these microenvironment components could indicate better or poorer overall survival after therapy in Chapter 2, we decided to further take advantage of the tunability feature of our *in vitro* model developed in Chapter 3 by systematically testing combinations of the glial cells in the microenvironment and their effect on measures of malignancy after standard of care therapy.

We generated new predictive survival curves based on the quartiles of astrocyte and microglia cell counts, instead of cell coverage that was used in the predictive curves from Chapter 2. These cell-count predictive survival curves suggest changing the proportions of astrocytes has little effect on overall patient survival (**Figure 6.1A**), whereas changing the ratio of microglia does affect overall patient survival (**Figure 6.1B**). Specifically, the model

suggests a 0.036 increase in the proportion of microglia is associated with a 10% increase in hazard of death (hazard ratio: 1.1; 90% confidence interval: 0.846 1.149). The increase of 0.036 is 10% of the range of values observed for each of these variables. A 0.036 increase in the proportion of astrocytes is associated with a 1.4% decrease in hazard (Hazard ratio: 0.986; 90% confidence interval: 0.846 to 1.149).

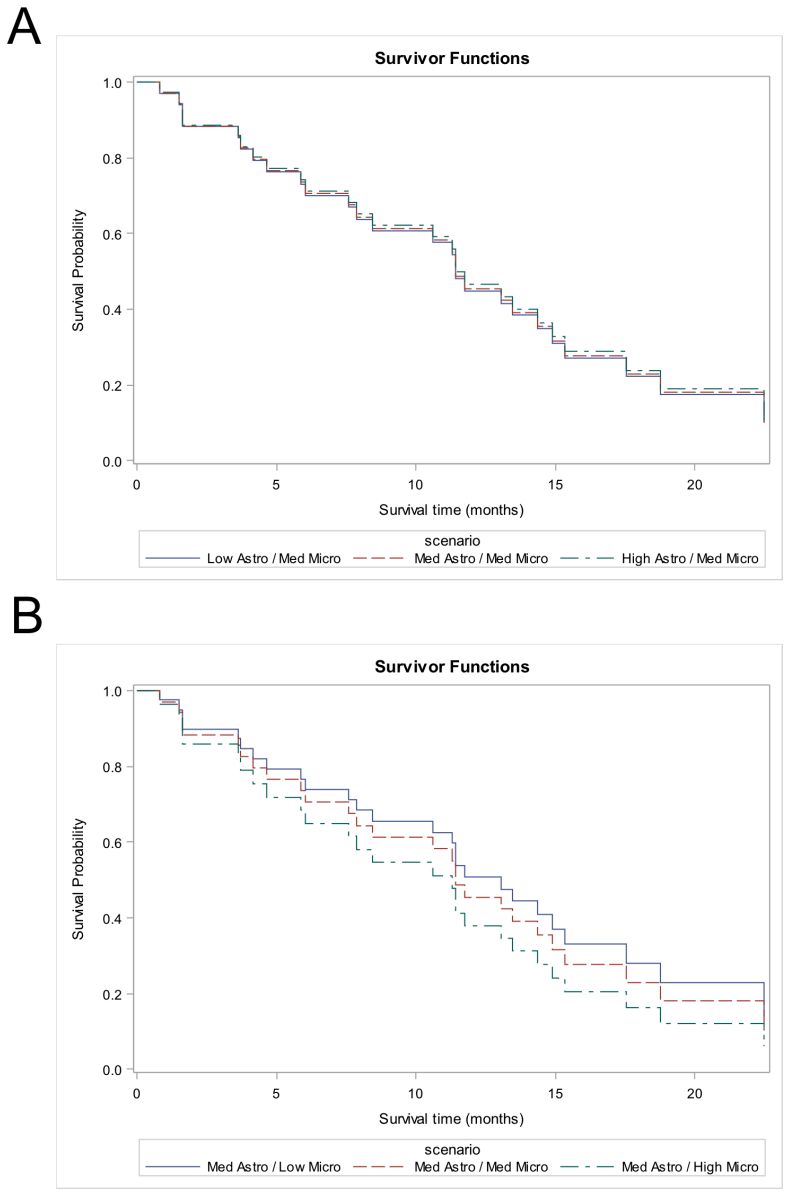

Figure 6.1: Predictive survival curves from adjusting glial cell ratios. A) Adjusting ratios of astrocytes to the 75% (high) quartile (green line) and 25% (low) quartile (blue line)

did not significantly alter patient survival curves from the baseline 50% (med) quartile (red line). B) Adjusting ratios of microglia to the 75% (high) quartile decreased patient survival (green line) and to the 25% (low) quartile increased patient survival (blue line) from the baseline 50% (med) quartile (red line).

In Chapter 4, we identified glioblastoma stem cells derived from patient G528 as more malignant when cultured alone, and less malignant when cultured with the full cellular microenvironment, which was also reflected in the significantly higher median overall survival of the murine xenografts. Because G528 glioblastoma stem cells appear becomes less malignant within a physiologically relevant microenvironment than our G34 glioblastoma stem cells, we thought it would be interesting to see how manipulating the microenvironment might affect the malignancy of the G528 glioblastoma stem cells, and how that can affect the response to standard of care therapy. From our predictive survival curves (**Figure 6.1**), we hypothesized altering astrocyte composition will not significantly affect measures of malignancy, while altering microglia composition will significantly affect the measures.

We treated gels incorporating varying ratios of astrocytes and microglia with a constant number of G528 glioblastoma stem cells, with 2Gy radiation therapy (RT) followed by gravity-driven fluid flow of 100μM temozolomide (TMZ) chemotherapy mimicking interstitial flow. We found a significant decrease in cell survival ($p < 0.0001$) when treating with the standard of care (RT+TMZ, black bars) compared to no treatment (white bars), although no significant differences were found across the varying microenvironments (**Figure 6.2A**). When looking at invasion without the standard of care treatment, we found invasion of G528 glioblastoma stem cells changed depending on the microenvironment

composition, with lower microglia present leading to decreased invasion, while increased microglia present lead to increased invasion (**Figure 6.2B**, white bars). Adjusting the astrocyte composition did not significantly change the invasion of G528 glioblastoma stem cells. Treating with the standard of care significantly decreased invasion ($p = 0.0047$) across all the microenvironment compositions, with relatively similar invasion of G528 glioblastoma stem cells for all conditions (**Figure 6.2B**, black bars). While the microenvironment composition did not significantly affect the changes in CD71+ stemness of G528 glioblastoma stem cells with or without standard of care treatment, there was an increase in CD71+ stemness of G528 glioblastoma stem cells with standard of care treatment, suggesting the standard of care treatment may be selecting for a more malignant population of cancer cells that are resistant to therapies (**Figure 6.2C**). Standard of care therapy significantly increased the Ki67+ proliferation of G528 glioblastoma stem cells over non-treated across all microenvironment conditions (**Figure 6.2D**, $p = 0.0005$). The microenvironment condition with high microglia resulted in particularly high population of Ki67+ proliferating G528 glioblastoma stem cells, while adjusting astrocyte populations did not significantly alter the increased Ki67+ proliferating population.

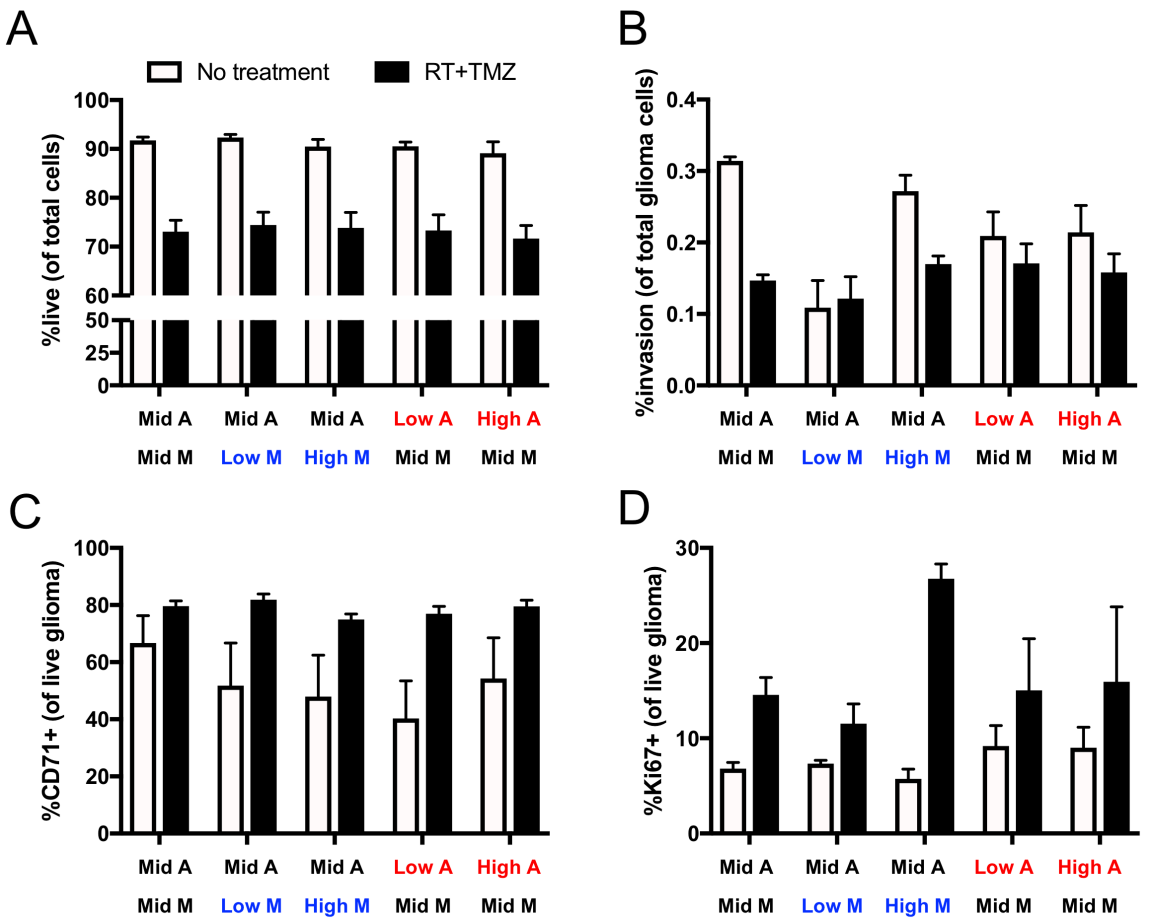

Figure 6.2: Effects of standard of care therapy and altering microenvironment composition on measures of glioblastoma malignancy. A) Treating with the standard of care radiation therapy and temozolomide chemotherapy (RT+TMZ, black bars) significantly reduced cell survival across all microenvironment conditions compared to no treatment (white bars). $p < 0.0001$. Standard of care treatment reduced B) invasion, but increased C) CD71+ stemness as well as D) Ki67+ proliferation across multiple microenvironment conditions.

These *in vitro* results support our predicted survival curves findings and hypotheses. Altering the astrocyte ratios did not significantly change invasion, proliferation, stemness, or death of the glioma cells after standard of care therapy compared with the baseline average model. Furthermore, increasing the microglia ratio to the upper quartile increased invasion of G528 glioblastoma stem cells, and significantly increased the Ki67+ proliferation

of G528 glioblastoma stem cells after standard of care therapy. With treatment, the goal is to minimize each of the malignant outcomes, i.e. minimize cell survival, invasion, proliferation, and stemness, in order to prevent recurrence. When we incorporated this data into a classical screening design of experiment analysis to determine how much of an effect the ratios had on each outcome measure, we found altering the ratios of glial cells with standard of care treatment significantly minimized cell survival ($p = 0.0489$) and invasion ($p = 0.00707$) but did not minimize proliferation ($p = 0.94744$) or stemness ($p = 0.63701$).

6.4.2 Potential for in vitro therapeutic response to predict in vivo survival using G34 patient-derived glioblastoma stem cells

Having demonstrated the use of our system for assessing standard of care therapeutic response as well as the potential for identifying novel therapeutic targets, we next utilized our 3D *in vitro* microenvironment model as a platform to screen chemotherapeutics. Collaborating neuro-oncologist, Dr. Benjamin Purow, selected a panel of clinically relevant chemotherapeutics of interest – BCNU, carboplatin, irinotecan, temozolomide, methotrexate, and etoposide – that all pass through the blood brain barrier and are used in the clinic to treat glioblastomas as well as other types of brain tumors. Specifically, temozolomide is the standard of care, while BCNU, irinotecan, and carboplatin are used as second-line treatments. Etoposide and methotrexate are used to treat other brain tumors, such as metastases to the brain. Temozolomide and BCNU are both alkylating agents [116]. Irinotecan and etoposide are topoisomerase inhibitors [117, 118], and carboplatin is a platinum agent [119].

We first applied the panel of chemotherapeutics to our glioblastoma stem cells derived from patient G34 alone in spheroid culture to develop 8-point dose-response curves for death, via live/dead flow cytometry staining, and determine the IC50 for cell survival, which is the dose at which half of the cell survival is inhibited (**Figure 6.3A**). Using physiologically-relevant interstitial flow, which we had identified as a strong contributor to malignant outcomes in Chapter 4, we then dosed our full *in vitro* model, using G34 glioblastoma stem cells with astrocytes and microglia, with a range of concentrations of the same panel of chemotherapeutics to determine the IC50 for cell survival as well (**Figure 6.3B**). We found significantly different cell survival IC50 doses between the G34 glioblastoma stem cells in spheroids and within our full 3D *in vitro* model. These findings indicate a significantly different dose is necessary to kill half of the cells when the cancer cells are along growing in spheroids than when the cancer cells are in a 3D matrix with glial cells, demonstrating one possible reason why therapies identified with spheroid screening assays fail upon translation to patients.

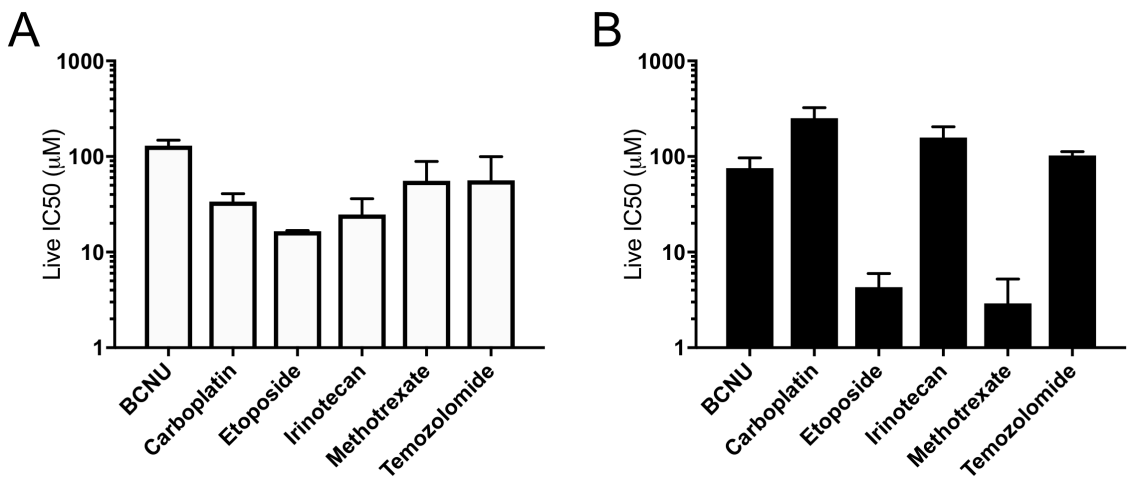

Figure 6.3: Comparison of cell survival of G34 glioblastoma stem cells IC50 across six chemotherapeutics. G34 glioblastoma stem cells have significantly differing cell survival IC50 when treated in A) traditional spheroid assay compared to B) within our 3D *in vitro* microenvironment model.

If we were to hypothesize how effective each of the chemotherapeutics are based on the cell survival IC50 for the spheroid data, we would think etoposide is the most effective, followed by irinotecan, carboplatin, methotrexate, temozolomide, and BCNU as the lease effective of the six chemotherapeutics. However, if we utilized the cell survival IC50 for the *in vitro* microenvironment model, we could hypothesize methotrexate is the most effective, then etoposide, BCNU, temozolomide, irinotecan, and carboplatin as the least effective.

To determine whether the spheroid data or our 3D *in vitro* model is more predictive of in vivo survival, we orthotopically implanted G34 patient-derived glioblastoma stem cells into NOD-SCID mice. After seven days, tumors were visible by MRI, and we began intraperitoneal injections of chemotherapeutics. Mice were dosed for five days according to the schedule listed in Table 6.2 (**Figure 6.4A**). At the end of the survival study, we found

statistically significant differences in overall survival across many of the cohorts (**Figure 6.4B, C**). The median overall survival was highest for the two alkylating agents, BCNU (25 days) and temozolomide (16 days), which are also the two drugs used most frequently in clinic for glioblastoma patient treatment. Topoisomerase inhibitors irinotecan (16 days) and etoposide (15 days) were the next highest median overall survival class, while carboplatin (15 days) and methotrexate (14 days) did not significantly improve median overall survival over the vehicle treatment (14 days). These trends were almost the complete opposite of what we had hypothesized based on our 3D *in vitro* model data for cell survival IC50. Since the trends also did not corroborate our hypothesis from the spheroid data, we believed there were likely many other factors contributing, other than simply cell survival post-treatment.

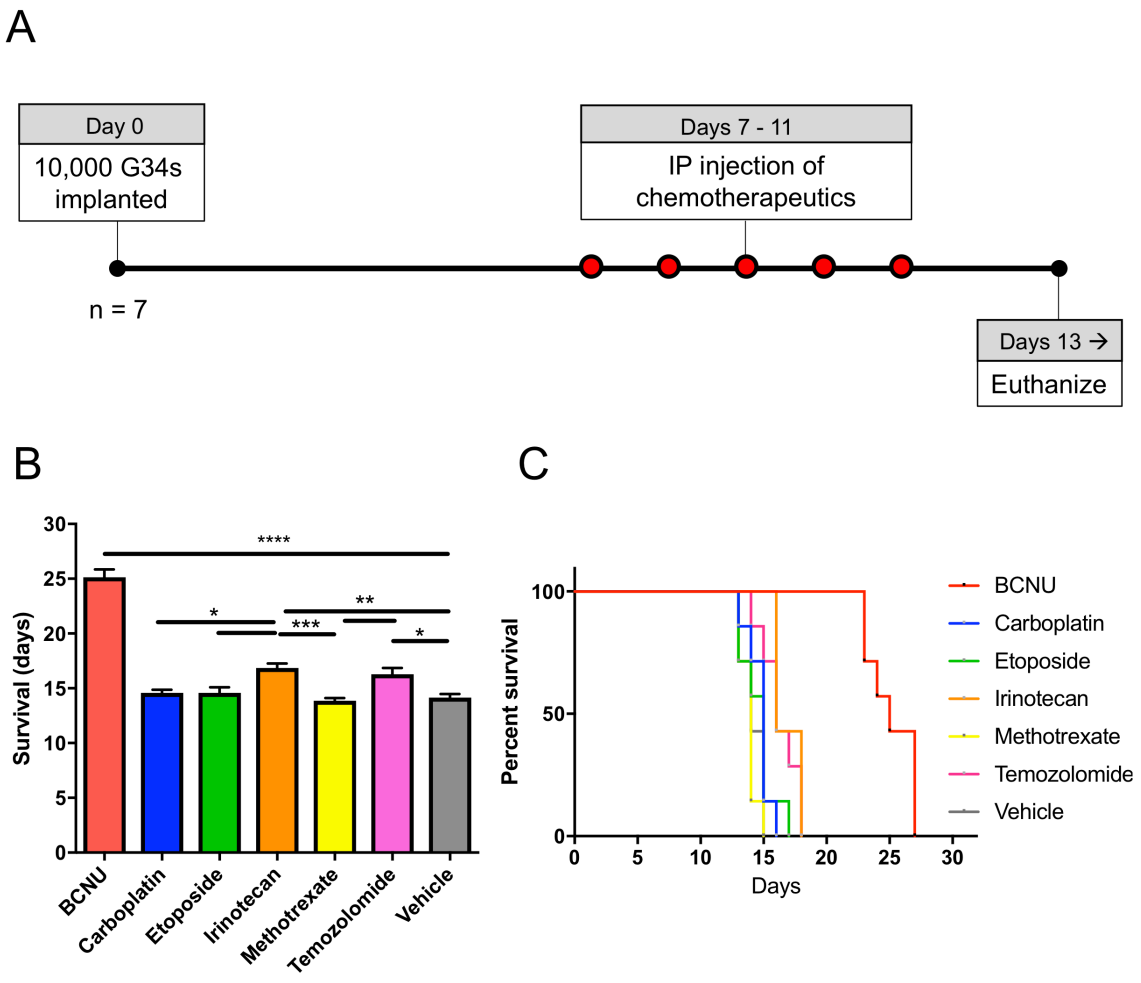

Figure 6.4: G34-inoculated murine xenograft survival study. A) 10,000 G34 glioblastoma stem cells were orthotopically implanted into seven groups of seven mice. Mice received five days of intraperitoneal chemotherapeutic injections according to Table 6.2. Overall survival of each cohort as B) bar graphs and C) Kaplan-Meier curves. *p<0.05, **p<0.01, ***p<0.001, ****p<0.0001.

Because of this, we expanded our *in vitro* model analysis to assess our other outcome measures - proliferation (Ki67+), stemness (CD71+) and invasion (%invasion) – in response to the panel of clinically relevant chemotherapeutics to determine how the chemotherapeutics may be differentially affecting these commonly overlooked outcomes. While we tested a wide range of doses for each chemotherapeutic, we specifically examined

the effects at the dose below the cell survival IC50 as we wanted to see the effects of the drug without significantly diminishing our cells from cytotoxicity. This dose is also the most clinically-relevant dose, in order to minimize whole body toxicology problems. At the dose below the cell survival IC50, we normalized the response to the response of the vehicle dosing and present each outcome as a fold change from the vehicle (**Figure 6.5**). BCNU resulted in the highest median overall survival *in vivo* and our *in vitro* data indicates while there was an increase in CD71+ stem populations in the dose of BCNU below the cell survival IC50 over the vehicle, Ki67+ proliferation was slightly lower, and invasion was about the same as the vehicle (**Figure 6.5A**). Methotrexate was the worst performing drug *in vivo*, yet our *in vivo* data suggests there was little difference in CD71+ stemness, Ki67+ proliferation, and invasion at the dose of methotrexate below the cell survival IC50 over the vehicle (**Figure 6.5E**). With the standard of care temozolomide, we saw similar trends as methotrexate *in vitro* – little difference in CD71+ stemness, Ki67+ proliferation, and invasion at the dose of temozolomide below the cell survival IC50 over the vehicle (**Figure 6.5F**). Comparing all of our *in vitro* data with the median overall survival in xenografts found increasing invasion correlated with improved overall survival (**Figure 6.6**, $\rho = 0.74$, $p = 0.096$), while all other *in vitro* outcomes did not correlate ($p > 0.2$).

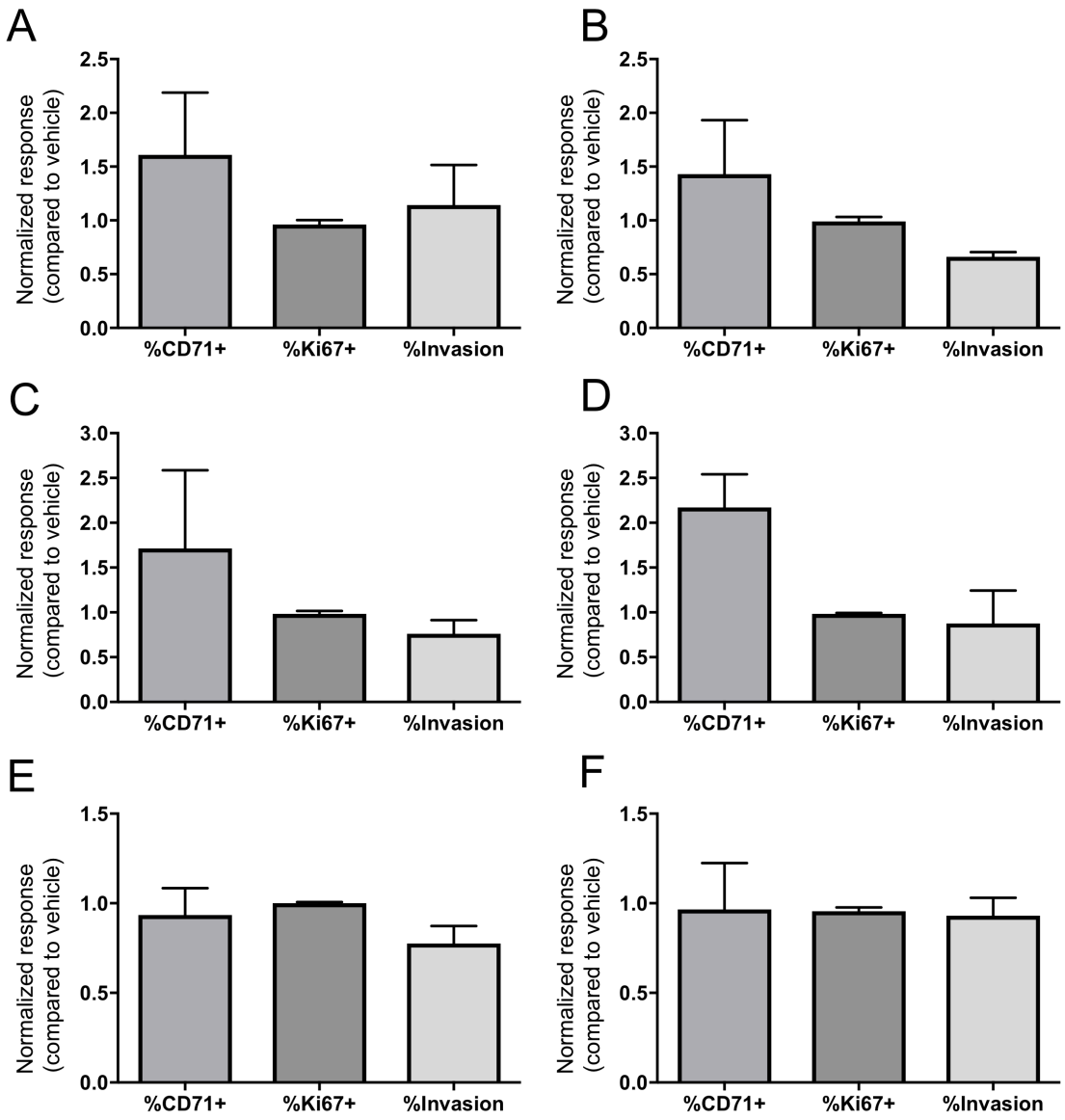

Figure 6.5: Therapeutic response of G34 glioblastoma stem cells in our microenvironment model for three parameters with six different chemotherapies. Percentage of CD71+ stem cells, Ki67+ proliferating cell, and cells invaded through the porous membrane at the dose below the IC50 for each drug normalized to the corresponding response with vehicle dosing for six clinically relevant chemotherapeutics – A) BCNU, B) carboplatin, C) etoposide, D) irinotecan, E) methotrexate, and F) temozolomide.

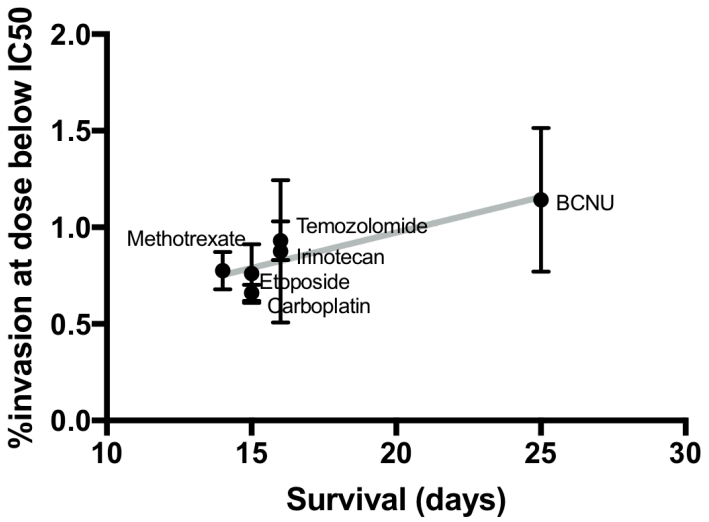

Figure 6.6: Comparison of G34 *in vitro* invasion measurements with xenograft overall survival. For G34 glioblastoma stem cells, there was a trend for increased in vitro invasion correlating with xenograft overall survival for our panel of six chemotherapeutics ($\rho = 0.74$, $p = 0.096$).

6.4.3 Expansion of in vitro and in vivo studies to G528 patient-derived glioblastoma stem cells

We then expanded our analyses to determine if we could utilize our *in vitro* therapeutic response assessment to predict overall survival using our G528 patient-derived glioblastoma stem cells, which were previously found to be less aggressive in the microenvironment than G34 in Chapter 4. Similar to the G34 glioblastoma stem cells, we found significantly different IC50s for cell survival ($p < 0.0001$) when the G528 glioblastoma stem cells were grown in spheroids (**Figure 6.7A**) compared to when they were grown in 3D incorporating astrocytes and microglia (**Figure 6.7B**). The cell survival IC50 data for spheroids suggests methotrexate as the most effective, followed by etoposide, carboplatin, BCNU, temozolomide, and finally irinotecan as the least effective. The cell survival IC50 data for

our 3D *in vitro* model suggests etoposide is the most effective, followed by carboplatin, irinotecan, BCNU, methotrexate, and finally temozolomide as the least effective. This pattern is of concern particularly because both spheroids and our 3D *in vitro* model predicted temozolomide as not effective in inhibiting cell survival, yet this is the chemotherapeutic given to all glioblastoma patients as part of the standard of care.

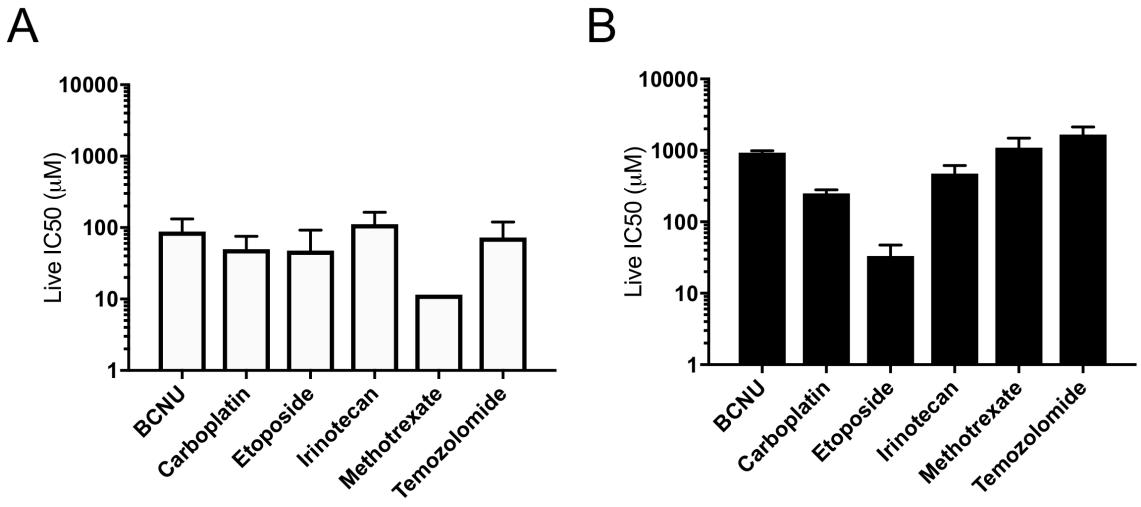

Figure 6.7: Comparison of cell survival of G528 glioblastoma stem cells IC50 across six chemotherapeutics. G528 glioblastoma stem cells have significantly differing cell survival IC50 when treated in A) traditional spheroid assay compared to B) within our 3D *in vitro* microenvironment model.

Because of this, we then expanded our analysis to assess invasion, stemness, and proliferation to determine if these differential outcomes may be more indicative than simply the cell survival. We again tested a wide range of doses for each chemotherapeutic but focused the analysis on the effects at the dose below the cell survival IC50 normalized to the effect using the vehicle dosing. At the dose below the cell survival IC50, we saw different effects than with our G34 patient-derived glioblastoma stem cells depending on the drug

(**Figure 6.8**). While BCNU (**Figure 6.8A**) and methotrexate (**Figure 6.8E**) trended similarly between G34 and G528, the other four drugs did not. Since invasion appeared as the most correlative response with our G34 studies, it was of interest that invasion increased at the dose below the cell survival IC50 over the vehicle with carboplatin (**Figure 6.8B**), etoposide (**Figure 6.8C**), and irinotecan (**Figure 6.8D**), but decreased at the dose below the cell survival IC50 over the vehicle for temozolomide (**Figure 6.8F**).

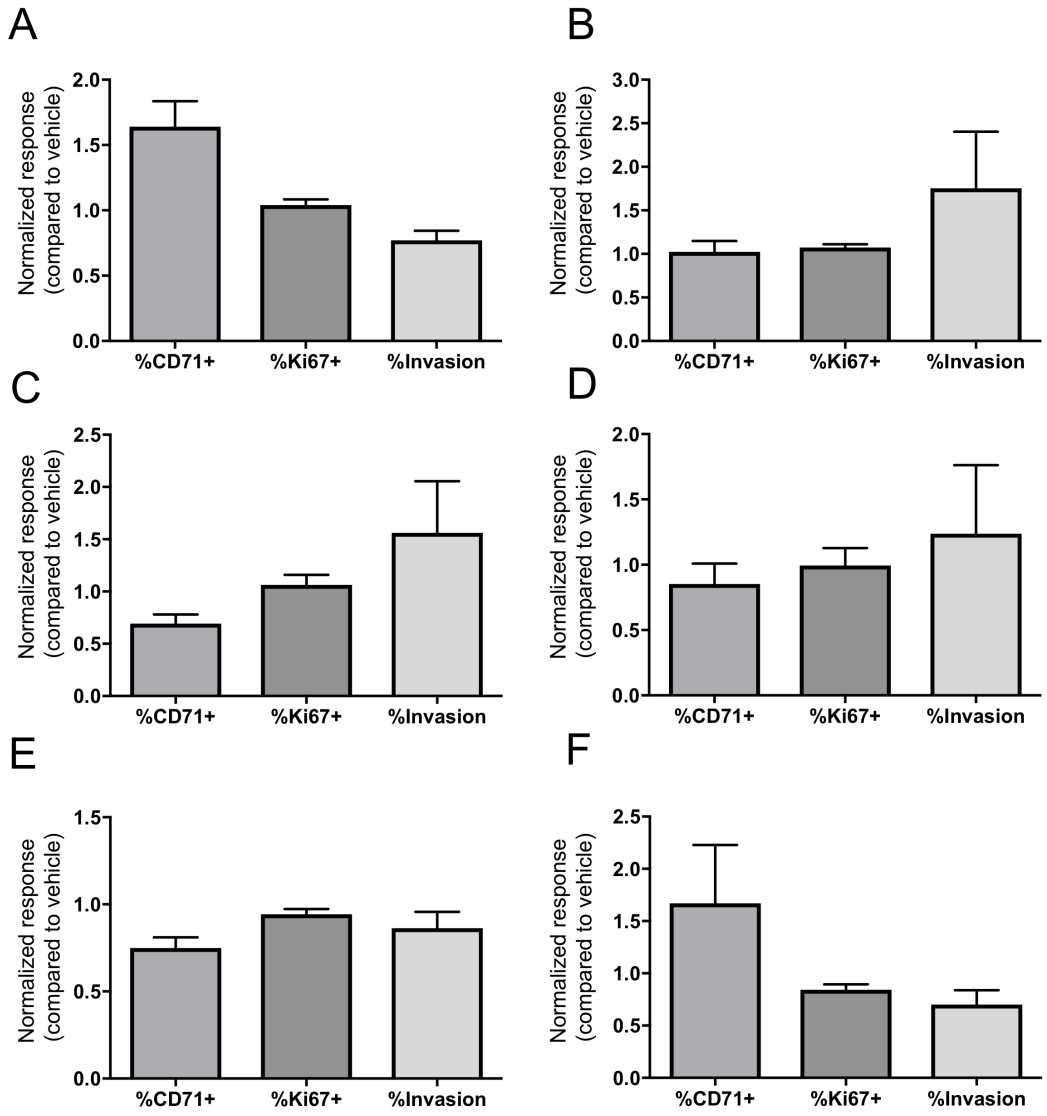

Figure 6.8: Therapeutic response of G528 glioblastoma stem cells in our microenvironment model for three parameters with six different chemotherapies.

Percentage of CD71+ stem cells, Ki67+ proliferating cell, and cells invaded through the porous membrane at the dose below the IC50 for each drug normalized to the corresponding response with vehicle dosing for six clinically relevant chemotherapeutics – A) BCNU, B) carboplatin, C) etoposide, D) irinotecan, E) methotrexate, and F) temozolomide.

For our *in vivo* study, we conducted a smaller study using chemotherapeutics of differing mechanisms – carboplatin (platinum agent), irinotecan (topoisomerase inhibitor), and temozolomide (alkylating agent) (**Figure 6.9**). These three drugs also had differing *in vitro* effects between our glioblastoma stem cells derived from G34 and G528 when incorporating into our 3D *in vitro* microenvironment model. 400,000 G528 glioblastoma stem cells were orthotopically implanted into murine xenografts for tumors to be visible via MRI by day 7 when intraperitoneal chemotherapeutic injections began (**Figure 6.9A**). The median overall survival for G528 xenografts treated with carboplatin (24 days) did not improve over the vehicle (25.5 days), while irinotecan improved survival to 31 days, and temozolomide increased median overall survival to 47 days (**Figure 6.9 B, C**). Each cohort's overall survival times were significantly higher ($p < 0.0001$) than the corresponding cohort with G34-inoculation, further reflecting the less aggressive phenotype of G528 glioblastoma stem cells when incorporated in tissue. Interestingly, while increased *in vitro* invasion was correlated with increased overall survival *in vivo* for the G34 study, the opposite was observed with our G528 study, although not statistically significant (**Figure 6.10**).

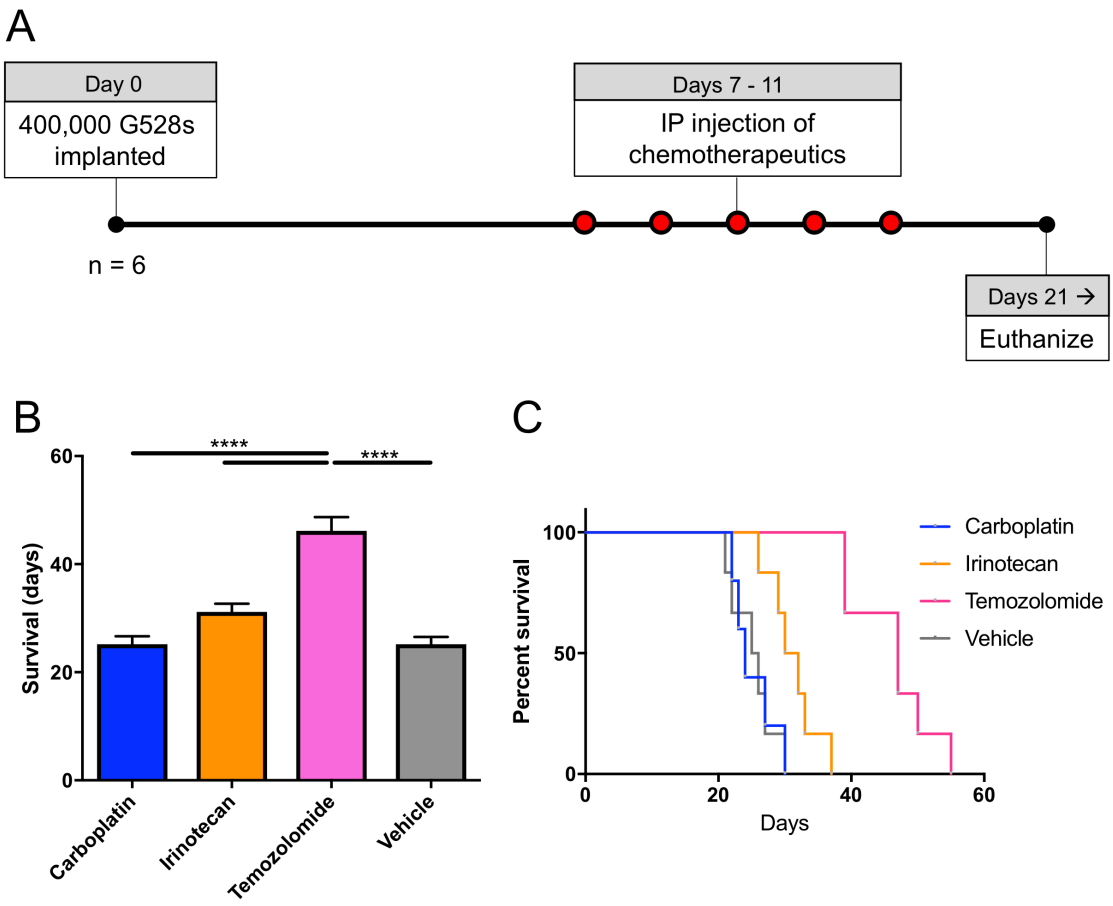

Figure 6.9: G528-inoculated murine xenograft survival study. A) 400,000 G528 glioblastoma stem cells were orthotopically implanted into four groups of 6 mice. Mice received five days of intraperitoneal chemotherapeutic injections according to Table 6.2 for carboplatin, irinotecan, temozolomide, and vehicle treatments. Overall survival of each cohort as B) bar graphs and C) Kaplan-Meier curves. ***p<0.001.

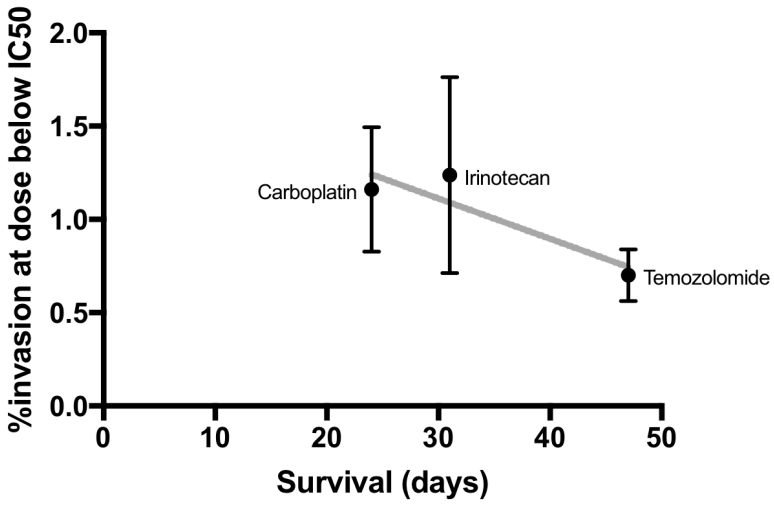

Figure 6.10: Comparison of G528 *in vitro* invasion measurements with xenograft overall survival. For G528 glioblastoma stem cells, there was a trend for decreased in vitro invasion correlating with xenograft overall survival for carboplatin, irinotecan, and temozolomide chemotherapies.

6.5 Discussion

This chapter presents the first steps for using our 3D *in vitro* human microenvironment model to test and identify therapeutic response in a variety of applications. We utilized our system to demonstrate mimicking the standard of care treatment combining radiation therapy with temozolomide chemotherapy, as well as screen a panel of clinically-relevant chemotherapeutics. Finally, we conducted murine xenograft survival studies to show the potential for prediction and validation of our *in vitro* findings. Instead of solely examining the traditional outcome measure of cell death in response to therapeutics [25, 148, 263], we assessed multiple outcome measures known to contribute to therapeutic resistance, including invasion, proliferation, and selection of malignant stem populations [23, 246, 282]. The importance of assessing multiple outcome measures was

significant as our experiments indicated therapeutics affect malignant outcomes differently. For example, our findings indicated a drug may be successful at halting proliferation of the cancer cells, but the cells can still be invasive and thus still be malignant.

Replicating the standard of care treatment regimen on models with varying microenvironment compositions is the first demonstration of combining both radiation therapy and chemotherapy treatments in an 3D *in vitro* model. Our data suggests the microenvironment consisted of higher microglia does lead to more malignant phenotypes, similar to the changes observed using our predictive survival curves generated in this chapter, as well as earlier in Chapter 2 [35]. This finding also parallels other studies indicating the malignant contributions of microglia to glioblastoma aggression and progression [37, 42, 45, 222]. Although we did not find significant differences between the microenvironment compositions tested, this could be due to keeping the concentration of the other glial component constant to control the number of conditions tested. More radical combinations would likely reveal significant changes in malignancy. Not only is this the first demonstration of combining both components of standard of care therapy (radiation therapy with temozolomide chemotherapy) in a 3D *in vitro* model, it is also the first model to mimic patient-defined ratios and test multiple combinations in a physiologically-relevant manner.

Our goal was to utilize our *in vitro* model as a screening platform to hopefully identify which chemotherapeutics may be successful in increasing overall survival *in vivo*. While we currently do not have enough power to definitively predict the *in vivo* survival result using our in vitro model results, we were able to show the improvements of using a

3D *in vitro* model of the microenvironment to identify multiparametric therapeutic response over the traditional single-cell screens for viability. The finding that increased *in vitro* invasion correlated with increased overall survival *in vivo* for our G34 study seemed counterintuitive, since increased invasion is associated with recurrence [140, 240, 283]. A closer analysis on the changes *in vivo*, such as with immunohistochemistry, would provide more details explaining this result. Although our sample size is currently too small to run full statistical analyses on our outcome measures, the trends that we observed lead towards future hypothesis development and power analysis for larger cohorts.

For our animal studies, we treated at a single consistent dose, only modified based on weight of mouse, despite finding in our *in vitro* model that the two patient-derived glioblastoma stem cells had different IC50s. While testing a range of doses with the animal study would have been useful for corroborating the significant differences we found in in vitro IC50s, this would have greatly escalated the number of animals needed, and thus not follow one of the rules of animal testing – to reduce the number of animals needed. Furthermore, in the clinic, patients all receive the same dose. Creating patient-specific 3D *in vitro* models would allow testing to determine an optimal dose for each patient instead of relying on the same dose for all patients, which may not be effective for all patients.

Chapter 7: Discussion

7.1 Discussion of overall thesis

This dissertation represents many first steps towards a better understanding of how the complex tumor microenvironment affects glioblastoma malignancy. First, we studied patient tumor resections to gain an understanding of the native cellular landscape of patient tumors and from this analysis, we created patient-defined cellular microenvironment profiles for predictive survival curves. To specifically study, manipulate, and understand the cellular microenvironment, we then designed and optimized a 3D *in vitro* human model of the invasive cellular glioblastoma tumor microenvironment capable of assessing multiple outcomes contributing to cancer malignancy. We then utilized the tissue-engineered model to systematically test cellular microenvironment contributions to glioblastoma malignancy, and compared our *in vitro* model with *in vivo* murine xenografts. Finally, we demonstrated the potential of the 3D *in vitro* microenvironment model as a platform for identifying therapeutic response. In order to discover and develop treatments that will increase the currently dismal patient survival times, advanced experimental models that more accurately mimic the complex glioblastoma physiology are necessary. The tissue-engineered model presented in this dissertation is the first patient-tunable 3D *in vitro* model of the glioblastoma microenvironment specifically mimicking the post-resection infiltrative edge. The translational possibilities for this highly physiologically-relevant technology to benefit patients in clinic are innumerable.

7.1.1 Contributions of the tumor microenvironment to patient survival

We began our investigation of the cellular glioblastoma tumor microenvironment by elucidating contributions of the cellular microenvironment to overall patient survival using patient tumor resections. Utilizing histological markers to identify the cellular populations, we analyzed patient tumor resections for cellular microenvironment composition and grouped the patients according to their cellular microenvironment profiles. With these distinct profiles, we developed predictive survival curves indicating the potential contributions of these cellular microenvironment to predicting overall patient survival. We then created hypothetical patient profiles based on the unique microenvironment composition patterns identified throughout our cohort, and developed resulting predicted survival curves. Although we found high variability in the histological markers across our entire patient cohort and incorporated this variability in the hypothetical patient profiles, a change in a single cellular marker composition was typically the difference between the best and worst prognosis. Links between the glioblastoma microenvironment and patient survival were unknown previously, so our significant findings relating the cellular composition with overall survival patient are particularly novel. We focused our study solely on glial cells, namely astrocytes, microglia, and oligodendrocytes, but as we discussed throughout this thesis, there are many more components to the glioblastoma tumor microenvironment that can be identified in patients through techniques other than immunohistochemistry. Circulating markers for angiogenesis, such as VEGF, and inflammation, such as TNFα and IL6, have

been identified through analysis of patient blood samples, have been found elevated but were not associated with survival or progression-free survival [284].

7.1.2 Significance and advantages of tissue-engineered models

In order to systematically test the discovered contributions of the cellular microenvironment, we needed to develop a robust and tunable platform. We developed a tissue-engineered model of the cellular glioblastoma tumor microenvironment specifically mimicking the post-resection infiltrative edge. Experimental tools for studying cancer typically derive from, or model the tumor bulk, and dismiss the critical interactions between the tumor bulk and surrounding parenchyma. The infiltrative edge contains the cells most dangerous to the patient because these cells will invade surrounding healthy tissue and lead to inevitable recurrence [285, 286]. Therefore, models focusing on the tumor bulk are not the best platform for understanding the regions associated with the poor outcomes for glioblastoma patients. In fact, modeling this specific region is important because after standard of care surgical resection of the tumor bulk, the remaining infiltrative edge is what is exposed to the subsequent radiation therapy and chemotherapy. However, this is certainly a difficult region to model, particularly with *in vivo* models. For *in vivo* orthotopic implanted tumors, it is near impossible to inoculate a tumor and then resect it without compromising the animal's health. Tissue-engineered 3D *in vitro* models are a controllable platform for specifically mimicking regions of interest, and we utilized this technology to replicate the invasive edges of glioblastoma tumors. We incorporated human astrocytes and human microglia with patient-derived glioblastoma stem cells at a ratio determined from quantifying

the respective populations of each cell in the invasive tumor regions via immunohistochemistry in patient tumor resections. Since our ratio was patient-defined, we ensured this model resembles glioblastoma patient physiology. Our three human cell populations are seeded into a predominantly hyaluronan 3D matrix, to mirror the primary extracellular matrix component of the brain. This is a key advantage over many complex tissue-engineered models of glioblastoma which solely comprise of collagen, and/or incorporate Matrigel ®, a basement membrane cocktail derived from mouse sarcomas containing 60% laminin, 30% collagen IV, 8% entactin with a variety of growth factors such as TGFβ, EGF, and PDGF [287]. While this combination of proteins certainly may be relevant to cancers such as breast and lung, these components do not reflect the glioblastoma extracellular matrix and microenvironment composition. Furthermore, Matrigel suffers from lot-to-lot variability and is not derived from a human source, leading to potentially inconsistent results as well as immune response.

Extending past the design of the *in vitro* model, we also optimized our model for multiparametric assessment of malignant outcomes. Incorporating our cell-gel mixture into a tissue culture insert with a porous membrane at the bottom allows us to utilize the popular Boyden Chamber assay technique for assessing invasion and migration of cells. Because glioblastoma is one of the most invasive cancers, it is essential to study this outcome measure. After removing the cell-gel mixture from the tissue culture insert, we degrade the matrix, leaving only our cells and use flow cytometry to allow for single cell, quantitative, and fast assessments of multiple outcomes affecting anti-tumor therapy failure. For this

work, we optimized a panel assessing cell death via live/dead staining, proliferation via the Ki67 marker, and stemness via the CD71 marker. We decided on these specific parameters for our model because glioblastoma recurrence occurs not just because the cancer cells continue to survive after therapy, these cancer cells can become stem-like and proliferate to form new tumors [23]. Since we utilize flow cytometry as our primary means for analysis, the breadth of markers available for flow cytometry are applicable to this system. Previous studies in our lab have demonstrated the usage of flow cytometry to quantitatively analyze uptake of doxorubicin [257], a commonly used fluorescent chemotherapeutic agent in the clinical management of breast cancer [288]. Although flow cytometry is extremely advantageous for specific single-cell quantification of interactions in the tumor microenvironment and the resulting changes, tissue complexity is lost, and the degradation of the extracellular matrix can cause altered receptor expression [74]. Since this work focuses specifically on cellular contributions, flow cytometry is an appropriate, valuable, and efficient technology for analysis.

Another key advantage for the model we developed is its versatility. Due to the pipettable liquid form of the cell-gel solution prior to homogenous gelation at 37°C, our model is easily adaptable to other vessels and platforms, such as microfluidic devices to study other disease-related phenomenon such as pressure and chemical gradient changes [259, 260]. Furthermore, the "tissue" aspect of the tissue-engineered model implies many analysis techniques traditionally used to study tissues can also be utilized to study this model. If adapting the model to study hypotheses concerning the extracellular matrix or

specific cell-cell interactions, alternative analysis methods – such as immunohistochemical staining or protein and gene expression could be utilized. In fact, in Chapter 5 of this dissertation, we demonstrated this versatility by analyzing of our model using Luminex and ELISA assays to assess protein content. We have also analyzed various other 3D *in vitro* models in our lab using various imaging as well as molecular biology techniques, such as MRI and western blotting.

Once our design and outcome measures were optimized, we used our *in vitro* model to hone in on our findings from Chapter 2 about how the cellular microenvironment composition can predict patient survival and determine how components of cellular microenvironment contribute to measures of glioblastoma malignancy. Although it is increasingly apparent that the tumor microenvironment plays a major role in the development and progression of cancer [26, 27], the glioblastoma tumor microenvironment, in particular, is relatively understudied, in large part due to the limits of glioblastoma experimental models to accurately and simply study it. Glioblastoma is a cancer that simultaneously grows and invades, making it highly integrated and difficult to separate from surrounding brain parenchyma. Current research on the cellular glioblastoma tumor microenvironment focuses only on the contributions of either astrocytes or microglia [32, 42, 244, 245] to glioma cell invasion as well as glioblastoma patient survival. We took advantage of the tunability aspect of our *in vitro* model to study both the individual and synergistic contributions of astrocytes and microglia to invasion, proliferation and stemness of glioblastoma stem cells derived from three different patients. Our studies in Chapter 2

indicated changing a single cellular composition was the difference between our best and worst predicted prognoses, and so we focused our conditions to single cellular changes. We found the extent and combination of responses was dependent on the combination of cells incorporated as well as the patient from which the cells were derived from. Specifically, when cultured alone within our 3D hyaluronan matrix, the glioblastoma stem cells derived from patient G528 appeared more malignant than our other two patients, G2 and G34. But when incorporating the glioblastoma stem cells in the tumor microenvironment, with astrocytes and microglia, the phenotypes switched – G2 and G34 glioblastoma stem cells appeared more malignant than G528 in the physiologically-relevant microenvironment. This differential response when including glial cell components suggested a phenomenon we later explored in more depth in Chapter 5, that the astrocytes and microglia are secreting additional signals that were altering the behaviors of the glioblastoma stem cells.

Upon further investigation of our patient-derived glioblastoma stem cells, we discovered the trends could be potentially contributed to the genetic subtype. G2 and G34 patients could be assigned to the mesenchymal subtype, while G528 is classical. Based on this information, we selected one patient from the mesenchymal subtype (G34) to compare with G528 using orthotopically implanted murine xenografts of the patient-derived glioblastoma stem cell. G34-inoculated murine xenografts had a median overall survival of 13 days, while G528 was significantly longer at 25.5 days. This significant difference in xenograft survival indicates G34 glioblastoma stem cells are more malignant than G528 *in vivo*, and this was indicated from *in vitro* data incorporating the microenvironment more

representative of *in vivo* native tissue. With the potential to replicate *in vivo* behaviors in an *in vitro* platform, we can hopefully move pre-clinical research away from cost, labor, and time intensive animal models and experiments. 3D *in vitro* models provide more specific control over microenvironment features, faster experiment times, and significantly lower costs than animal studies.

7.1.3 Translational capacity of 3D in vitro microenvironment models

Other than understanding how the complex glioblastoma microenvironment contributes to this cancer's growth, the most important consideration is how can we utilize this information to benefit patients. With our tunable 3D *in vitro model*, demonstrate the ability to alter the microenvironment to reflect those of different patients and attempt to assess patient-specific therapeutic response. We first manipulated our standard ratio of cancer cells to astrocytes to microglia (6:1:1) used in the previous portions of this dissertation to other quartile ratios identified within our patient cohort, thus further demonstrating the tunability aspect of our model, as well as its potential to be used for patient-specific modeling. Recreation of tissues outside the patient body using tissue engineering methods offers the ability to potentially examine a patient's own tissues in a controlled setting [143, 195]. These systems combine the benefits of mimicking tissue-level structures and interactions with the ease and manipulability of higher throughput screening platforms. Aside from precision medicine applications, they can also be used to test important scientific hypotheses related to disease related to the complex interactions that arise in a complete tissue and thus offer opportunities for drug discovery and development [78, 197].

We expanded to then demonstrate the potential of our 3D *in vitro* model to be used as a high throughput screening system by assessing therapeutic response of a panel of six clinically relevant chemotherapeutics. Several screening strategies measuring cell death – genomic profiling, tissue microarrays with molecular profiling, and therapeutic testing of either single treatment monolayer (2D) cell cultures or patient-derived spheroid cell cultures – have been experimentally employed to predict patient outcomes prior to treatment [25]. Not only does our 3D *in vitro* model incorporate several components of the microenvironment, it also has the capability of assessing multiple outcomes other than cell death in response to therapy, such as invasion, proliferation, and selection for cancer stem cells, to better understand therapeutic response and glioblastoma progression.

We not only compared therapeutic response from our 3D *in vitro* model to the traditional spheroid assays, we also conducted *in vivo* survival studies with our panel of chemotherapeutics using murine xenograft models orthotopically implanted with the same patient-derived glioblastoma stem cells. Patient-derived xenograft (PDX) models, where primary tumor cells from a patient are implanted directly into an immunocompromised rodent, are the current gold-standard of personalized medicine. PDX models add in whole body information that is missed with standard cell culture, providing a useful tool for drug efficacy and toxicological studies [289]. Not only has there been poor translation from these preclinical models to clinical trials, many drugs successfully screened through in vitro studies have failed in animal studies [289]. Animal models of glioma have largely been validated using molecular biology to determine similarities in gene expression to patients [264, 289].

Expanding the characterization of our 3D *in vitro* model to molecular biology by expanding the gene expression changes will likely add another angle for potential of correlation.

Utilizing a 3D *in vitro* model of the microenvironment allowed us to both test more therapies for less cost and in less time, as well as reduce the use of these murine models without losing the information that is valuable within these microenvironmental contexts. We tested a range of chemotherapeutic doses for our *in vitro* studies, which would not only have been difficult and costly to do *in vivo*, it is also would not be ethical. These factors greatly limit the scalability of using patient-derived xenograft models as high-throughput screening platforms for personalized medicine. Furthermore, single doses of chemotherapeutics are how these drugs are administered in clinic. More complex dosing strategies both *in vitro* and *in vivo* may be more predictive, and this is most feasible using an *in vitro* system. While our 3D *in vitro* model screening studies did not conclusively predict the overall survival patterns of our *in vivo* murine xenografts treated with chemotherapeutics, we did find potential trends between *in vitro* invasion and *in vivo* overall survival. We had hoped to correlate the post-therapy changes observed *in vitro* with *in vivo* immunohistochemistry, similar to the correlative results described in Chapter 4, however the poor tissue integrity of the brains in this survival study made staining and quantification difficult. This analysis certainly is useful information for assessing the correlative capacity of our *in vitro* model, and therefore could be performed with a repeat study not assessing overall survival, where the animals are sacrificed at earlier time point before the brains become so damaged. Genomic analyses on both our *in vitro* model and the harvested brain

tissue could also elucidate correlations between the two. Regardless, one potentially large contributing factor to our inability to directly correlate our *in vitro* results with the murine survival study is our 3D *in vitro* model is built as a fully humanized model, and therefore is not designed to mimic xenograft microenvironments where patient-derived cancer cells are interacting with native mouse cells and tissue. Although it would certainly be useful for our 3D *in vitro* human model to predict patterns from pre-clinical animal models, the ultimate goal is to assess and predict patient outcomes.

7.1.4 Limitations and potential improvements to our design

The predictive capacity of our current model is limited by the lack of information on the medical histories of the patients from which our glioblastoma stem cells are derived. Because of this, we are unable to directly correlate our *in vitro* findings with patient prognosis outcomes, such as progression-free survival and overall survival, and are forced to end with PDX models as our final *in vivo* translation point. The ideal experimental design for assessing the capability of a 3D *in vitro* model for predicting patient outcomes in clinic would be to begin with glioblastoma stem cells directly harvested from a patient whose entire medical history is known, as well as induced pluripotent stem cells harvested from this patient that we could direct towards differentiation into astrocytes and microglia. From the patient's tumor resection, we would analyze the astrocyte and microglia composition using our techniques described in Chapters 2 and 3, and then incorporate the patient's own tumor cells and stromal cells into a 3D *in vitro* model to create patient-specific that is completely tuned from the original tumor of the patient. We would systematically analyze

the microenvironment like in Chapter 4 and compare these patient-specific outcomes to those from our baseline tumor model from Chapters 3 and 4 to understand how aggressive these tumors are at a baseline without any treatment, and then treat the 3D *in vitro* model with standard of care radiation therapy and temozolomide chemotherapy, like in Chapter 6, to determine how the patient will respond to the standard of care. The *in vitro* results we gather from this data can then be compared with the original patient medical history, and we can determine which of, or if, our parameters contribute to glioblastoma recurrence, progression-free survival, or overall survival. Concurrently, we would use murine xenografts inoculated with these directly derived glioblastoma cells to not only compare the results our *in vitro* model versus the PDX model, but also to determine whether the fully humanized and completely patient-specific 3D *in vitro* model or the murine xenograft model has higher predictive capability of patient outcomes. We can then screen a panel of chemotherapeutics, and targeted agents as applicable, in the model. While we certainly will not have concurrent response to these various therapeutic regiments from the original patient, we will be able to gather sensitivity and specificity information to show the proof-of-concept for utilizing this model for clinical robustness.

Glioblastoma presents an interesting and unique scenario in how we develop and implement therapeutics pre-clinically and clinically. Currently, every glioblastoma patient receives the same standard of care treatment, even though recent evidence suggests molecular dissimilarities that may correlate with therapeutic response [290]. Prior to this dissertation work, there had been no published research on the interpatient heterogeneity of

the tumor microenvironment and how changes in the surrounding tissue may influence therapeutic potential. Little work experimentally has even been approached to examine the role of the general microenvironment in therapeutic development and response, though it is increasingly the subject of review articles [27, 36, 291, 292] and calls for funding. This is partially due to the lack of good tools to study specifically the microenvironment, and even fewer tools to specifically study the brain tumor microenvironment, a unique niche with a seemingly insurmountable cancer. This dissertation demonstrates the potential of an *in vitro* system to replicate the *in vivo* microenvironment in the context of cellular biology and pathology, thus providing a tool for scientists and clinicians for novel testing of microenvironment-specific hypotheses. Although there is still room for improvement with this model, particularly with molecular biology and signaling pathway characterization, we are transforming the types of questions that can be probed and the throughput of therapies and targets that can be tested. By incorporating multiple cell populations as well as multiple outcome measures of therapeutic screening, we may shift the perspective of current screenings away from simply cell survival and growth, and more towards a holistic view of cancer therapeutic failure.

7.2 Future directions

This dissertation represents early progress in identifying the role of the cellular tumor microenvironment in glioblastoma malignancy via development of a 3D *in vitro* model of this region. Our findings proved our overarching hypothesis that incorporating glioblastoma

cells in an *in vitro* microenvironment more accurately representing that of native *in vivo* tissue will more similarly mimic *in vivo* phenotypes than traditional *in vitro* studies. However, there is still much more to investigate to fully prove this hypothesis. Our studies were limited to three patient-derived glioblastoma stem cells, so how do glioblastoma cells derived from other patients within the mesenchymal and classical subtypes, or even the proneural subtype, behave in our *in vitro* model and in *in vivo* xenografts? Are our *in vitro* assessments of invasion, proliferation, and stemness post-therapy predictive of the respective changes in these populations *in vivo*? How does the combination of cell death, invasion, proliferation, and stemness outcomes contribute to overall survival both in animal studies? Further than animal models, can we ultimately predict patient outcomes using an *in vitro* model? Answering these questions will only open the door to even more hypotheses, but building this platform paves the beginning for finally understanding the complex glioblastoma tumor microenvironment and hopefully identifying a therapeutic regimen that will significantly increase patient survival.

Utilizing an *in vitro* model comprised of as many components of the glioblastoma tumor microenvironment as the model presented here brings the potential to discover novel therapeutic targets that would never have been discovered from screening on cancer cells alone. We now know many individual microenvironment components, such as interstitial flow and signaling from astrocytes or microglia, contribute to glioblastoma cell invasion, but previous models did not allow for studying how these microenvironment components can be working together to contribute to glioblastoma malignancy across multiple outcomes. In

fact, early studies in our lab have identified a particularly interesting small molecule inhibitor that is only effective in the context of flow with the cellular microenvironment, and without flow or without the cellular microenvironment, it has no effect. Before the development of our model, discovery of this mechanism at a pre-clinical stage would have been impossible. We have also demonstrated capabilities of the system to identify potential paracrine signaling communications that would be missed without studying glioblastoma with its microenvironment. Although cancer cells are self-sufficient and readily capable of self-survival, they also hijack surrounding normal cells to create highly aggressive environments to support tumor growth. With the ability to study glioblastoma cells in the context of the microenvironment, the potential for drug discovery and new targets has greatly expanded, and we can hopefully identify treatment strategies to benefit glioblastoma patients and significantly increased the overall survival.

Our system specifically models the invasive interface of the tumor, but this can be adapted to model tumor bulk and therefore assess other microenvironmental influences on drug response such as hypoxia and pH fluctuations seen at the tumor core [258]. We incorporated two stromal cell types in addition to the cancer cells in a 3D matrix certainly makes our model more physiologically-relevant than traditional experimental models of glioblastoma, there are still many components of the tumor microenvironment that can be included. We identified oligodendrocyte and endothelial cell populations within our tumor resections in Chapter 2 as contributors to patient survival, but did not include these cell populations in our design. Furthermore, our lab has observed gradients of cancer cellular

density in breast tumors and have mimicked this *in vitro* through layering of multiple cell-gel solutions [293], a design that is certainly relevant to the invasive edge of glioblastoma tumors. Other than cellular components and extracellular matrix, chemical and physical gradients and structures also can be incorporated [257]. However, incorporation of every element within the tissue would drastically reduce the ease of use of a system and can cause difficulties in outcome measures. Therefore, careful formulation of the specific question, hypothesis, or objective should be considered before design of the system. This is followed by collection of relevant information to enable appropriate modeling either through literature or prior *in vivo* data. Regardless, the techniques of tissue engineering can be easily translated to study the complexities of tumor biology.

The work in this thesis demonstrates the ease in implementation and highly versatile characteristics of *in vitro* modeling. While 3D tissue-engineered models are certainly advantageous over animal models for testing multiple conditions simultaneously, there is a physical limit to the complexity and timeline that is reasonable for scientists to setup and test at the benchtop. As such, computational, or *in silico*, modeling gains ground. Specifically, one type of computation modeling, agent-based modeling, focuses on the dynamic interactions of objects in a rule-based system to predict and describe complex temporal and spatial biological interactions [294]. All computational models are developed based on data, but agent-based models are specifically generated from rules determined by interpreted data [295] making them particularly powerful for modeling complex biological interactions such as those present in tumor microenvironments. Furthermore, the potential

for agent-based models to identify emergent behavior through incorporating multiple components together is exceptionally useful. Previous studies in our lab have used agent-based modeling to model effects of interstitial flow on brain cancer cell invasion via CXCR4-CXCL12 autologous chemotaxis and CD44 mechanotransduction [78], as well as contributions of drug transport in breast cancer therapeutic response [293].

Albeit with different purposes, the governing principles from these two models, including the interplay between cancer cells and the microenvironment and the progression of chemotherapeutic drugs through a realistic matrix could be applied to a new agent-based model for modeling glioblastoma. With the numerous components included within our *in vitro* model and the multiple outcome measures, agent-based modeling would be a powerful tool for characterizing our *in vitro* findings. A key limitation of using agent-based modeling is the rules are determined by known experimental results, therefore restricting the model to capture the typical behaviors of cells already observed. However, once the model incorporates reliable parameters determined experimentally, it can be applied, more generally, to describe the glioblastoma microenvironment in a variety of conditions, while minimizing the costs associated with *in vitro* and *in vivo* studies. This thesis encompasses a wide range of experimental data that can be integrated into a robust agent-based modeling platform with the ability to test multiple complex combinations of glial cell ratios, and chemotherapeutic dosing patterns in a much more efficient manner than to test all these combinations *in vitro*. Moreover, agent-based modeling could help hone in on key therapeutic strategies for further investigation *in vitro* and potentially *in vivo*, as well.

This thesis demonstrates analysis of patient tumor resections to build a physiologically-relevant multicellular model of the glioblastoma tumor microenvironment. Precise modeling of the microenvironment can contribute to personalized patient care, and the methods described throughout this thesis can be applied to different cancer types and metastases, and neurological disorders. We have previously collaborated with neural stem cell researchers to develop models of Alzheimer's using our basic *in vitro* model. Our lab studies both brain and breast cancer, and we have also begun development of a 3D *in vitro* model of the breast cancer metastasis to the brain microenvironment. By analyzing the microenvironment of patient pathological resections from both primary breast tumors and brain metastases, we were able to identify the relative composition of important microenvironment components to inform the design of a 3D *in vitro* model of the brain metastatic breast cancer microenvironment and study tumor-stroma interactions as well as eventually elucidate therapeutic response.

In the last four years working on this thesis, the field of cancer tissue engineering has greatly expanded. This multidisciplinary field encompasses cancer researchers at the basic science level and traditional tissue engineers. Bridging these is necessary to fully understand the physical complexities of cancers in order to develop more effective therapeutic strategies. With these exciting collaborations, cancer tissue engineering will play an instrumental role in the effort to better understand cancer mechanisms and pathology and develop personalized medicine platforms.

References

1. Heron M, Division of Vital Statistics (2016) National Vital Statistics Reports. Deaths: leading causes for 2013. *Natl Vital Stat Reports* 65(2):1–95.

2. Siegel RL, Miller KD, Jemal A (2018) Cancer statistics, 2018. *CA Cancer J Clin* 68(1):7–30.

3. Hess KR, Broglio KR, Bondy ML (2004) Adult glioma incidence trends in the United States, 1977-2000. *Cancer* 101(10):2293–2299.

4. Stupp R, et al. (2009) Effects of radiotherapy with concomitant and adjuvant temozolomide versus radiotherapy alone on survival in glioblastoma in a randomised phase III study: 5-year analysis of the EORTC-NCIC trial. *Lancet Oncol* 10(5):459–466.

5. Claes A, Idema AJ, Wesseling P (2007) Diffuse glioma growth: a guerilla war. *Acta Neuropathol* 114(5):443–458.

6. Holland EC (2000) Glioblastoma multiforme: the terminator. *Proc Natl Acad Sci U S A* 97(12):6242–4.

7. Wild-Bode C, Weller M, Rimner A, Dichgans J, Wick W (2001) Sublethal Irradiation Promotes Migration and Invasiveness of Glioma Cells. *Cancer Res* 61(6).

8. Gliemroth J, Feyerabend T, Gerlach C, Arnold H, Terzis AJA (2003) Proliferation, migration, and invasion of human glioma cells exposed to fractionated radiotherapy in vitro. *Neurosurg Rev* 26(3):198–205.

9. Louis DN, et al. (2016) The 2016 World Health Organization Classification of Tumors of the Central Nervous System: a summary. *Acta Neuropathol* 131(6):803–820.

10. Scherer HJ (1940) Cerebral astrocytomas and their derivatives. *Am J Cancer* 40(2):159–198.

11. Bloch O, et al. (2012) Impact of extent of resection for recurrent gliobalstoma on overall survival. *J Neurosurg* 117(December):1032–1038.

12. Bucci B, et al. (2006) Fractionated ionizing radiation exposure induces apoptosis through caspase-3 activation and reactive oxygen species generation. *Anticancer Res* 26(6B):4549–57.

13. Lehnert BE, Iyer R (2002) Exposure to low-level chemicals and ionizing radiation: reactive oxygen species and cellular pathways. *Hum Exp Toxicol* 21(2):65–69.

14. Hochberg FH, Pruitt A (1980) Assumptions in the radiotherapy of glioblastoma. *Neurology* 30(9):907–11.

15. Hegi ME, et al. (2004) Clinical Trial Substantiates the Predictive Value of O-6-Methylguanine-DNA Methyltransferase Promoter Methylation in Glioblastoma Patients Treated with Temozolomide. *Clin Cancer Res* 10:1871–1874.

16. Brandes AA, et al. (2009) Recurrence Pattern After Temozolomide Concomitant With and Adjuvant to Radiotherapy in Newly Diagnosed Patients With Glioblastoma: Correlation With MGMT Promoter Methylation Status. *J Clin Oncol* 27:1275–1279.

17. Hegi ME, et al. (2005) *MGMT* Gene Silencing and Benefit from Temozolomide in

Glioblastoma. *N Engl J Med* 352(10):997–1003.

18. Deangelis LM, Burger PC, Green SB, Cairncross JG (1998) Malignant glioma: Who benefits from adjuvant chemotherapy? *Ann Neurol* 44(4):691–695.

19. Attenello FJ, et al. (2008) Use of Gliadel (BCNU) Wafer in the Surgical Treatment of Malignant Glioma: A 10-Year Institutional Experience. *Ann Surg Oncol* 15(10):2887–2893.

20. Ferrara N, Hillan KJ, Gerber H-P, Novotny W (2004) Case history: Discovery and development of bevacizumab, an anti-VEGF antibody for treating cancer. *Nat Rev Drug Discov* 3(5):391–400.

21. Maysinger D, Morinville A (1997) Drug delivery to the nervous system. *Trends Biotechnol* 15(10):410–418.

22. Xie Q, Mittal S, Berens ME (2014) Targeting adaptive glioblastoma: An overview of proliferation and invasion. *Neuro Oncol* 16(12):1575–1584.

23. Calabrese C, et al. (2007) A Perivascular Niche for Brain Tumor Stem Cells. *Cancer Cell* 11(1):69–82.

24. Pollard SM, et al. (2009) Glioma Stem Cell Lines Expanded in Adherent Culture Have Tumor-Specific Phenotypes and Are Suitable for Chemical and Genetic Screens. *Cell Stem Cell* 4(6):568–580.

25. Kunz-Schughart LA, Freyer JP, Hofstaedter F, Ebner R (2004) The use of 3-D cultures for high-throughput screening: the multicellular spheroid model. *J Biomol Screen* 9(4):273–85.

26. Correia AL, Bissell MJ (2012) The tumor microenvironment is a dominant force in multidrug resistance. *Drug Resist Updat* 15(1–2):39–49.

27. Swartz MA, et al. (2012) Tumor microenvironment complexity: Emerging roles in cancer therapy. *Cancer Res* 72(10):2473–2480.

28. Sherriff J, et al. (2013) Patterns of relapse in glioblastoma multiforme following concomitant chemoradiotherapy with temozolomide. *Br J Radiol* 86. doi:10.1259/bjr.20120414.

29. Geer CP, Grossman SA (1997) Interstitial fluid flow along white matter tracts: A potentially important mechanism for the dissemination of primary brain tumors. *J Neurooncol* 32(3):193–201.

30. Scherer HJ (1940) Cerebral Astrocytomas and Their Derivatives. *Am J Cancer* 40(2):159–198.

31. Ohgaki H, Kleihues P (2013) The definition of primary and secondary glioblastoma. *Clin Cancer Res* 19(4):764–772.

32. Zhai H, Heppner FL, Tsirka SE (2011) Microglia/macrophages promote glioma progression. *Glia* 59(3):472–485.

33. Placone AL, Qui??ones-Hinojosa A, Searson PC (2015) The role of astrocytes in the progression of brain cancer: complicating the picture of the tumor microenvironment. *Tumor Biol*. doi:10.1007/s13277-015-4242-0.

34. Alves TR, et al. (2011) Glioblastoma cells: A heterogeneous and fatal tumor interacting with the parenchyma. *Life Sci* 89(15):532–539.

35. Yuan JX, Bafakih FF, Mandell JW, Horton BJ, Munson JM (2016) Quantitative Analysis of the Cellular Microenvironment of Glioblastoma to Develop Predictive Statistical Models of Overall Survival. *J Neuropathol Exp Neurol*.

36. Charles NA, Holland EC, Gilbertson R, Glass R, Kettenmann H (2011) The brain tumor microenvironment. *Glia* 59(8):1169–1180.

37. Bettinger I, Thanos S, Paulus W (2002) Microglia promote glioma migration. *Acta Neuropathol* 103(4):351–355.

38. Markovic DS, Glass R, Synowitz M, Rooijen N Van, Kettenmann H (2005) Microglia stimulate the invasiveness of glioma cells by increasing the activity of metalloprotease-2. *J Neuropathol Exp Neurol* 64(9):754–62.

39. Hambardzumyan D, Gutmann DH, Kettenmann H (2015) The role of microglia and macrophages in glioma maintenance and progression. *Nat Neurosci* 19(1):20–27.

40. Coniglio S, Eugenin E (2012) Microglial stimulation of glioblastoma invasion involves epidermal growth factor receptor (EGFR) and colony stimulating factor 1 receptor (CSF-1R) signaling. *Mol Med* 18(3):1.

41. Zhou W, et al. (2015) Periostin Secreted by Glioblastoma Stem Cells Recruits M2 Tumor-associated Macrophages and Promotes Malignant Growth. *Nat Cell Biol* 17(2):170–182.

42. Ye X, et al. (2012) Tumor-associated microglia/macrophages enhance the invasion of glioma stem-like cells via TGF-β1 signaling pathway. *J Immunol* 189:444–53.

43. Sofroniew M V., Vinters H V. (2010) Astrocytes: biology and pathology. *Acta*

Neuropathol 119(1):7–35.

44. Lee J, et al. (2009) Glioma-induced remodeling of the neurovascular unit. *Brain Res* 1288:125–34.

45. Le DM, et al. (2003) Exploitation of astrocytes by glioma cells to facilitate invasiveness: a mechanism involving matrix metalloproteinase-2 and the urokinase-type plasminogen activator-plasmin cascade. *J Neurosci* 23(10):4034–43.

46. Barbero S, et al. (1969) Stromal Cell-derived Factor 1 Stimulates Human Glioblastoma Cell Growth through the Activation of Both Extracellular Signal-regulated Kinases 1/2 and Akt 1. *Cancer Res* 63.

47. Chen W, et al. (2015) Glioma cells escaped from cytotoxicity of temozolomide and vincristine by communicating with human astrocytes. *Med Oncol* 32(3):43.

48. Marchetti D, Li J, Shen R (2000) Astrocytes Contribute to the Brain-metastatic Specificity of Melanoma Cells by Producing Heparanase 1. *Cancer Res* 60:4767–4770.

49. Clement V, Sanchez P, de Tribolet N, Radovanovic I, Ruiz i Altaba A (2007) HEDGEHOG-GLI1 Signaling Regulates Human Glioma Growth, Cancer Stem Cell Self-Renewal, and Tumorigenicity. *Curr Biol* 17(2):165–172.

50. Kostianovsky AM, Maier LM, Anderson RC, Bruce JN, Anderson DE (2008) Astrocytic regulation of human monocytic/microglial activation. *J Immunol* 181(8):5425–32.

51. Hanahan D, Weinberg RA (2000) The hallmarks of cancer. *Cell* 100(1):57–70.

52. Jain RK, et al. (2007) Angiogenesis in brain tumours. *Nat Rev Neurosci* 8(8):610–22.

53. Kamba T, McDonald DM (2007) Mechanisms of adverse effects of anti-VEGF therapy for cancer. *Br J Cancer* 96(12):1788–1795.

54. Narayana A, et al. (2009) Antiangiogenic therapy using bevacizumab in recurrent high-grade glioma: impact on local control and patient survival. *J Neurosurg* 110(1):173–180.

55. Jain RK (2013) Normalizing tumor microenvironment to treat cancer: bench to bedside to biomarkers. *J Clin Oncol* 31(17):2205–2218.

56. Leenders WPJ, Küsters B, de Waal RMW (2002) Vessel Co-Option: How Tumors Obtain Blood Supply in the Absence of Sprouting Angiogenesis. *Endothelium* 9(2):83–87.

57. Zagzag D, et al. (2006) Hypoxia-inducible factor 1 and VEGF upregulate CXCR4 in glioblastoma: implications for angiogenesis and glioma cell invasion. *Lab Invest* 86(12):1221–32.

58. Rong Y, Durden DL, Van Meir EG, Brat DJ (2006) 'Pseudopalisading' Necrosis in Glioblastoma: A Familiar Morphologic Feature That Links Vascular Pathology, Hypoxia, and Angiogenesis. *J Neuropathol Exp Neurol* 65(6):529–539.

59. Abbott NJ, Rönnbäck L, Hansson E (2006) Astrocyte–endothelial interactions at the blood–brain barrier. *Nat Rev Neurosci* 7(1):41–53.

60. Netti PA, Baxter LT, Boucher Y, Skalak R, Jain RK (1995) Time-dependent behavior of interstitial fluid pressure in solid tumors: implications for drug delivery. *Cancer Res* 55(22):5451–8.

61. Bellail AC, Hunter SB, Brat DJ, Tan C, Van Meir EG (2004) Microregional extracellular matrix heterogeneity in brain modulates glioma cell invasion. *Int J Biochem Cell Biol* 36(6):1046–1069.

62. Zamecnik J (2005) The extracellular space and matrix of gliomas. *Acta Neuropathol* 110(5):435–442.

63. Kalluri R, Zeisberg M (2006) Fibroblasts in cancer. *Nat Rev Cancer* 6(5):392–401.

64. Frantz C, Stewart KM, Weaver VM (2010) The extracellular matrix at a glance. *J Cell Sci* 123(Pt 24):4195–200.

65. Nelson AR, Fingleton B, Rothenberg ML, Matrisian LM (2000) Matrix metalloproteinases: biologic activity and clinical implications. *J Clin Oncol* 18(5):1135–49.

66. Kessenbrock K, Plaks V, Werb Z (2010) Matrix Metalloproteinases: Regulators of the Tumor Microenvironment. *Cell* 141(1):52–67.

67. Jadin L, et al. (2015) Hyaluronan expression in primary and secondary brain tumors. *Ann Transl Med* 3(6):80.

68. Park JB, Kwak H-J, Lee S-H (2008) Role of hyaluronan in glioma invasion. *Cell Adh Migr* 2(3):202–207.

69. Gilg AG, et al. (2008) Targeting hyaluronan interactions in malignant gliomas and their drug-resistant multipotent progenitors. *Clin Cancer Res* 14(6):1804–13.

70. Wiranowska M, et al. (2010) Modulation of hyaluronan production by CD44 positive glioma cells. *Int J Cancer* 127(3):532–542.

71. Zhang H, Kelly G, Zerillo C, Jaworski DM, Hockfield S (1998) Expression of a cleaved brain-specific extracellular matrix protein mediates glioma cell invasion In vivo. *J Neurosci* 18(7):2370–6.

72. Wade A, et al. (2013) Proteoglycans and their roles in brain cancer. *FEBS J* 280(10):2399–2417.

73. Butcher DT, Alliston T, Weaver VM (2009) A tense situation: forcing tumour progression. *Nat Rev Cancer* 9(2):108–22.

74. Lu P, Takai K, Weaver VM, Werb Z (2011) Extracellular matrix degradation and remodeling in development and disease. *Cold Spring Harb Perspect Biol* 3(12):a005058.

75. Yu H, Mouw JK, Weaver VM (2011) Forcing form and function: biomechanical regulation of tumor evolution. *Trends Cell Biol* 21(1):47–56.

76. Kumar S, Weaver VM (2009) Mechanics, malignancy, and metastasis: the force journey of a tumor cell. *Cancer Metastasis Rev* 28(1–2):113–27.

77. Munson JM, Shieh AC (2014) Interstitial fluid flow in cancer: implications for disease progression and treatment. *Cancer Manag Res* 6:317–28.

78. Kingsmore KM, et al. (2016) Interstitial flow differentially increases patient-derived glioblastoma stem cell invasion via CXCR4, CXCL12, and CD44-mediated mechanisms. *Integr Biol*. doi:10.1039/C6IB00167J.

79. Munson JM, Bellamkonda R V., Swartz MA (2013) Interstitial Flow in a 3D Microenvironment Increases Glioma Invasion by a CXCR4-Dependent Mechanism.

Cancer Res 73(5).

80. Gromov P, et al. (2013) Tumor interstitial fluid — A treasure trove of cancer biomarkers. *Biochim Biophys Acta - Proteins Proteomics* 1834(11):2259–2270.

81. Wiig H, Swartz MA (2012) Interstitial Fluid and Lymph Formation and Transport: Physiological Regulation and Roles in Inflammation and Cancer. *Physiol Rev* 92(3):1005–1060.

82. Iliff JJ, et al. (2012) A paravascular pathway facilitates CSF flow through the brain parenchyma and the clearance of interstitial solutes, including amyloid β. *Sci Transl Med* 4(147):147ra111.

83. Fleury ME, Boardman KC, Swartz MA (2006) Autologous Morphogen Gradients by Subtle Interstitial Flow and Matrix Interactions. *Biophys J* 91(1):113–121.

84. Hoelzinger DB, Demuth T, Berens ME (2007) Autocrine factors that sustain glioma invasion and paracrine biology in the brain microenvironment. *J Natl Cancer Inst* 99(21):1583–93.

85. Shih AH, Holland EC (2006) Platelet-derived growth factor (PDGF) and glial tumorigenesis. *Cancer Lett* 232(2):139–47.

86. Wesolowska A, et al. (2008) Microglia-derived TGF-beta as an important regulator of glioblastoma invasion--an inhibition of TGF-beta-dependent effects by shRNA against human TGF-beta type II receptor. *Oncogene* 27(7):918–930.

87. Kenig S, Alonso MBD, Mueller MM, Lah TT (2010) Glioblastoma and endothelial cells cross-talk, mediated by SDF-1, enhances tumour invasion and endothelial

proliferation by increasing expression of cathepsins B, S, and MMP-9. *Cancer Lett* 289(1):53–61.

88. Ehtesham M, Mapara KY, Stevenson CB, Thompson RC (2009) CXCR4 mediates the proliferation of glioblastoma progenitor cells. *Cancer Lett* 274(2):305–312.

89. Pedersen P-H, et al. (1994) Heterogeneous response to the growth factors [EGF, PDGF (bb), TGF-α, bFGF, IL-2] on glioma spheroid growth, migration and invasion. *Int J Cancer* 56(2):255–261.

90. Dieterich LC, et al. (2012) Transcriptional profiling of human glioblastoma vessels indicates a key role of VEGF-A and TGFβ2 in vascular abnormalization. *J Pathol* 228(3):378–390.

91. Leventhal C, Rafii S, Rafii D, Shahar A, Goldman SA (1999) Endothelial Trophic Support of Neuronal Production and Recruitment from the Adult Mammalian Subependyma. *Mol Cell Neurosci* 13(6):450–464.

92. Ramírez-Castillejo C, et al. (2006) Pigment epithelium–derived factor is a niche signal for neural stem cell renewal. *Nat Neurosci* 9(3):331–339.

93. Zhu VF, Yang J, Lebrun DG, Li M (2012) Understanding the role of cytokines in Glioblastoma Multiforme pathogenesis. *Cancer Lett* 316(2):139–50.

94. Vredenburgh JJ, et al. (2007) Phase II trial of bevacizumab and irinotecan in recurrent malignant glioma. *Clin Cancer Res* 13(4):1253–1259.

95. Wen PY, et al. (2006) Phase I/II study of imatinib mesylate for recurrent malignant gliomas: North American Brain Tumor Consortium Study 99-08. *Clin Cancer Res*

12(16):4899–907.

96. Bonnet D, Dick JE (1997) Human acute myeloid leukemia is organized as a hierarchy that originates from a primitive hematopoietic cell. *Nat Med* 3(7):730–737.

97. Jordan CT, Guzman ML, Noble M (2006) Cancer Stem Cells. *N Engl J Med* 355:1253–61.

98. Wakimoto H, et al. (2012) Maintenance of primary tumor phenotype and genotype in glioblastoma stem cells. *Neuro Oncol* 14(2):132–144.

99. Eramo A, et al. (2006) Chemotherapy resistance of glioblastoma stem cells. *Cell Death Differ* 13(7):1238–1241.

100. Bjerkvig R, Tysnes BB, Aboody KS, Najbauer J, Terzis AJA (2005) Opinion: The origin of the cancer stem cell: current controversies and new insights. *Nat Rev Cancer* 5(11):899–904.

101. Yuan X, et al. (2004) Isolation of cancer stem cells from adult glioblastoma multiforme. doi:10.1038/sj.onc.1208311.

102. Park JK, et al. (2010) Scale to predict survival after surgery for recurrent glioblastoma multiforme. *J Clin Oncol* 28(24):3838–43.

103. Filatova A, Acker T, Garvalov BK (2013) The cancer stem cell niche(s): The crosstalk between glioma stem cells and their microenvironment. *Biochim Biophys Acta - Gen Subj* 1830(2):2496–2508.

104. Bao S, et al. (2006) Glioma stem cells promote radioresistance by preferential activation of the DNA damage response. *Nature* 444(7120):756–760.

105. Liu L, et al. (2017) Mechanoresponsive stem cells to target cancer metastases through biophysical cues. *Sci Transl Med* 9(400).

106. Chen R, et al. (2010) A Hierarchy of Self-Renewing Tumor-Initiating Cell Types in Glioblastoma. *Cancer Cell* 17(4):362–375.

107. Wang J, et al. (2008) CD133 negative glioma cells form tumors in nude rats and give rise to CD133 positive cells. *Int J Cancer* 122(4):761–768.

108. Schonberg DL, et al. (2015) Preferential Iron Trafficking Characterizes Glioblastoma Stem-like Cells. *Cancer Cell* 28(4):441–455.

109. Daniels TR, Delgado T, Rodriguez JA, Helguera G, Penichet ML (2006) The transferrin receptor part I: Biology and targeting with cytotoxic antibodies for the treatment of cancer. *Clin Immunol* 121(2):144–158.

110. Kikyo N, et al. (1994) Purification and characterization of a cell growth factor from a human leukemia cell line: immunological identity with ferritin. *Cancer Res* 54(1):268–271.

111. Coffman LG, Parsonage D, D'Agostino R, Torti FM, Torti S V (2009) Regulatory effects of ferritin on angiogenesis. *Proc Natl Acad Sci U S A* 106(2):570–5.

112. Hanahan D, Weinberg RA (2011) Hallmarks of Cancer: The Next Generation. *Cell* 144(5):646–674.

113. Cummings BS, Schnellmann RG, Schnellmann RG (2004) Measurement of cell death in mammalian cells. *Curr Protoc Pharmacol* Chapter 12:Unit 12.8.

114. Krysko D V., Vanden Berghe T, D'Herde K, Vandenabeele P (2008) Apoptosis and

necrosis: Detection, discrimination and phagocytosis. *Methods* 44(3):205–221.

115. A novel assay for apoptosis Flow cytometric detection of phosphatidylserine expression on early apoptotic cells using fluorescein labelled Annexin V (1995) *J Immunol Methods* 184(1):39–51.

116. Friedman HS, Kerby T, Calvert H (2000) Temozolomide and treatment of malignant glioma. *Clin Cancer Res* 6(7):2585–2597.

117. Pommier Y, Pourquier P, Fan Y, Strumberg D (1998) Mechanism of action of eukaryotic DNA topoisomerase I and drugs targeted to the enzyme. *Biochim Biophys Acta - Gene Struct Expr* 1400(1–3):83–106.

118. Xu Y, Villalona-Calero MA (2002) Irinotecan: mechanisms of tumor resistance and novel strategies for modulating its activity. *Ann Oncol* 13(12):1841–1851.

119. Reedijk J (1987) The mechanism of action of platinum antitumor drugs. *Pure Appl Chem* 59(2):181–192.

120. Ohgaki H, Kleihues P (2007) Genetic pathways to primary and secondary glioblastoma. *Am J Pathol* 170(5):1445–53.

121. Wong AJ, et al. (1992) Structural alterations of the epidermal growth factor receptor gene in human gliomas. *Proc Natl Acad Sci* 89(7):2965–2969.

122. Houillier C, et al. (2006) Prognostic impact of molecular markers in a series of 220 primary glioblastomas. *Cancer* 106(10):2218–2223.

123. Duerr E-M, et al. (1998) PTEN mutations in gliomas and glioneuronal tumors. *Oncogene* 16(17):2259–2264.

124. Yan H, et al. (2009) Mutations in Gliomas. *N Engl J Med* 360(8):765–773.

125. Cuddapah VA, Robel S, Watkins S, Sontheimer H (2014) A neurocentric perspective on glioma invasion. *Nat Rev Neurosci* 15(7):455–465.

126. Beauchesne P, Patrick (2011) Extra-Neural Metastases of Malignant Gliomas: Myth or Reality? *Cancers (Basel)* 3(1):461–477.

127. Friedl P, Wolf K (2003) Tumour-cell invasion and migration: diversity and escape mechanisms. *Nat Rev Cancer* 3(5):362–374.

128. Chintala SK, Rao JK (1996) Invasion of human glioma: role of extracellular matrix proteins. *Front Biosci* 1(November):d324–d339.

129. Rubenstein BM, Kaufman LJ (2008) The Role of Extracellular Matrix in Glioma Invasion: A Cellular Potts Model Approach. *Biophys J* 95(12):5661–5680.

130. Mohamed MM, Sloane BF (2006) Cysteine cathepsins: multifunctional enzymes in cancer. *Nat Rev Cancer* 6(10):764–775.

131. Groves MD, et al. (2006) Phase II trial of temozolomide plus marimastat for recurrent anaplastic gliomas: A relationship among efficacy, joint toxicity and anticonvulsant status. *J Neurooncol* 80(1):83–90.

132. Groves MD, et al. (2002) Phase II trial of temozolomide plus the matrix metalloproteinase inhibitor, marimastat, in recurrent and progressive glioblastoma multiforme. *J Clin Oncol* 20(5):1383–8.

133. Fellner S, et al. (2002) Transport of paclitaxel (Taxol) across the blood-brain barrier in vitro and in vivo. *J Clin Invest* 110(9):1309–18.

134. Jordan MA, Toso RJ, Thrower D, Wilson L (1993) Mechanism of mitotic block and inhibition of cell proliferation by taxol at low concentrations. *Proc Natl Acad Sci U S A* 90(20):9552–6.

135. Perou CM, et al. (2000) Molecular portraits of human breast tumours. *Nature* 406(6797):747–752.

136. Verhaak RGW, et al. (2010) Integrated Genomic Analysis Identifies Clinically Relevant Subtypes of Glioblastoma Characterized by Abnormalities in PDGFRA, IDH1, EGFR, and NF1. *Cancer Cell* 17(1):98–110.

137. Vogel CL, et al. (2002) Efficacy and Safety of Trastuzumab as a Single Agent in First-Line Treatment of HER2 -Overexpressing Metastatic Breast Cancer. *J Clin Oncol* 20(3):719–726.

138. Patel AP, et al. (2014) Single-cell RNA-seq highlights intratumoral heterogeneity in primary glioblastoma. *Science* 344(6190):1396–401.

139. Wang J, et al. (2016) Clonal evolution of glioblastoma under therapy. *Nat Genet* 48(7):768–76.

140. Giese A, Westphal M (1996) Glioma invasion in the central nervous system. *Neurosurgery* 39(2):235-50; discussion 250–2.

141. Allen M, Bjerke M, Edlund H, Nelander S, Westermark B (2016) Origin of the U87MG glioma cell line: Good news and bad news. *Sci Transl Med* 8(354):354re3.

142. Hutmacher DW, et al. (2009) Translating tissue engineering technology platforms into cancer research. *J Cell Mol Med* 13(8a):1417–1427.

143. Yamada KM, Cukierman E (2007) Modeling Tissue Morphogenesis and Cancer in 3D. *Cell* 130(4):601–610.

144. Liang C-C, Park AY, Guan J-L (2007) In vitro scratch assay: a convenient and inexpensive method for analysis of cell migration in vitro. *Nat Protoc* 2(2):329–333.

145. Yuhas JM, Li AP, Martinez AO, Ladman AJ (1977) A Simplified Method for Production and Growth of Multicellular Tumor Spheroids. *Cancer Res* 37(10):3639–3643.

146. Mehta G, Hsiao AY, Ingram M, Luker GD, Takayama S (2012) Opportunities and challenges for use of tumor spheroids as models to test drug delivery and efficacy. *J Control Release* 164(2):192–204.

147. Marusyk A, et al. (2016) Spatial Proximity to Fibroblasts Impacts Molecular Features and Therapeutic Sensitivity of Breast Cancer Cells Influencing Clinical Outcomes. *Cancer Res* 76(22):6495–6506.

148. Hirschhaeuser F, et al. (2010) Multicellular tumor spheroids: An underestimated tool is catching up again. *J Biotechnol* 148(1):3–15.

149. Kunz-Schughart L (1999) Multicellular tumor spheroids: intermediates between monolayer culture and in vivo tumor. *Cell Biol Int* 23(3):157–161.

150. Lin R-Z, Chang H-Y (2008) Recent advances in three-dimensional multicellular spheroid culture for biomedical research. *Biotechnol J* 3(9–10):1172–1184.

151. Nyga A, Cheema U, Loizidou M (2011) 3D tumour models: novel in vitro approaches to cancer studies. *J Cell Commun Signal* 5(3):239–248.

152. Albini A, et al. (1987) A Rapid in Vitro Assay for Quantitating the Invasive Potential of Tumor Cells. *Cancer Res* 47(12):3239–3245.

153. Albini A, Benelli R (2007) The chemoinvasion assay: a method to assess tumor and endothelial cell invasion and its modulation. *Nat Protoc* 2(3):504–511.

154. Huszthy PC, et al. (2012) In vivo models of primary brain tumors: pitfalls and perspectives. *Neuro Oncol* 14(8):979–993.

155. Dai C, Holland EC (2001) Glioma models. *Biochim Biophys Acta - Rev Cancer* 1551(1):M19–M27.

156. de Vries NA, Beijnen JH, van Tellingen O (2009) High-grade glioma mouse models and their applicability for preclinical testing. *Cancer Treat Rev* 35(8):714–723.

157. Pilkington GJ, Bjerkvig R, De Ridder L, Kaaijk P (1997) In vitro and in vivo models for the study of brain tumour invasion. *Anticancer Res* 17(6 B):4107–4109.

158. Shapiro WR, Basler GA, Chernik NL, Posner JB (1979) Human brain tumor transplantation into nude mice. *J Natl Cancer Inst* 62(3):447–53.

159. Weiner NE, et al. (1999) A Syngeneic Mouse Glioma Model for Study of Glioblastoma Therapy. *J Neuropathol Exp Neurol* 58(1):54–60.

160. Sonabend AM, Lesniak MS, Ulasov I V (2007) Emerging role of new transgenic mouse models in glioma research. *Expert Rev Anticancer Ther* 7(sup1):S7–S13.

161. Fomchenko EI, Holland EC (2006) Mouse models of brain tumors and their applications in preclinical trials. *Clin Cancer Res* 12(18):5288–97.

162. Begley CG, Ellis LM (2012) Raise standards for preclinical cancer research. *Nature*

483(7391):531–533.

163. Rubin EH, Gilliland DG (2012) Drug development and clinical trials—the path to an approved cancer drug. *Nat Rev Clin Oncol* 9(4):215–222.

164. Humpel C (2015) Organotypic brain slice cultures. *Neuroscience* 305:86–98.

165. Ohnishi T, Matsumura H, Izumoto S, Hiraga S, Hayakawa T (1998) A Novel Model of Glioma Cell Invasion Using Organotypic Brain Slice Culture1. *CANCER Res* 58:2935–2940.

166. Jung S, et al. (2002) Brain tumor invasion model system using organotypic brain-slice culture as an alternative to in vivo model. *J Cancer Res Clin Oncol* 128(9):469–476.

167. Opitz-Araya X, Barria A (2011) Organotypic hippocampal slice cultures. *J Vis Exp* (48). doi:10.3791/2462.

168. Muzio L, Consalez G (2013) Modeling human brain development with cerebral organoids. *Stem Cell Res Ther* 4(6):154.

169. Kelava I, Lancaster MA (2016) Dishing out mini-brains: Current progress and future prospects in brain organoid research. *Dev Biol* 420(2):199–209.

170. Lancaster MA, et al. (2013) Cerebral organoids model human brain development and microcephaly. *Nature* 501(7467):373–9.

171. Sachs N, Clevers H (2014) Organoid cultures for the analysis of cancer phenotypes. *Curr Opin Genet Dev* 24:68–73.

172. Camp JG, Treutlein B (2017) Human development: Advances in mini-brain

technology. *Nature* 545(7652):39–40.

173. Lutolf MP, Hubbell JA (2005) Synthetic biomaterials as instructive extracellular microenvironments for morphogenesis in tissue engineering. *Nat Biotechnol* 23(1):47–55.

174. Khademhosseini A, Langer R, Borenstein J, Vacanti JP (2006) Microscale technologies for tissue engineering and biology. *Proc Natl Acad Sci U S A* 103(8):2480–7.

175. Chitcholtan K, Sykes PH, Evans JJ (2012) The resistance of intracellular mediators to doxorubicin and cisplatin are distinct in 3D and 2D endometrial cancer. *J Transl Med* 10(1). doi:10.1186/1479-5876-10-38.

176. F. Rehfeldt, A. Engler, A. Eckhardt, F. Ahmed DD (2007) Cell responses to the mechanochemical microenvironment—Implications for regenerative medicine and drug delivery. *Adv Drug Deliv Rev* 59(13):1329–1339.

177. Weigelt B, Geyer FC, Reis-Filho JS (2010) Histological types of breast cancer: how special are they? *Mol Oncol* 4(3):192–208.

178. Ulrich TA, de Juan Pardo EM, Kumar S (2009) The mechanical rigidity of the extracellular matrix regulates the structure, motility, and proliferation of glioma cells. *Cancer Res* 69(10):4167–74.

179. Ulrich TA, Jain A, Tanner K, MacKay JL, Kumar S (2010) Probing cellular mechanobiology in three-dimensional culture with collagen–agarose matrices. *Biomaterials* 31(7):1875–1884.

180. Rape AD, Zibinsky M, Murthy N, Kumar S (2015) A synthetic hydrogel for the high-throughput study of cell–ECM interactions. *Nat Commun* 6(1):8129.

181. Xiao W, Sohrabi A, Seidlits SK (2017) Integrating the glioblastoma microenvironment into engineered experimental models. *Futur Sci OA*:FSO189.

182. Haessler U, Kalinin Y, Swartz M a, Wu M (2009) An agarose-based microfluidic platform with a gradient buffer for 3D chemotaxis studies. *Biomed Microdevices* 11(4):827–35.

183. Stroock AD, Fischbach C (2010) Microfluidic culture models of tumor angiogenesis. *Tissue Eng Part A* 16(7):2143–6.

184. Duinen V Van, Trietsch SJ, Joore J, Vulto P, Hankemeier T (2015) Microfluidic 3D cell culture : from tools to tissue models. *Curr Opin Biotechnol* 35:118–126.

185. Pedron S, Becka E, Harley BA (2015) Spatially Gradated Hydrogel Platform as a 3D Engineered Tumor Microenvironment. *Adv Mater* 27(9):1567–1572.

186. Griffith LG, Naughton G (2002) Tissue Engineering--Current Challenges and Expanding Opportunities. *Science (80-)* 295(5557).

187. Yu J, et al. (2007) Induced Pluripotent Stem Cell Lines Derived from Human Somatic Cells. *Science (80-)* 318(5858).

188. Atala A, Kasper FK, Mikos AG (2012) Engineering Complex Tissues. *Sci Transl Med* 4(160).

189. Haessler U, Pisano M, Wu M, Swartz MA (2011) Dendritic cell chemotaxis in 3D under defined chemokine gradients reveals differential response to ligands CCL21 and

CCL19. *Proc nation* 108:3–8.

190. Wlodkowic D, Cooper JM (2010) Tumors on chips: oncology meets microfluidics. *Curr Opin Chem Biol* 14(5):556–567.

191. Kim BJ, Wu M (2012) Microfluidics for mammalian cell chemotaxis. *Ann Biomed Eng* 40(6):1316–27.

192. Packer M, et al. (2001) Effect of Carvedilol on Survival in Severe Chronic Heart Failure. *N Engl J Med* 344(22):1651–1658.

193. Paez JG, et al. (2004) EGFR Mutations in Lung Cancer: Correlation with Clinical Response to Gefitinib Therapy. *Science (80-)* 304(5676).

194. Michiels S, Koscielny S, Hill C (2005) Prediction of cancer outcome with microarrays: a multiple random validation strategy. *Lancet* 365(9458):488–492.

195. Elliott NT, Yuan F (2011) A Review of Three-Dimensional In Vitro Tissue Models for Drug Discovery and Transport Studies. *J Pharm Sci* 100(1):59–74.

196. Burdett E, Kasper FK, Mikos AG, Ludwig JA (2010) Engineering Tumors: A Tissue Engineering Perspective in Cancer Biology. *Tissue Eng Part B Rev* 16(3):351–359.

197. Verbridge SS, Chandler EM, Fischbach C (2010) Tissue-Engineered Three-Dimensional Tumor Models to Study Tumor Angiogenesis. *Tissue Eng Part A* 16(7):2147–2152.

198. Dolacek T, Propp JM, Stroup NE, Kruchko C (2012) CBTRUS Statistical Report : Primary Brain and Central Nervous System Tumors Diagnosed in the United States in 2006-2010. *Neuro Oncol* 14:v1–v49.

199. Lefranc F, Brotchi J, Kiss R (2005) Possible future issues in the treatment of glioblastomas: special emphasis on cell migration and the resistance of migrating glioblastoma cells to apoptosis. *J Clin Oncol* 23(10):2411–22.

200. Munson JM, et al. (2012) Anti-invasive adjuvant therapy with imipramine blue enhances chemotherapeutic efficacy against glioma. *Sci Transl Med* 4(127):127ra36.

201. Gritsenko PG, Ilina O, Friedl P (2012) Interstitial guidance of cancer invasion. *J Pathol* 226(2):185–199.

202. Inda M-M, et al. (2010) Tumor heterogeneity is an active process maintained by a mutant EGFR-induced cytokine circuit in glioblastoma. *Genes Dev* 24(16):1731–45.

203. Parsons DW, et al. (2008) An Integrated Genomic Analysis of Glioblastoma Multiforme. *Science (80-)* 321:1807–1813.

204. Burger PC, Green SB (1987) Patient age, histologic features, and length of survival in patients with glioblastoma multiforme. *Cancer* 59(9):1617–1625.

205. Turcan S, et al. (2012) IDH1 mutation is sufficient to establish the glioma hypermethylator phenotype. *Nature* 483(7390):479–483.

206. Songtao Q, et al. (2012) IDH mutations predict longer survival and response to temozolomide in secondary glioblastoma. *Cancer Sci* 103(2):269–273.

207. Shinojima N, et al. (2003) Prognostic Value of Epidermal Growth Factor Receptor in Patients with Glioblastoma Multiforme. *Cancer Res* 63:6962–6970.

208. Schumacher T, et al. (2014) A vaccine targeting mutant IDH1 induces antitumour immunity. *Nature* 512(7514):324–327.

209. Karpel-Massler G, Schmidt U, Unterberg A, Halatsch M-E (2009) Therapeutic inhibition of the epidermal growth factor receptor in high-grade gliomas: where do we stand? *Mol Cancer Res* 7(7):1000–1012.

210. Rubin JB (2009) Only in congenial soil: the microenvironment in brain tumorigenesis. *Brain Pathol* 19(1):144–9.

211. Quail DF, Joyce JA (2013) Microenvironmental regulation of tumor progression and metastasis. *Nat Med* 19(11):1423–1437.

212. Dvorak HF, Weaver VM, Tlsty TD, Bergers G (2011) Tumor microenvironment and progression. *J Surg Oncol* 103(6):468–474.

213. Leek RD, Harris AL (2002) Tumor-associated macrophages in breast cancer. *J Mammary Gland Biol Neoplasia* 7(2):177–89.

214. Bingle L, Brown NJ, Lewis CE (2002) The role of tumour-associated macrophages in tumour progression: Implications for new anticancer therapies. *J Pathol* 196(3):254–265.

215. Bhowmick NA, Neilson EG, Moses HL (2004) Stromal fibroblasts in cancer initiation and progression. *Nature* 432(7015):332–337.

216. Surowiak P, et al. (2007) Occurence of stromal myofibroblasts in the invasive ductal breast cancer tissue is an unfavourable prognostic factor. *Anticancer Res* 27(4 C):2917–2924.

217. Lorger M (2012) Tumor microenvironment in the brain. *Cancers* 4(1):218–43.

218. Gill BJ, et al. (2014) MRI-localized biopsies reveal subtype-specific differences in

molecular and cellular composition at the margins of glioblastoma. *Proc Natl Acad Sci U S A* 111(34):12550–5.

219. Zagzag D, et al. (2000) Expression of hypoxia-inducible factor 1alpha in brain tumors: association with angiogenesis, invasion, and progression. *Cancer* 88(11):2606–18.

220. Rempel SA, Dudas S, Ge S, Gutie JA (2000) Identification and Localization of the Cytokine SDF1 and Its Receptor , CXC Chemokine Receptor 4 , to Regions of Necrosis and Angiogenesis in Human Glioblastoma. *Clin Cancer Res* 6:102–111.

221. Lai A, et al. (2011) Phase II study of bevacizumab plus temozolomide during and after radiation therapy for patients with newly diagnosed glioblastoma multiforme. *J Clin Oncol* 29(2):142–148.

222. Roggendorf W, Strupp S, Paulus W (1996) Distribution and characterization of microglia/macrophages in human brain tumors. *Acta Neuropathol* 92(3):288–293.

223. Shearer KD, Fragoso YD, Clagett-Dame M, McCaffery PJ (2012) Astrocytes as a regulated source of retinoic acid for the brain. *Glia* 60(12):1964–1976.

224. Rangaraju S, Gearing M, Jin L-W, Levey A (2015) Potassium Channel Kv1.3 Is Highly Expressed by Microglia in Human Alzheimer's Disease. *J Alzheimer's Dis* 44(3):797–808.

225. Poff AM, et al. (2015) Non-Toxic Metabolic Management of Metastatic Cancer in VM Mice: Novel Combination of Ketogenic Diet, Ketone Supplementation, and Hyperbaric Oxygen Therapy. *PLoS One* 10(6):e0127407.

226. Ma F, et al. (2014) The Requirement of CD8+ T Cells To Initiate and Augment

Acute Cardiac Inflammatory Response to High Blood Pressure. *J Immunol* 192(7):3365–3373.

227. Leon SP, Folkerth R, Black PM, Ph MD (1996) Microvessel Density Is a Prognostic Indicator for Patients with Astroglial Brain Tumors. *Cancer* 77(2):362–372.

228. Schiffer D, Chio A, Giordana MT, Leone M, Soffietti R (1988) Prognostic Value of Histologic Factors in Adult Cerebral Astrocytoma. *Cancer* 61:1386–1393.

229. Finak G, et al. (2008) Stromal gene expression predicts clinical outcome in breast cancer. *Nat Med* 14(5):518–27.

230. Peferoen L, Kipp M, van der Valk P, van Noort JM, Amor S (2014) Oligodendrocyte-microglia cross-talk in the central nervous system. *Immunology* 141(3):302–313.

231. Adam SA, et al. (2012) ALDH1A1 is a Marker of Astrocytic Differentiation during Brain Development and Correlates with Better Survival in Glioblastoma Patients. *Brain Pathol* 22(6):788–797.

232. Wei J, Gabrusiewicz K, Heimberger A (2013) The controversial role of microglia in malignant gliomas. *Clin Dev Immunol* 2013. doi:10.1155/2013/285246.

233. Watters JJ, Schartner JM, Badie B (2005) Microglia function in brain tumors. *J Neurosci Res* 81(3):447–455.

234. Badie B, Schartner J (2001) Role of microglia in glioma biology. *Microsc Res Tech* 54(2):106–113.

235. Morris CS, Esiri MM (1991) Immunocytochemical study of macrophages and microglial cells and extracellular matrix components in human CNS disease. 1.

Gliomas. *J Neurol Sci* 101(1):47–58.

236. Lin JHC, et al. (2002) Connexin 43 enhances the adhesivity and mediates the invasion of malignant glioma cells. *J Neurosci* 22(11):4302–4311.

237. Bonavia R, Inda MDMM -d.-M, Cavenee WK, Furnari FB (2011) Heterogeneity Maintenance in Glioblastoma: A Social Network. *Cancer Res* 71(12):4055–4060.

238. Stupp R, Hegi ME, Gilbert MR, Chakravarti A (2007) Chemoradiotherapy in malignant glioma: standard of care and future directions. *J Clin Oncol* 25(26):4127–36.

239. Tuettenberg J, et al. (2009) Recurrence pattern in glioblastoma multiforme patients treated with anti-angiogenic chemotherapy. *J Cancer Res Clin Oncol* 135(9):1239–1244.

240. Hatzikirou H, Basanta D, Simon M, Schaller K, Deutsch A (2012) "Go or grow": the key to the emergence of invasion in tumour progression? *Math Med Biol* 29(1):49–65.

241. Wu M, Swartz M (2014) Modeling tumor microenvironments in vitro. *J Biomech Eng* 136(February):1–7.

242. Xu F, et al. (2011) A three-dimensional in vitro ovarian cancer coculture model using a high-throughput cell patterning platform. *Biotechnol J* 6(2):204–212.

243. Kenny HA, et al. (2015) Quantitative high throughput screening using a primary human three-dimensional organotypic culture predicts in vivo efficacy. *Nat Commun* 6:6220.

244. Rath BH, et al. (2013) Astrocytes Enhance the Invasion Potential of Glioblastoma

Stem-Like Cells. *PLoS One* 8(1):e54752.

245. Placone AL, Quiñones-Hinojosa A, Searson PC (2016) The role of astrocytes in the progression of brain cancer: complicating the picture of the tumor microenvironment. *Tumor Biol* 37(1):61–69.

246. Giese A (2003) Cost of Migration: Invasion of Malignant Gliomas and Implications for Treatment. *J Clin Oncol* 21(8):1624–1636.

247. Pollard SM, et al. (2009) Glioma stem cell lines expanded in adherent culture have tumor-specific phenotypes and are suitable for chemical and genetic screens. *Cell Stem Cell* 4(6):568–80.

248. Lee J, et al. (2006) Tumor stem cells derived from glioblastomas cultured in bFGF and EGF more closely mirror the phenotype and genotype of primary tumors than do serum-cultured cell lines. *Cancer Cell* 9(5):391–403.

249. Heddleston JM, Li Z, McLendon RE, Hjelmeland AB, Rich JN (2009) The hypoxic microenvironment maintains glioblastoma stem cells and promotes reprogramming towards a cancer stem cell phenotype. *Cell Cycle* 8(20):3274–84.

250. de Vries N a, Beijnen JH, van Tellingen O (2009) High-grade glioma mouse models and their applicability for preclinical testing. *Cancer Treat Rev* 35(8):714–23.

251. Fillmore HL, et al. (1999) An in vivo rat model for visualizing glioma tumor cell invasion using stable persistent expression of the green fluorescent protein. *Cancer Lett* 141(1–2):9–19.

252. Gutmann DH (2009) Modeling human brain tumors in mice. *Brain Pathol* 19(1):108–

11.

253. Pedron S, Becka E, Harley BAC (2013) Regulation of glioma cell phenotype in 3D matrices by hyaluronic acid. *Biomaterials* 34(30):7408–7417.

254. Griffith LG, Swartz MA (2006) Capturing complex 3D tissue physiology in vitro. *Nat Rev Mol Cell Biol* 7(3):211–224.

255. Beier D, et al. (2007) CD133+ and CD133− Glioblastoma-Derived Cancer Stem Cells Show Differential Growth Characteristics and Molecular Profiles. *Cancer Res* 67(9).

256. Liu G, et al. (2006) Analysis of gene expression and chemoresistance of CD133 + cancer stem cells in glioblastoma. *Mol Cancer* 5(1):67.

257. Harris AR, Yuan JX, Munson JM (2018) Assessing multiparametric drug response in tissue engineered tumor microenvironment models. *Methods* 134–135:20–31.

258. Ivey JW, Bonakdar M, Kanitkar A, Davalos R V., Verbridge SS (2016) Improving cancer therapies by targeting the physical and chemical hallmarks of the tumor microenvironment. *Cancer Lett* 380(1):330–339.

259. Diao J, et al. (2006) A three-channel microfluidic device for generating static linear gradients and its application to the quantitative analysis of bacterial chemotaxis. *Lab Chip* 6(3):381–388.

260. Kim BJ, et al. (2013) Cooperative Roles of SDF-1α and EGF Gradients on Tumor Cell Migration Revealed by a Robust 3D Microfluidic Model. *PLoS One* 8(7):e68422.

261. Gupta PB, et al. (2009) Identification of Selective Inhibitors of Cancer Stem Cells by High-Throughput Screening. *Cell* 138(4):645–659.

262. Torrance CJ, Agrawal V, Vogelstein B, Kinzler KW (2001) Use of isogenic human cancer cells for high-throughput screening and drug discovery. *Nat Biotechnol* 19(10):940–945.

263. Macarron R, et al. (2011) Impact of high-throughput screening in biomedical research. *Nat Publ Gr* 10. doi:10.1038/nrd3368.

264. Gao H, et al. (2015) High-throughput screening using patient-derived tumor xenografts to predict clinical trial drug response. *Nat Med* 21(11):1318–1325.

265. Castells M, Thibault B, Delord J-P, Couderc B (2012) Implication of Tumor Microenvironment in Chemoresistance: Tumor-Associated Stromal Cells Protect Tumor Cells from Cell Death. *Int J Mol Sci* 13(12):9545–9571.

266. Tchou J, Conejo-Garcia J (2012) Targeting the tumor stroma as a novel treatment strategy for breast cancer: shifting from the neoplastic cell-centric to a stroma-centric paradigm. *Adv Pharmacol* 65:45–61.

267. Sounni NE, Noel A (2013) Targeting the Tumor Microenvironment for Cancer Therapy. *Clin Chem* 59(1).

268. Ye C, Liu J, Ren F, Okafo N (2000) Design of experiment and data analysis by JMP® (SAS institute) in analytical method validation. *J Pharm Biomed Anal* 23(2–3):581–589.

269. Wang H, et al. (2009) Targeting Interleukin 6 Signaling Suppresses Glioma Stem Cell Survival and Tumor Growth. *Stem Cells* 27(10):2393–2404.

270. Fontana A, Hengartner H, de Tribolet N, Weber E (1984) Glioblastoma cells release

interleukin 1 and factors inhibiting interleukin 2-mediated effects. *J Immunol* 132(4):1837–44.

271. Chang C-Y, et al. (2005) Prognostic and clinical implication of IL-6 expression in glioblastoma multiforme doi:10.1016/j.jocn.2004.11.017.

272. Chen W, et al. (2016) Human astrocytes secrete IL-6 to promote glioma migration and invasion through upregulation of cytomembrane MMP14. *Oncotarget* 7(38):62425–62438.

273. Zhu VF, Yang J, LeBrun DG, Li M (2012) Understanding the role of cytokines in Glioblastoma Multiforme pathogenesis. *Cancer Lett* 316(2):139–150.

274. Brat DJ, Bellail AC, Van Meir EG (2005) The role of interleukin-8 and its receptors in gliomagenesis and tumoral angiogenesis. *Neuro Oncol* 7(2):122–133.

275. Infanger DW, et al. (2013) Glioblastoma Stem Cells Are Regulated by Interleukin-8 Signaling in a Tumoral Perivascular Niche. *Cancer Res* 73(23):7079–7089.

276. Zhou Y, et al. (2005) The chemokine GRO-α (CXCL1) confers increased tumorigenicity to glioma cells. *Carcinogenesis* 26(12):2058–2068.

277. Chen Q, et al. (2016) Carcinoma–astrocyte gap junctions promote brain metastasis by cGAMP transfer. *Nature* 533(7604):493–498.

278. Plowman J, et al. (1994) Preclinical antitumor activity of temozolomide in mice: efficacy against human brain tumor xenografts and synergism with 1,3-bis(2-chloroethyl)-1-nitrosourea. *Cancer Res* 54(14):3793–9.

279. Huysentruyt LC, Shelton LM, Seyfried TN (2010) Influence of methotrexate and

cisplatin on tumor progression and survival in the VM mouse model of systemic metastatic cancer. *Int J Cancer* 126(1):65–72.

280. Patel VJ, et al. (2000) Schedule-dependent activity of temozolomide plus CPT-11 against a human central nervous system tumor-derived xenograft. *Clin Cancer Res* 6(10):4154–4157.

281. Auffinger B, et al. (2014) Conversion of differentiated cancer cells into cancer stem-like cells in a glioblastoma model after primary chemotherapy. *Cell Death Differ* 21(10):1119–1131.

282. Persson AI, Weiss W a (2009) The side story of stem-like glioma cells. *Cell Stem Cell* 4(3):191–2.

283. Anand Cuddapah V, Robel S, Watkins S, Sontheimer H (2014) A neurocentric perspective on glioma invasion. *Nat Publ Gr* 15. doi:10.1038/nrn3765.

284. Reynés G, et al. (2011) Circulating markers of angiogenesis, inflammation, and coagulation in patients with glioblastoma. *J Neurooncol* 102(1):35–41.

285. Barker FG, et al. (1998) Survival and functional status after resection of recurrent glioblastoma multiforme. *Neurosurgery* 42(4):709-20; discussion 720–3.

286. Chaichana KL, et al. (2013) Multiple resections for patients with glioblastoma: prolonging survival. *J Neurosurg* 118(4):812–20.

287. Xiao W, Sohrabi A, Seidlits SK (2017) Integrating the glioblastoma microenvironment into engineered experimental models. *Futur Sci OA* 3(3):FSO189.

288. Nicolini A, et al. (2006) Metastatic breast cancer: an updating. *Biomed Pharmacother*

60(9):548–556.

289. Tentler JJ, et al. (2012) Patient-derived tumour xenografts as models for oncology drug development. *Nat Rev Clin Oncol* 9(6):338–350.

290. Phillips HS, et al. (2006) Molecular subclasses of high-grade glioma predict prognosis, delineate a pattern of disease progression, and resemble stages in neurogenesis. *Cancer Cell* 9(3):157–173.

291. Placone AL, Quiñones-Hinojosa A, Searson PC (2016) The role of astrocytes in the progression of brain cancer: complicating the picture of the tumor microenvironment. *Tumor Biol* 37(1):61–69.

292. Hoelzinger DB, Demuth T, Berens ME (2007) Autocrine Factors That Sustain Glioma Invasion and Paracrine Biology in the Brain Microenvironment. *J Natl Cancer Inst* 99(21):1583–1593.

293. Logsdon DK, Beeghly GF, Munson JM (2017) Chemoprotection Across the Tumor Border: Cancer Cell Response to Doxorubicin Depends on Stromal Fibroblast Ratios and Interstitial Therapeutic Transport. *Cell Mol Bioeng* 10(5):463–481.

294. Martin KS, Blemker SS, Peirce SM (2015) Agent-based computational model investigates muscle-specific responses to disuse-induced atrophy. *J Appl Physiol* 118(10).

295. An G (2015) Integrating physiology across scales and formalizing hypothesis exploration with agent-based modeling. *J Appl Physiol* 118(10).